HYBUILD
Hybrid Energy Storage for Buildings

Project Title:

Innovative compact HYbrid electrical/thermal storage systems for low energy BUILDings

Project Acronym:

HYBUILD

Deliverable Report

Deliverable number:

D4.4

Deliverable title:

Report on system performance

Related task:	4.1, 4.3, 4.4
Lead beneficiary:	ENG
Authors and institutions:	Alessandro Rossi (ENG), Matteo Verber (ENG), Giuseppe Raveduto (ENG), Federico Trentin (EURAC), Mattia Dallapiccola (EURAC), Chiara Dipasquale (EURAC), Gabriel Zsembinszki (UDL), Cèsar Fernández (UDL), David Vérez (UDL), Luisa F. Cabeza (UDL)
Due date:	31/03/2021 (M42)

DISSEMINATION LEVEL		
PU	Public, fully open, e.g. web	X
CO	Confidential, restricted under conditions set out in Model Grant Agreement	
CI	Classified, information as referred to in Commission Decision 2001/844/EC.	

DOCUMENT STATUS HISTORY		
Date	Description	Partner
2019/09/30	First extended ToC	ENG
2021/03/15	Complete Draft	ENG
2021/03/26	Reviewed	ENG
2021/03/31	Finalised version	COMSA
2022/06/29	Reviewed	ENG, EURAC
2022/06/29	Accepted	COMSA

Table of contents

Publishable executive summary

This document is part of EU Horizon 2020-funded project HYBUILD, whose final target is the development of two innovative compact hybrid electrical/thermal storage systems for stand-alone and district-connected buildings, both in Mediterranean and Continental climatic conditions. It is the last deliverable foreseen inside WP4, "Smart control and System integration" and focuses on the report of the HYBUILD system performance.

The deliverable describes and analyses the (simulated) performances of the HYBUILD system when applied to the two reference buildings already defined in D1.1 and reported in all previous deliverables inside WP4. Both results from dynamic simulation and the two optimisation approaches proposed inside the project are analysed.

Dynamic simulations of thermal and electric systems integrated into the building could become fundamental for analysis of complex systems. Especially when dealing with storages, both thermal and electric, static calculation are not enough for studying all the involved effects. Moreover, the influence of each component on the whole system can be analysed only if all the components are integrated and simulated together. For these reasons, the document presents the modular structure used for developing the simulation environment where each component and sub-system of the energy plant constitutes a module, building included. This approach allows a smart development of the overall building system model, making easy the eventual update of sub systems numerical models without losing the already created connections with other sub-systems.

In the first part of the deliverable, sub-systems and results from dynamic simulation are reported. For the sake of simplicity and due to the level of detail adopted for estimating energy consumption, simplified models are adapted and made suitable for thermal and electric analysis, with respect to the ones studied in detail at technology level in WP3. The unique simulation environment adopted for the whole system allows to perform energy analysis, from an hourly to a yearly basis. Finally, an additional advantage of a numerical model of the overall system (HVAC + storage systems + building) is the possibility to implement and test the adopted control strategies.

The present document also describes the working scenarios for the two systems configurations, in the Mediterranean and in the Continental climate. Depending on the external conditions and building energy demand, the generation sources or storages are used in order to minimize the energy consumption. The results are reported in terms of the PIs already defined in WP1 for the two studied HYBUILD systems and allow a useful evaluation of systems performance at both sub-system level and overall building system level.

The main conclusion of this first part of the deliverable is that an overview of the whole system is fundamental when dealing with optimization of the control strategy in complex systems, as the ones proposed in HYBUILD, where the interactions between the different components become crucial.

In the second part of the deliverable, the results of two optimised control systems, based on Artificial Intelligence, are discussed.

Optimisation of the control of such a complex system as HYBUILD is one of the major challenges of the project. Rule-based control strategies are usually implemented in energy systems, which consider well-defined and suitable operation rules based on various parameters thresholds. However, besides a basic rule-based control implementation, the complexity of systems such as the one developed within HYBUILD requires the implementation of a smart control able to improve the behaviour of the system as compared to the basic control. In this report, the results

of the research carried out by UDL with respect to the smart control implementation based on cost and energy performance policies are presented.

The research carried out at UDL and presented here are the continuation of previous results obtained for the theoretical Mediterranean HYBUILD system based on a cost optimisation strategy already reported in deliverable D4.3, where the full methodology of the deep reinforcement learning (DRL) techniques applied were presented in detail. In this last deliverable of WP4, a model robustness check was performed and presented to confirm the validity of the results obtained using simple models developed for the theoretical system components. Moreover, an optimisation strategy from a system efficiency perspective was investigated, and the results are shown in comparison with the results obtained using a cost-optimisation strategy. The share of renewable was used as a performance indicator relating to the system efficiency.

The results obtained confirmed that the simple models used in the cost-optimisation strategy based on DRL techniques were accurate enough for the purpose of this research. Moreover, the results showed that the share of renewable could be enhanced from 52% in the case of the cost-optimisation strategy to 62% in the case of the energy efficiency optimisation strategy. However, from an economic point of view, the latter optimisation strategy is not suitable, since the operation cost corresponding to the tested period increased from 11.3 € to 27 €.

In light of the results obtained, further investigation should be carried out to improve the smart control strategy based on energy efficiency-related policies, which should combine cost and environmental criteria to obtain an optimal compromise between economic, social, and environmental benefits.

The optimiser provided by ENG relies upon an optimisation framework able to handle more objectives at the same time. It has been implemented through a heuristic algorithm, the Non-dominated Sorting Genetic Algorithm II (NSGA II), in which the main objectives are the provision of flexibility services to the grid operators, guaranteeing the economic management of the energy operations, and the user comfort, in terms of fulfilment of the energy demand for the space cooling or heating and availability of domestic hot water. In this case, the solution proposed allows to leverage on the storage systems, in particular the electrical battery and the latent storage, not only for handling internal energy management but also for addressing the request from the grid operators. This is part of a wider framework of Demand Response (DR) implementation in the field of building energy management. A typical DR mechanism has been envisioned: a grid operator sends a flexibility service request signal consisting of a power profile to be followed by the building. This service request drives the optimisation. The system fulfills the request, guaranteeing at the same time the comfort of the inhabitants, always seen as priority.

The main conclusion of this second approach reported in the deliverable is that the participation to DR programs could be feasible in this context, exploiting the flexibility allowed by the adoption of a HYBUILD solution for the energy management of the building. The proposed algorithm, based on NSGA-II approach, is also quick enough to adopt not only a day-ahead approach but also an infra-day adaptation within reasonable execution time in case of needs of re-adaptations: the study performed on the algorithm at variation of configuration parameters demonstrated in fact that higher execution times allows better results only under particular circumstances. First of all, when the complexity of the system is high, the constraints over the optimisation variables have a higher impact over the additional freedom enabled by a higher number of optimisation parameters. In general, it is important to identify all the technical constraints, in order to better shape the optimisation and tailor the implementation to the specific case.

Acronyms and Abbreviations

ADS	Adsorption Chiller
AGL	Aglantzia (simulated system)
AI	Artificial Intelligence
B	Battery *(in formulas)* / Power charged or discharged from the battery
BEMS	Building Energy Management System
BESS	Battery Energy Storage System
CON	Continental
CONTRL	Controller/equipment (electrical system)
COP	Coefficient Of Performance
CV	Control Volume
DHW	Domestic Hot Water
DISTR	Distribution system
DR	Demand-Response
DRL	Deep Reinforcement Learning
DSO	Distribution Service Operator
EER	Energy Efficiency Ratio
EL	Electrical system
ENG	Engineering Ingegneria Informatica S.p.A.
EURAC	EURAC research
FE	Final Energy
HP	Compression chiller + PCM in HYBUILD MED system, Heat Pump in HYBUILD CON system
KPI	Key Performance Indicator
MED	Mediterranean
NSGA-II	Non-dominated Sorting Genetic Algorythm II
OM	Operational Modes
PCM	Phase Change Material
PV	Photovoltaic (system)
RBC	Rule Based Control
RPW-HEX	Refrigerant/PCM/Water - Heat EXchanger
SC	Space Cooling
Sc	Self-consumption
SCOP	Seasonal Coefficient Of Performance
SEER	Seasonal Energy Efficiency Ratio
SFH	Single Family House
SH	Space Heating
SH/C	Space Heating and Cooling emission system
sMFH	Small Multi-Family House
SPF	Seasonal Performance Factor
SR	Share of Renewable
SS	Self-sufficiency
STC	Solar Thermal Collector
UDL	Universidad de Lleida

1 Introduction

1.1 Aims and objectives

The current deliverable reports and analyses the final results obtained in WP4 within the different frameworks which have been designed, developed and studied during the entire duration of the WP. The main scope is to describe the performance of the HYBUILD system from different perspectives: the dynamic simulation performed by EURAC, the cost and efficiency optimization studied and developed by UDL, and the flexibility optimization, intended as the ability of the building to fulfill external requests exploiting its peculiar components, proposed by ENG. Being the last deliverable foreseen in WP4, it builds upon the outcomes of previously released WP4 deliverables D4.1 [1], D4.2 [2] and D4.3 [3]. In particular, the focus of this deliverable is on the reference buildings adopting the HYBUILD solution for the Mediterranean and Continental climates, as already defined and described in the past deliverables. This deliverable does not analyse the performance of the real demo sites, which will be evaluated later and reported in later deliverables, once experimental results are available from the operational phase.

In this sense, the results analysed here will represent a benchmark and a reference for the real demo site performance evaluation. Demo site owners and partners involved in post-processing analisys at various levels are the main target groups of the current deliverable. Moreover, the deliverable will be disclosed to the public, to all the readers interested about the HYBUILD project, its results, and in particular its performance versus either the basic rule-based or the optimized AI-based (Artificial Intelligence) control foreseen within the project and applied to the reference buildings.

1.2 Relations to other activities in the project

This deliverable is linked not only to the work performed in WP4, and specifically in T4.1 for the simulation activities, T4.3 for the optimisation, and T4.4 for the general implementation of the Building Energy Management System (BEMS), but also to other tasks pertaining to other WPs. Specifically, fundamental for the evaluation of the system result was the study and identification of PIs and KPIs performed in WP1, in particular within T1.5, whose definitions, included in D1.3, have been widely used in this deliverable. Component models reported in D3.1, have been adapted and used as well for the elicitation of the results from the dynamic simulation.

The work performed and reported in this deliverable will be used in WP6, specifically in T6.4, where the experimental results from demo sites will be acquired and studied, and their performance will be evaluated versus the same PIs and KPIs used in here.

1.3 Report structure

The deliverable is structured in five main sections, and one appendix.

The first section includes the general introduction and the scope of the document itself, as well as the work performed by the different partners.

In the second section, the structure used to model the HYBUILD systems in TRNSYS is reported. Detailed studies are carried out at technology level and reported in deliverable D3.1 [4]. For the sake of simplicity and due to the level of detail adopted for estimating energy consumption, simplified models are adapted and made suitable for thermal and electric analysis.

The third section presents results from TRNSYS simulations of HYBUILD MED and CON systems in the specific reference buildings considering the control logics extensively explained in D4.2 [2]. The results are reported in terms of the above mentioned and explained PIs.

The fourth section present cost and efficiency optimisation results, as well as the ones from the flexibility-based optimiser. The two approaches, even if different in both methodology and objectives, both allow to control the building in optimized way fulfilling the results each one aims to obtain.

In the last section, the conclusions are given.

In the appendix, some info about the software implementation are given, as well as the thermal control in the Continental case. This section is intended as an extension of the previous deliverables in the WP to describe the software updates implemented in the meanwhile.

1.4 Contributions of partners

EURAC is responsible for the modelling of the HYBUILD systems for Mediterranean and Continental climates in the specific reference building. The software TRNSYS is used to model HYBUILD systems and to assess, through dynamic simulations, performance of the two systems using PIs defined in D1.3 [5] with respect to sub-system and overall building system level. Moreover, dynamic simulations are also useful for other partners working in optimization to have a benchmark to compare the developed optimized control logics to evaluate their effective benefits. Energy models of the HYBUILD systems are also useful for other partners when sizing the system components.

UDL performed the implementation of the smart control using artificial intelligence techniques based on cost and energy efficiency perspectives. A robustness check of the models was performed, and the comparison of both optimisation strategies was shown. The most relevant results and conclusions were also provided.

ENG led the WP and the final editing of the deliverable. Moreover, ENG is responsible of the BEMS implementation and the flexibility optimiser. Results from tests have been collected and analysed. In appendix, a brief intro to the software developed so far is included.

Further direct and indirect contributions have been given by CSEM, who is maintaining the electrical rack implementing new firmware updates and indicators to support the system performance and bug fixing and tested the BEMS interface, PINK, who kindly provided the specifics of the thermal controller reported in appendix and logistic support in their demo site to be efficiently managed remotely, UCY, for the refinement of the basic control rules in AGL, FAHR, for the detailed memory mapping of their sorption module controller and testing of the BEMS interface, and CNR-ITAE, who collaborated with UDL and ENG with the lab test of the main subsystem that will be deployed in ALM and refined the basic control rules successfully tested in Messina together with ENG.

2 Introduction about HYBUILD Mediterranean and Continental systems

2.1 Resume about system structure

The HYBUILD Mediterranean (MED) and Continental (CON) systems have been already presented extensively in different reports [1] [2]. However, it is here important to recall some concepts to better understand how the system has been modelled in TRNSYS, which contains various outputs in terms of Performance Maps coming from WP2 (components level) and WP3 (sub-system level) or operational modes of the global systems (WP4).

2.1.1 Mediterranean system

The HYBUILD system foreseen for MED climate is already explained in D4.2 [2]. Below, a short description is reported, as well. Figure 1 shows the conceptual scheme of the system and its division in sub-parts developed for TRNSYS dynamic simulation. As it can be noted, six sub-systems are identified:

- Solar Thermal Collector (STC)
- Adsorption Chiller (ADS)
- Compression Chiller and PCM (HP)
- Distribution system (DISTR)
- Domestic Hot Water (DHW)
- Electrical system (EL)

Each of these subsystems is further detailed in the next sections.
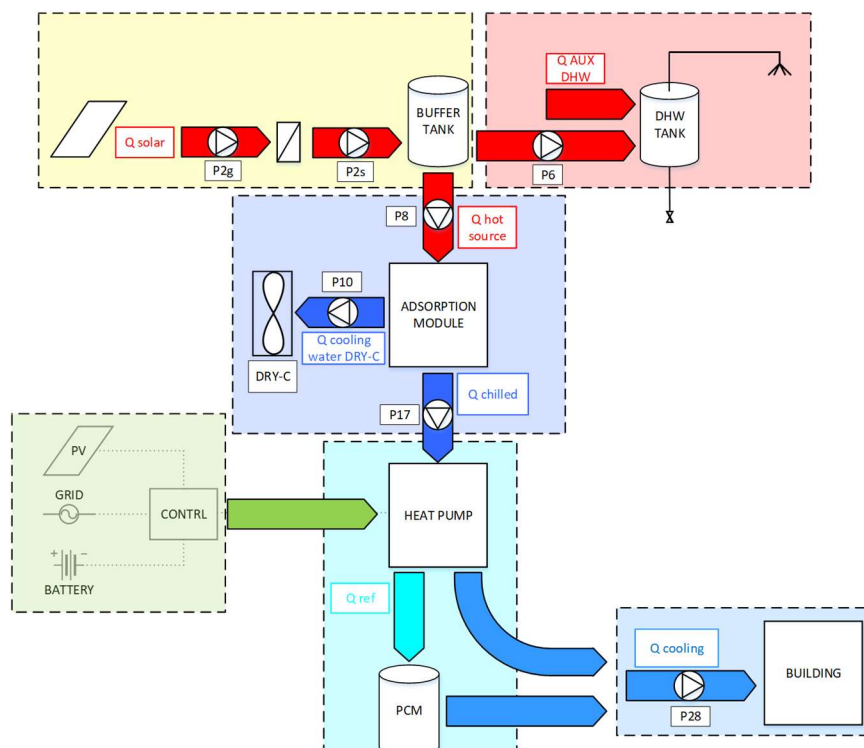
Figure 1 Conceptual scheme of HYBUILD MED system with sub-systems division. Sub-system colour legend: yellow -> STC, red -> DHW, dark blue -> ADS, light blue -> HP, blue -> DISTR, green -> EL

It is useful to remind here that the target building for HYBUILD MED system is a Single Family House (SFH) with 2 floors of 50 m^2 each in the Mediterranean climate (with the reference city of Athens). The target building and climate considered are explained in detail in D1.1 [6].

Solar Thermal Collector

Solar Thermal Collector (STC) circuit is composed basically by Fresnel solar collector (60 m^2) and buffer tank (800 l). To connect them, two circulating pumps (P2g and P2s) and a heat exchanger to separate water from water-glycol circuits are foreseen. Pumps P2g and P2s are fixed speed ones and their activation depends on two measured variables (Fresnel outlet water temperature, measured by sensor TT 105 in Figure 2 and buffer tank top temperature, measured by sensor TT 301 in Figure 2). Figure 2 reports the position of the sensors and components of STC sub-system.
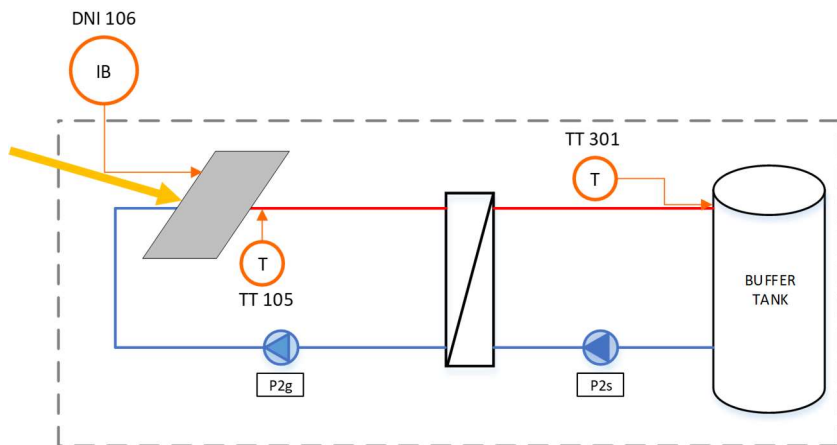

Figure 2 HYBUILD MED system, STC sub-system scheme with components and sensors used for sub-system control

The activation of P2g and P2s occurs if the four following conditions are verified at the same time:

- Solar thermal availability: STC water outlet temperature (TT 105) higher than 30 °C (with a hysteresis characterized by deadband limits of respectively +5°C and 0°C);
- Temperature difference between STC water outlet temperature (TT 105) and buffer tank top temperature (TT 301) higher than 5°C (the hysteresis deadband limits in this case are respectively 0°C and -5°C);
- NOT STC Stagnation: STC water outlet temperature lower than 120 °C (with a hysteresis characterized by deadband limits of respectively 0°C and -5°C);
- NOT Buffer Tank Boiling: buffer tank top temperature lower than 95°C (with a hysteresis characterized by deadband limits of respectively 0°C and -5°C).

The buffer tank considered is equipped with four double ports to allow connection of all the foreseen circuits. Figure 3 reports the buffer tank characteristics, in particular: position of the sensor, position of all the connections with various circuits and geometrical characteristics.
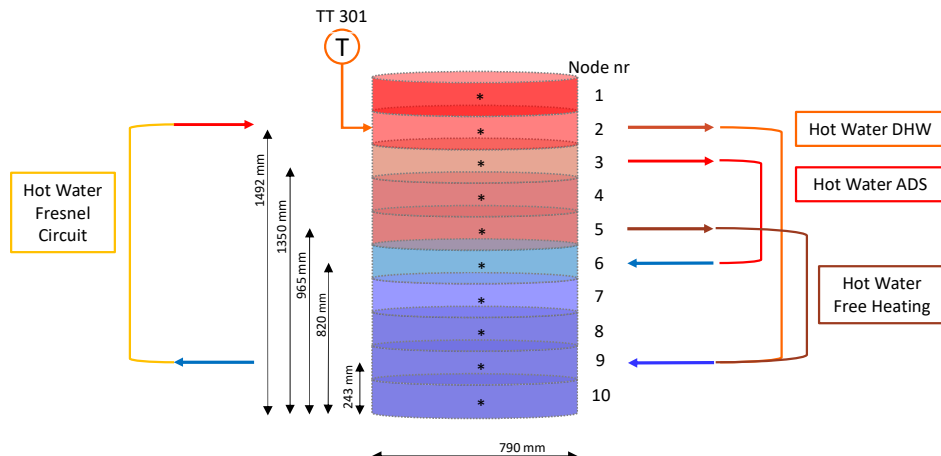
Figure 3 HYBUILD MED system, sensors, double ports and geometrical characteristics of the buffer tank

Adsorption module

Adsorption module´s scope is to cool down water coming from the condenser of compression chiller ensuring in this way optimal working condition for compression machine and therefore higher Energy Efficiency Ratio (EER). Figure 4 reports the adsorption module with its three main circuits, the components to which it is connected and the position of sensors that evaluate the device availability for operation. In particular:

- TT 301 evaluates hot water temperature;
- TT 702 evaluates cooling water temperature;
- TT 801 evaluates chilled water temperature.
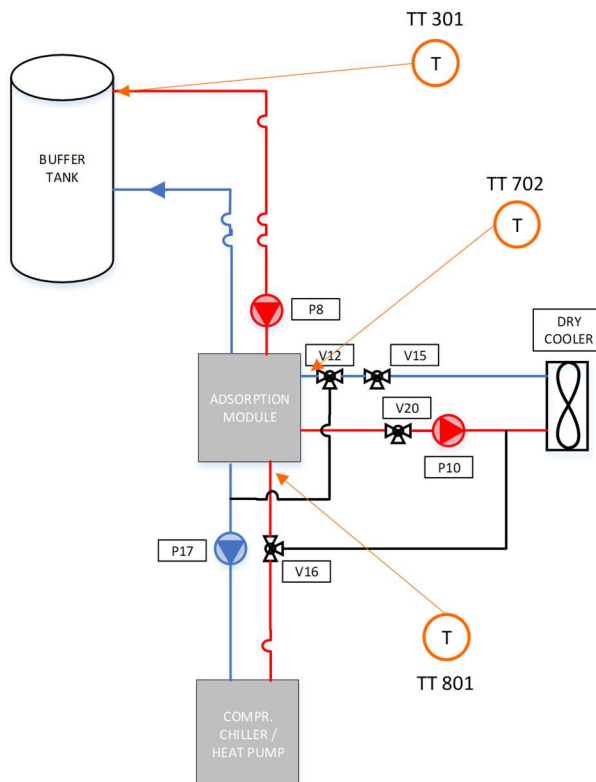
Figure 4 HYBUILD MED system, ADS sub-system scheme with components and sensors used for sub-system control

For the activation of adsorption module and its three related circulating pumps (P8, P10, P17) three conditions on the three circuits temperature must be satisfied at the same time:

- Hot water circuit inlet temperature in the range 65 – 95 °C;
- Cooling water temperature lower than 50°C (the hysteresis deadband limits in this case are respectively 0°C and -3°C);
- Chilled water temperature in the range 16 – 21 °C.

In the simulations, circulating pumps are considered constant speed pumps. Adsorption chiller and dry-cooler instead modulate their power internally to reach the desired condition that, in both cases, is an outlet temperature. In particular, for the adsorption chiller, the desired chilled water outlet temperature is equal to 20°C, while for the dry cooler it has been considered equal to ambient air temperature plus 2.3°C, to be consistent with the approach temperature reported in the dry cooler datasheet at nominal conditions.

If at least one of the previous conditions is not satisfied, adsorption module, P8 and P10 are switched off. If at the same time compression chiller is operating, valves V12 and V16 change their position connecting the condenser of the compression module directly to the dry cooler. In this way the compression chiller works temporarily as a water to air one and Figure 5 represents exactly this operative mode.
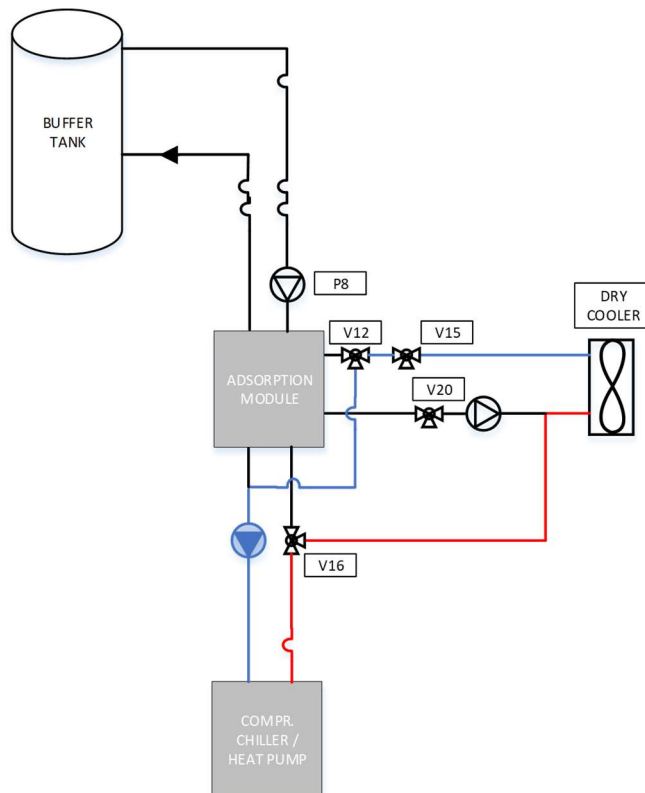

Figure 5 HYBUILD MED system, scheme of operational mode without ADS

Compression chiller and PCM

Compression chiller is the element that produces the energy for cooling the building. At this point some explanations about its different possible operational modes are necessary. This device in HYBUILD MED system is meant to work coupled with adsorption machine connected to its condenser side but, if the adsorption module is not available, the compression chiller condenser side can be connected directly to the dry cooler as explained above and shown in

Figure 5. On the other hand, the evaporator side, although can be also connected directly to the fan coils, is in general connected to the latent storage ensuring its charge. In this second way it is possible to separate the distribution part from the "generation" one that comprises compression chiller and adsorption module as well as the solar circuit.

Regarding the latent storage it constitutes one important part of HYBUILD MED system. Its scope is to store thermal energy using a PCM material that is generally maintained at temperatures in the range -2 - 12°C. The energy stored in the PCM tank is then used to cover building space cooling demand.

Although HYBUILD MED system main focus is to cover space cooling demand of the building, the possibility to cover space heating demand through the inversion of the hydraulic circuit is considered, too.

Distribution system

The distribution system delivers energy through fan coil units for heating and cooling the building to maintain the desired temperature. In fact, the HYBUILD MED system is able to cover also heating demand during winter. For this reason, below, an explanation of distribution circuit operations in different period of the year is reported.

Cooling season

During the cooling season, fan coil units are fed for most of the time from water that is cooled down passing through the Phase Change Material (PCM) storage tank that presents temperature in the range -2 – 12°C. Figure 6 reports this operational mode in continuous blue and red lines. As can be seen in the same figure, there is the possibility to directly connect compression chiller to the distribution system bypassing the PCM storage. However, from simulation it results that this condition, represented in Figure 6 by blue and red dotted lines, doesn´t occur due to the oversized chiller that is always able to maintain the PCM storage charged.

Fan coil units and distribution pump (P28) activation is governed by the thermostats of the considered zones, therefore occurs if:
- Temperature in the considered zone is higher than 25°C (the hysteresis deadband limits in this case are respectively 0°C and -0.5°C).
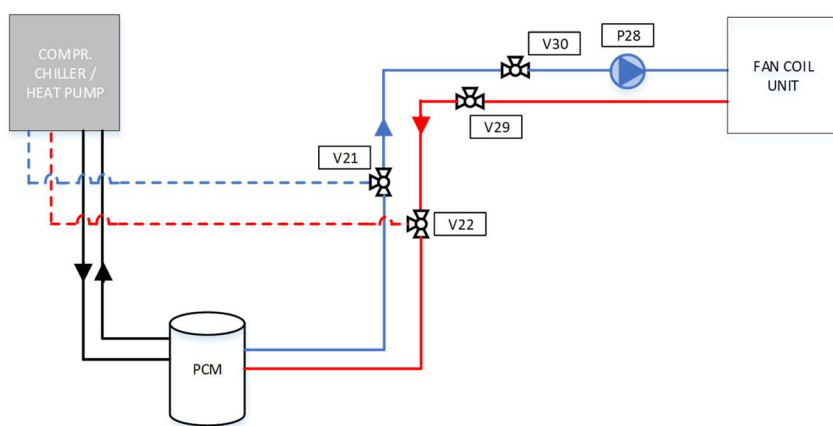

Figure 6 HYBUILD MED system, distribution circuit scheme during cooling season

Heating season

Although HYBUILD MED system aim is mainly to cover space cooling demand, also space heating demand can be satisfied. Moreover, one important feature of HYBUILD MED system is the possibility to exploit directly energy captured from STC to partly cover space heating demand

through free heating mode connecting buffer tank directly to fan coil units. This operational mode is shown in Figure 7. Free heating operational mode, that implies the activation of P28 and the position of valves V29 and V30 in bypass position is activated if both the two following conditions are satisfied at the same time:

- Temperature in one of the zones is lower than 20°C (the hysteresis deadband limits in this case are respectively +0.5°C and 0°C);
- Temperature at the node 5 of the buffer tank (see Figure 3) is higher than 40°C (the hysteresis deadband limits in this case are respectively +1°C and 0°C).
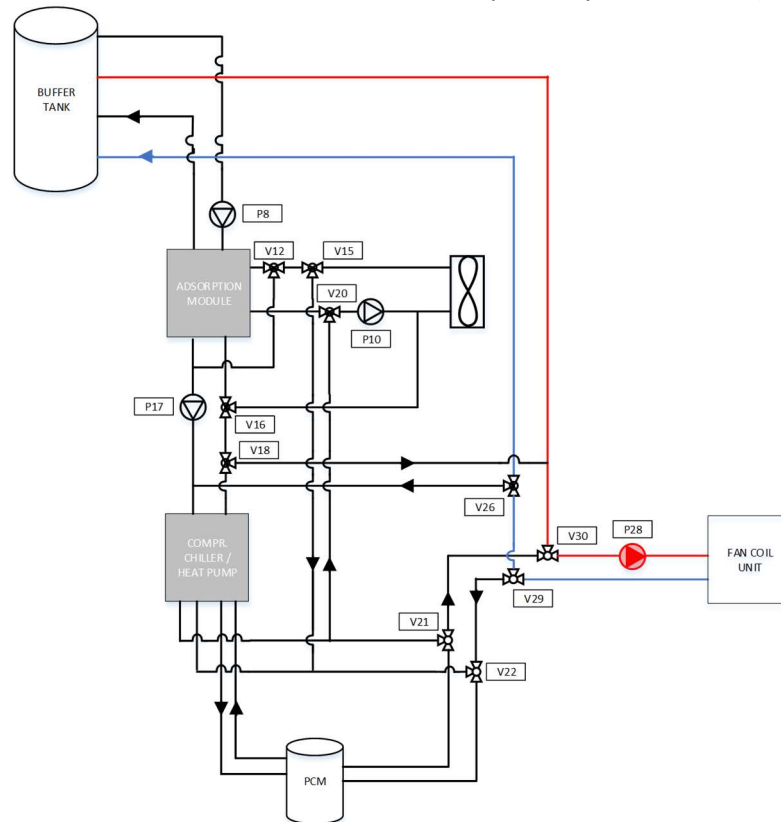

Figure 7 HYBUILD MED system, free heating scheme

When there is no availability from the buffer storage, i.e., its temperature at node 5 is lower than 40°C, space heating is covered in auxiliary mode. Figure 8 reports this modality where, using hydraulic valves, the compression chiller is used as an heat pump, delivering water at temperature around 40°C directly to fan coils.
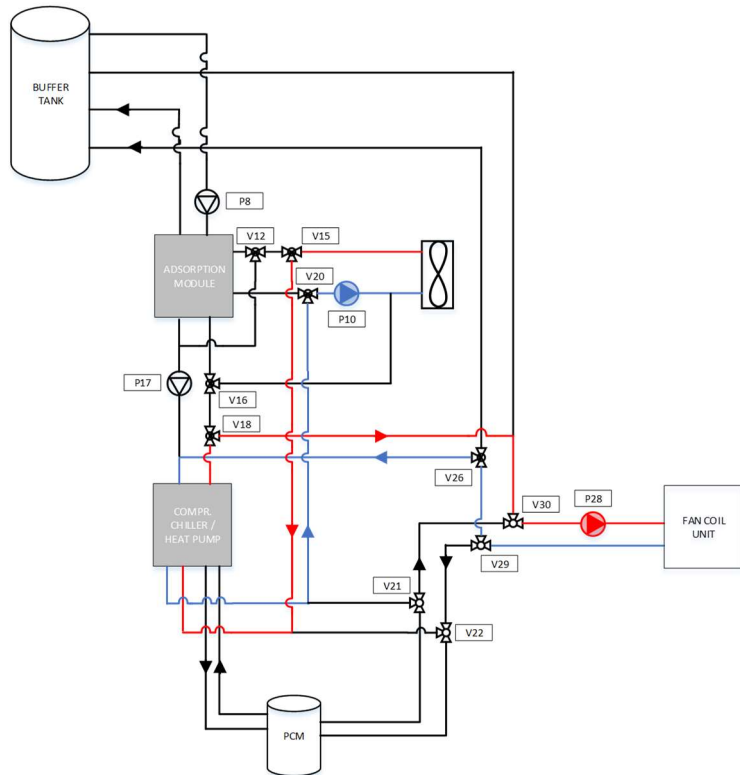
Figure 8 HYBUILD MED system, space heating delivered using the Compression Chiller

Domestic Hot Water

In HYBUILD MED system, DHW demand is covered by exploiting the solar source when available, and through an electrical resistance inside the DHW tank when the first option is not available. In particular, the conditions to charge the DHW tank using energy catched from solar thermal collectors through the buffer tank are the following and the relative scheme is reported in Figure 9:

- DHW tank top temperature lower than 50°C (the hysteresis deadband limits in this case are respectively +5°C and 0°C);
- Buffer tank top temperature higher than DHW tank top temperature (the hysteresis deadband limits in this case are respectively +5°C and 0°C).


Figure 9 HYBUILD MED system, DHW tank charging using buffer tank

If only the first condition is verified, as already mentioned, an electrical resistance is used to increase the temperature of water inside the DHW tank. This second scheme is reported in Figure 10.
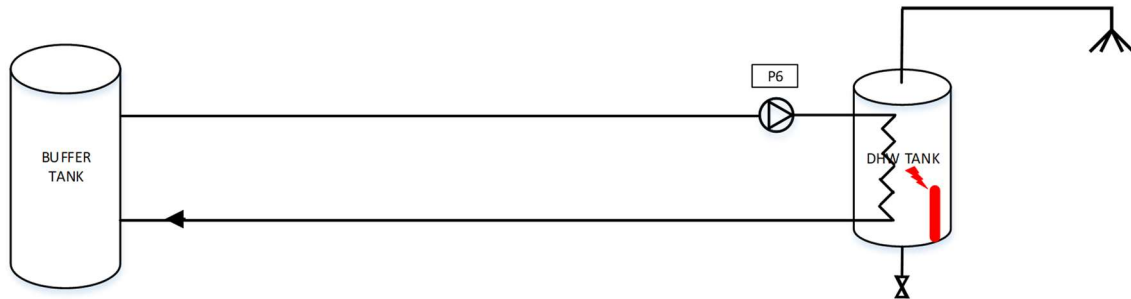
Figure 10 HYBUILD MED system, DHW tank charging using internal electrical resistance

Electrical system

The electrical side of the HYBUILD MED system is composed by three main components:

- Photovoltaic (PV) system with a nominal installed power of 3 kWp
- Battery Energy Storage System (BESS) with a total capacity of 7.3 kWh
- Controller/equipment (CONTRL) to manage the energy flow from the photovoltaic system, to/from the battery and to/from the grid.

It is important to highlight that in this system the PV+BESS sub-system can provide electricity only to the DC compression chiller (also called load) as shown in Figure 1, while the other system components (dry cooler, circulating pumps, etc.) are all connected to the external electrical grid. The logic used by the controller to manage the electrical energy fluxes is the following:

1. Priority is given to Self-consumption: if the compression chiller is operating and the photovoltaic system is producing, the energy produced by the photovoltaic system is sent to the compression chiller (load).
2. If the energy produced by the photovoltaic system is higher than the energy required by the load and at the same time the battery can be charged, the energy produced by PV is used firstly to cover the load and the remaining energy is used to charge the battery. If the battery is completely charged, the excess energy is sent to the grid.
3. If the energy from the photovoltaic system is lower than the energy required by the load, the battery is discharged. In case the photovoltaic production and the energy from the battery are not enough to cover the load demand, use energy from the grid.

Figure 11 represents in a graphical way the possible energy fluxes in the HYBUILD MED electrical system.
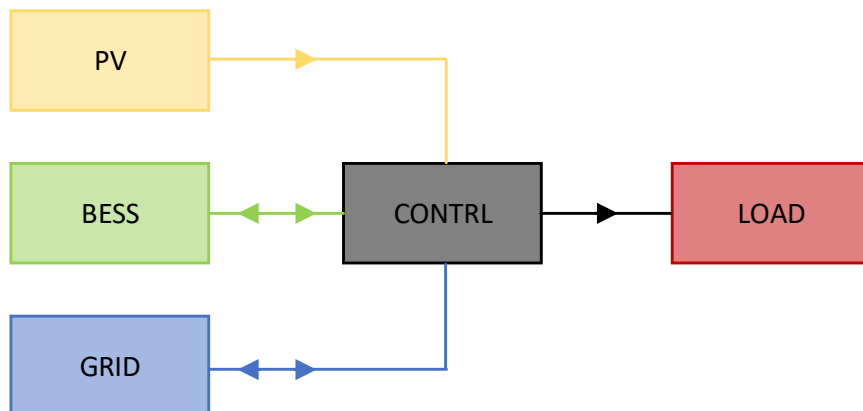

Figure 11 HYBUILD MED system energy fluxes in electrical system

2.1.2 Continental system

The HYBUILD system foreseen for Continental (CON) climate is explained in more details in D4.2 [2], however, as done for the HYBUILD MED system also in this case, a short description is reported. Figure 12 reports the conceptual scheme of the HYBUILD CON system and its division in sub-systems used in TRNSYS dynamic simulation. These sub-systems are:

- Heat Pump (HP)
- Refrigerant/PCM/Water - Heat EXchanger (RPW-HEX)
- Distribution (DISTR)
- Space heating and cooling emission system (SH/C)
- Domestic Hot Water (DHW)
- Electrical system (EL)

The various sub-systems are explained in detail in the following sections.
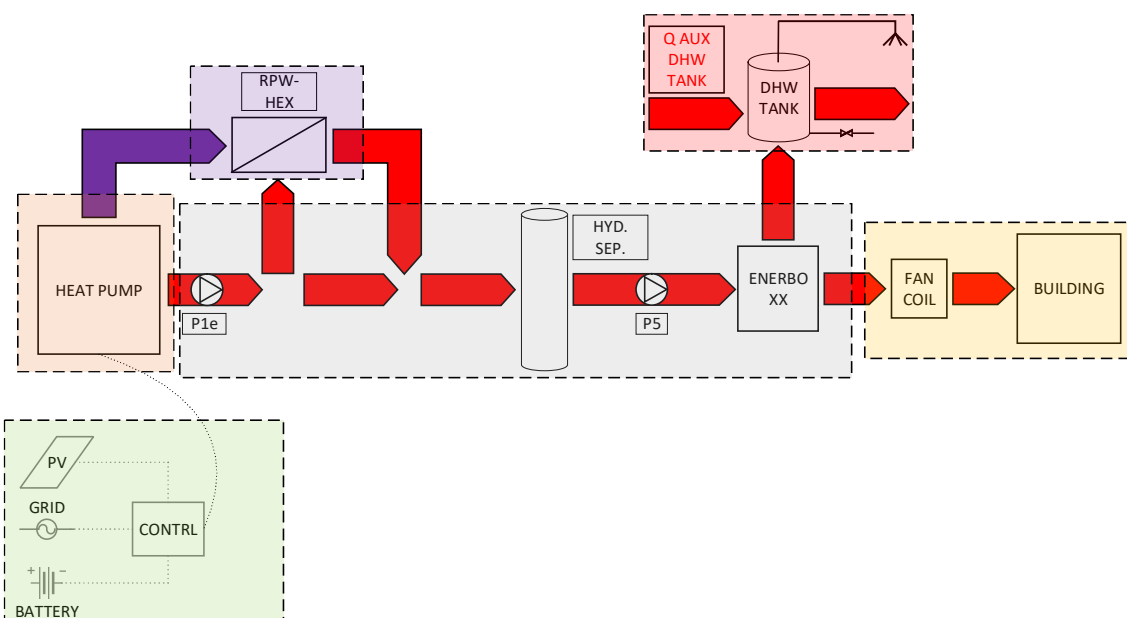

Figure 12 Conceptual scheme of HYBUILD CON system with sub-systems division. Sub-system colour legend: HP -> orange , RPW-HEX -> purple, DISTR -> grey, DHW -> red, SH/C -> yellow, EL -> green

It is important to note that, the target building for HYBUILD CON system, is a small Multi-Family House (sMFH) with 2 dwellings of 50 m^2 each per floor and five floors in the continental climate (with the reference city of Stuttgart). However, for the sake of clarity, in the next figures, only two dwellings (with the related components at dwelling level) are represented.

It is also important to mention here that the building considered for HYBUILD CON system has been changed during the project from the one reported in D1.1 [6]. Same characteristics in terms of geometry and number of dwellings and same reference climate (CON one, with Stuttgart as reference location) are considered, but higher envelope performance up to achieve a heating demand in the range of 50 kWh/m^2/y.

Heat pump

Heat pump is the element that produces the energy for space heating (SH), space cooling (SC) and ensure also decentralized DHW tanks charging. Being the distribution system a two-pipes circuit, the HP works in some predefined periods of the day in DHW mode, while for the rest of the day is available to cover SH or SC building demand (see DHW part in the following for more details about DHW tanks charging periods). One of the innovative solutions of HYBUILD CON system is the adoption of a latent storage (RPW-HEX) that is charged by the hot refrigerant gas

17

exiting the HP compressor before it enters the condenser when the machine is working in SH or SC mode without sensible decrements of HP performance. In this way, when the HP switches from SH or SC mode to DHW tanks charging mode, it is possible to use the HP only to pre-heat the water coming from the decentralized DHW tanks to a temperature of around 40-45°C [6] and use the energy previously stored in the RPW-HEX as a thermal boost to further increase the water temperature, to around 60°C, before sending it to the DHW tanks for their charging. The main advantage of this operational mode is represented by the fact that the HP Coefficient Of Performance (COP) for DHW tanks charging is similar to the COP of the machine in SH mode as it depends on water outlet temperature (40-45°C in this case) and higher with respect to the COP of the machine in DHW charging mode (when the machine should produce water with a temperature in the range 56-62°C). It is in any case important to note that, the considered HP, is also able to ensure DHW tanks charging without the latent storage contribution.

The HP activation in SH or SC mode is governed by basically two inputs:

- Single dwelling thermostats signal (TT ambient 1 and TT ambient 2 in Figure 13),
- Timer control to evaluate if the HP should work in SH/SC mode or in DHW tanks charging mode in the considered moment (timer in Figure 13)
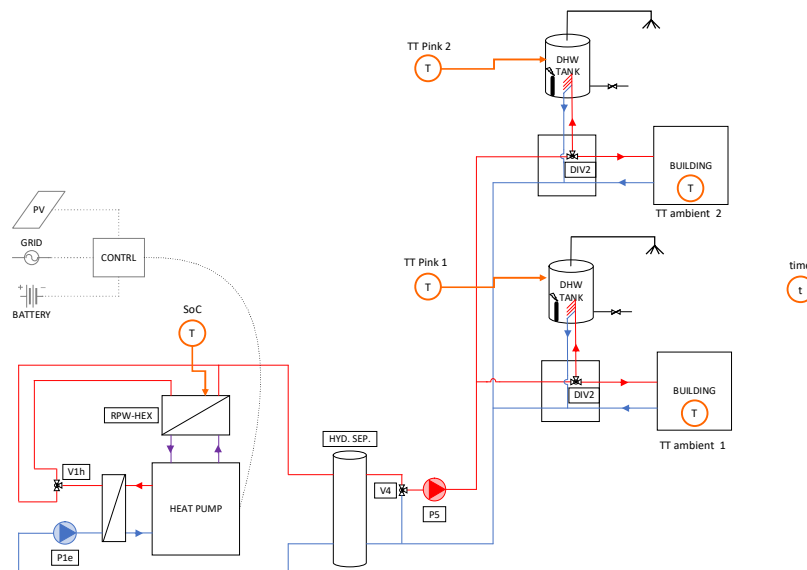

Figure 13 HYBUILD CON system scheme with components and sensors used for systems control

More specifically, the HP is activated in SH or SC mode if one of the following conditions is verified during the predefined working period:

- At least one dwelling is requiring space heating, that is indoor temperature is lower than 20°C ± 0.25°C;
- At least one dwelling is requiring space cooling, that is indoor temperature is higher than 25°C ± 0.25°C.

If, in addition to one of the previous conditions, the RPW-HEX can be charged, the HP works to cover SH or SC demand of the building and, at the same time, RPW-HEX is charged. If, on the other hand, there is SH or SC demand, but the RPW-HEX is already charged, the HP works to cover only SH or SC demand. In this last case the hot refrigerant gas exiting the HP compressor by-passes the RPW-HEX and is directly sent to the HP condenser.

Regarding instead HP activation in DHW charging mode, it is managed by slightly different input signals, in particular:

- Temperature sensor placed at node 1 of the specific DHW tank (TT Pink 1 and TT Pink 2 in Figure 13, for more detail about sensor position see TT Pink # in Figure 22)
- Timer control to evaluate if the HP should work in SH/SC or in DHW tanks charging mode in the considered moment (timer in Figure 13)

More specifically, the activation of HP in DHW tanks charging mode occurs if the following condition is verified during the predefined DHW charging periods:

- At least in one DHW tank, the temperature at the node 1 (see TT Pink # in Figure 22) of the tank is lower than 50°C (the hysteresis varying between 50 and 53°C).

Moreover, if at the same time the RPW-HEX can be discharged, the two devices (HP and RPW-HEX) work in series and HP only pre-heats the water to a temperature of 40-45°C with benefits in terms of performance and, therefore, electrical consumption of the machine. If energy in RPW-HEX is not available, the HP produces hot water at temperature around 56-62°C, ensuring the DHW tanks charging.

At the end of this paragraph it is considered useful to resume the various possible HP operational modes. Moreover, in the following points, also the labels used in TRNSYS model and in some graphs presented in next sections to identify the various schemes are reported. In addition to this, for each operational mode, a figure explains graphically the energy fluxes.

- Scheme SC_2_1: HP works to cover space heating demand and at the same time charges the RPW-HEX (Figure 14)
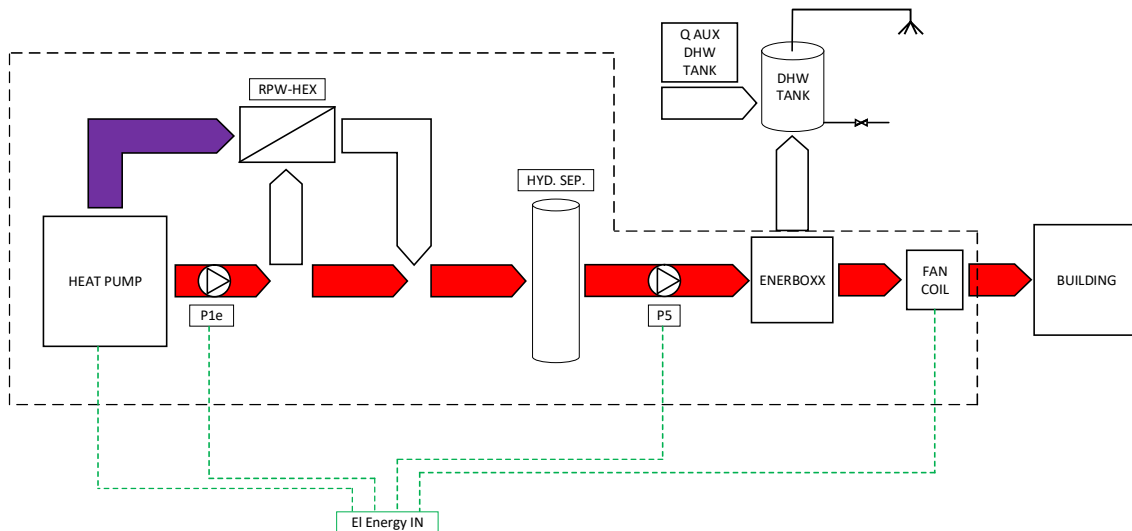

Figure 14 HYBUILD CON system scheme SC_2_1 (SH and RPW-HEX charging)

- Scheme SC_2_2: HP works to cover only space heating demand as the RPW-HEX is fully charged (Figure 15);
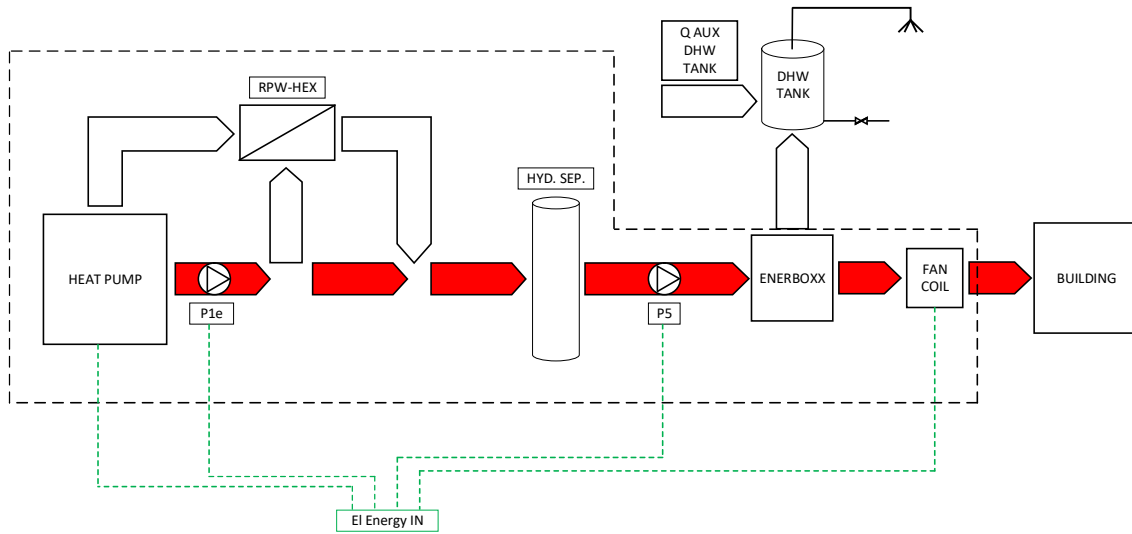
Figure 15 HYBUILD CON system scheme SC_2_2 (SH only)

- Scheme SC_3_1: HP works to cover space cooling demand and at the same time charges the RPW-HEX (Figure 16);
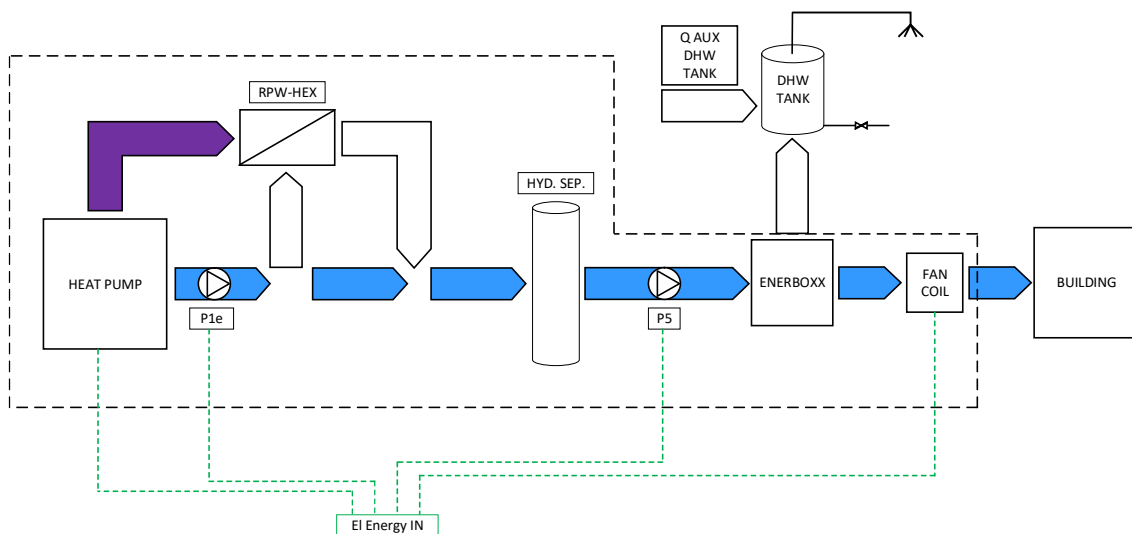
Figure 16 HYBUILD CON system scheme SC_3_1 (SC and RPW-HEX charging)

- Scheme SC_3_2: HP works to cover only space cooling demand as the RPW-HEX is fully charged (Figure 17);
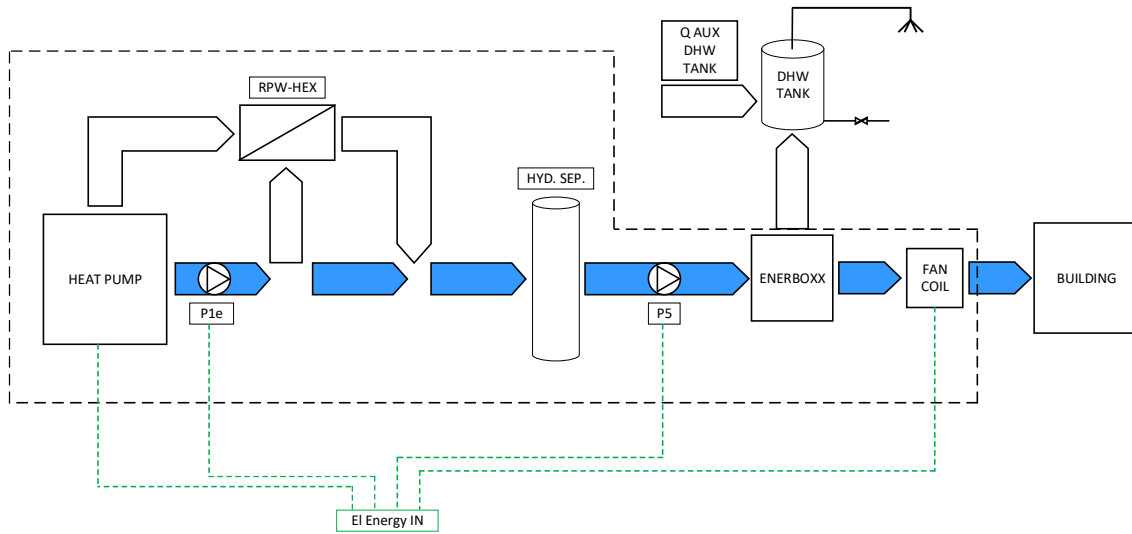
**Figure 17 HYBUILD CON system scheme SC_3_2 (SC only)**

- Scheme SC_4_1: HP works in series with RPW-HEX to charge DHW tanks (Figure 18);
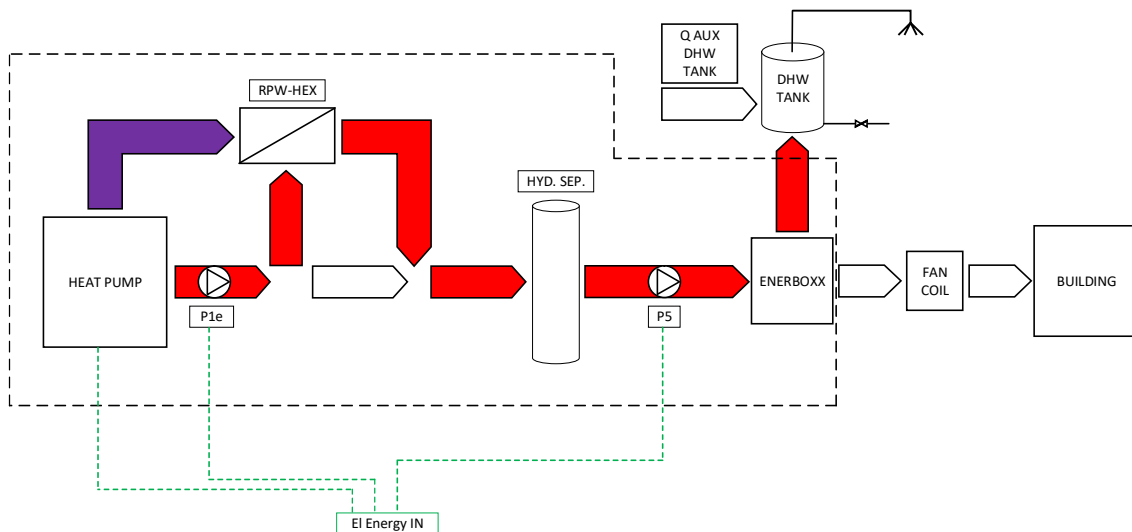
Figure 18 HYBUILD CON system scheme SC_4_1 (DHW tanks charging with HP and RPW-HEX working in series)

- Scheme SC_4_2: HP works alone to charge DHW tanks as RPW-HEX is not available (Figure 19).
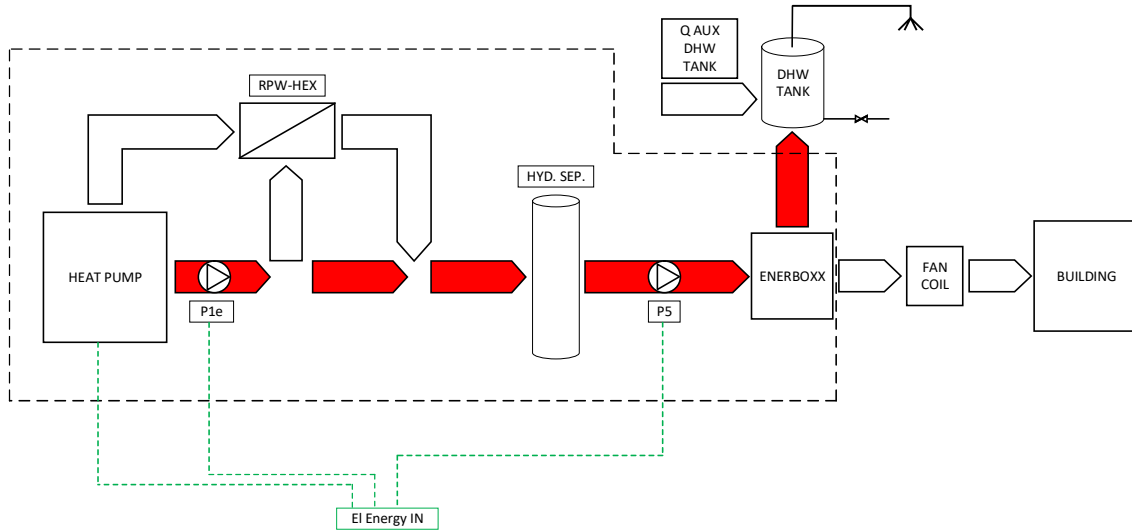
Figure 19 HYBUILD CON system scheme SC_4_2 (DHW tanks charging with HP only)

Refrigerant/PCM (Phase Change Material)/Water - Heat EXchanger (RPW-HEX)

As already mentioned in the previous part, the use of a RPW-HEX is one of the key aspects of HYBUILD CON system. The main purpose of this device is to store part of the sensible energy of refrigerant after being elaborated by the HP compressor when it works to cover SH or SC building demand and use the stored energy for DHW tanks, working in series with the HP. As previously said, the operational mode that foresees the use of HP and RPW-HEX in series, guarantees higher HP COP and, thus, lower electricity consumption with respect to the operational mode in which only HP is used for DHW tanks charging. The higher HP COP when the HP works coupled with RPW-HEX is due to the fact that, in this operational mode, HP only pre-heats the water to a temperature of 40-45 °C. Being the HP COP higher when the machine works with lower water outlet temperature this ensure an higher HP COP when the HP works coupled with RPW-HEX (producing water at 40-45 °C) with respect to when the HP alone guarantees the DHW tanks charging (producing water at 56-62°C).

The RPW-HEX thermal storage capacity considered in the simulations is 7 kWh. This value has been set according to some preliminary indications from other partners. Nevertheless, simulations with also different thermal storage capacity of the RPW-HEX (up to 10 kWh) have been performed and the related conclusions are reported in section 3.2.

Distribution

The distribution circuit is constituted by all the devices that allow the connection between generation units (HP and RPW-HEX) and decentralized units. The main components of the distribution circuit are the hydraulic separator, the circulating pumps P1e and P5, and the distribution pipes. To manage the distribution of hot water to DHW tank or to the fan coils, each dwelling has a hydraulic box (ENERBOXX in Figure 12). It is important to note that the distribution circuit is a two-pipes one, hence, the same two pipes are alternatively used to cover SH/SC dwellings´ demand and to charge the decentralized DHW tanks. The activation of P1e and P5 is related to HP operation, in particular, they are activated if the HP is running. These two circulating pumps are variable speed and the logic used to define the volume flowrate is the following:

- If the HP is working in DHW tanks charging mode, circulating pumps P1e and P5 elaborate the nominal volume flowrate;
- if the HP is working in SH/SC mode, circulating pumps P1e and P5 elaborate a volume flowrate proportional to the number of dwellings that are requiring SH/SC.

Space heating and cooling emission system

Space heating and cooling energy is delivered to the various dwellings through fan coil units to maintain the desired temperature.

Heating season:

During winter, fan coils are fed with mild/hot water. The temperature of water sent to fan coils is regulated based on external air temperature, through a climatic curve defined in Table 1.

Table 1 Climatic curve considered for space heating (emission units: fan coils)

T ambient air [°C]	T water outlet [°C]
20	30
-20	50

The activation of a fan coil unit of the specific apartment is managed by the thermostat of the considered dwelling and occurs if:
- Temperature in the considered dwelling is lower than 20°C ± 0.25°C.

Figure 20 reports the HYBUILD CON system when operating in space heating mode. As can be noted from the considered figure, the RPW-HEX is simultaneously charged (scheme SC_2_1).
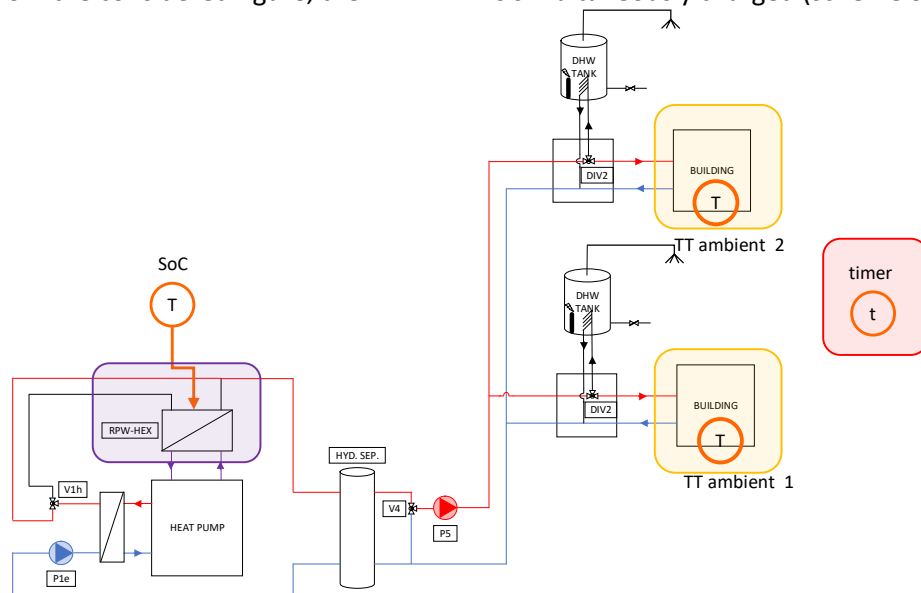
Figure 20 HYBUILD CON system, space heating scheme with also RPW-HEX charging (scheme SC_2_1). System components and sensors used for system control

Cooling season:

During summer, fan coils are fed with fresh water produced by the HP (at temperature of 7°C) during the SC periods of the day. The activation of a fan coil unit of the specific apartment is governed by the thermostat of the considered dwelling and occurs if:
- Temperature in the considered dwelling is higher than 25°C ± 0.25°C.

Figure 21 shows the HYBUILD CON system when operating in space cooling mode. Moreover, it is important to note that, at the same time, RPW-HEX is charged (scheme_SC_3_1).
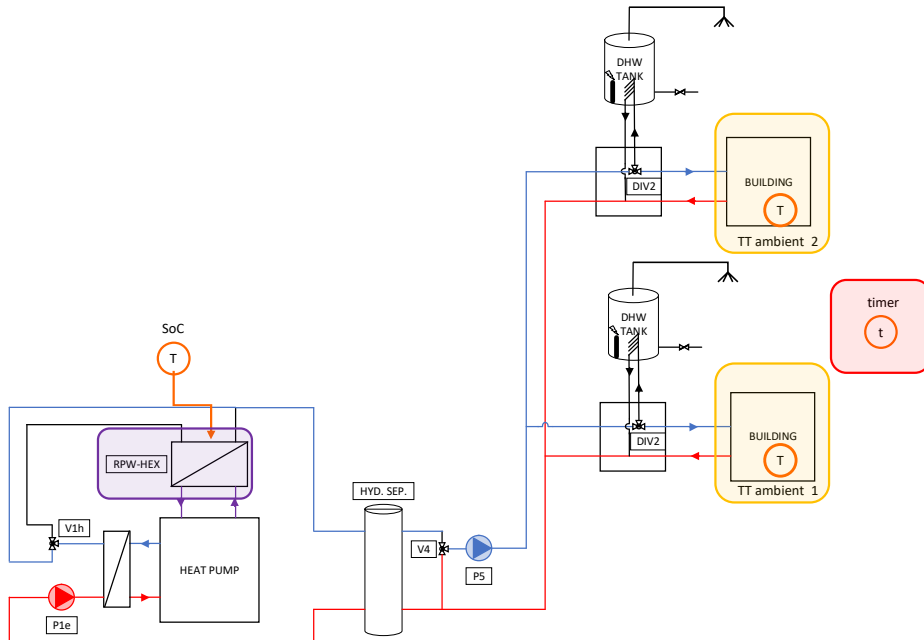
Figure 21 HYBUILD CON system, space cooling scheme with also RPW-HEX charging (scheme_SC_3_1). System components and sensors used for system control

Domestic Hot Water

As already explained in the previous paragraphs, the considered system is a two-pipes distribution system, where the same two pipes are used alternatively for SH/SC and for charging the decentralized DHW tanks. One decentralized DHW tank, with a capacity of 140 l, is installed in each dwelling. This stored volume allows to cover the DHW users' demand and to manage the tanks charging operations in particular moment of the day. DHW users´ peaks demand generally occur in the early morning (from 6:00 a.m. to 9:00 a.m.) and in the evening (from 5:00 a.m. to 9:00 p.m). For this reason, the DHW tanks charging phase is foreseen in two timeslots of two hours each from 3:00 a.m. to 5:00 a.m. and from 3:00 p.m. to 5:00 p.m. Moreover, the considered DHW tanks charging periods are also periods in which it can be acceptable to disconnect SH/SC system. Regarding the management of DHW charging sequence, the building considered for the CON climate has five floors and two dwellings per floor. In this work it is considered that two DHW tanks are charged at the same time starting with the two placed at the ground floor.

A DHW storage is considered to be charged during the DHW tanks charging phase if:

- the temperature at node 1 of the tank (TT Pink # in Figure 22) is lower than 50°C (the hysteresis varying between 50 and 53°C).

Once a DHW tank is fully charged, the charging of the DHW tank placed at the upper floor starts. This DHW tanks charging phase continues until one of the following conditions is reached:

- All DHW tanks are charged;
- The timeslot for DHW tanks charging ends.

Figure 23 reports the decentralized DHW tanks charging phase. In the same figure, HP and RPW-HEX work in series (scheme SC_4_1).
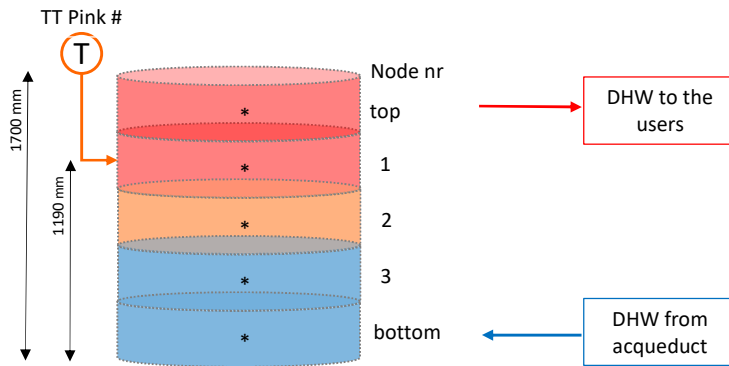
Figure 22 HYBUILD CON system, decentralized DHW tanks scheme, temperature sensor position and geometrical characteristics
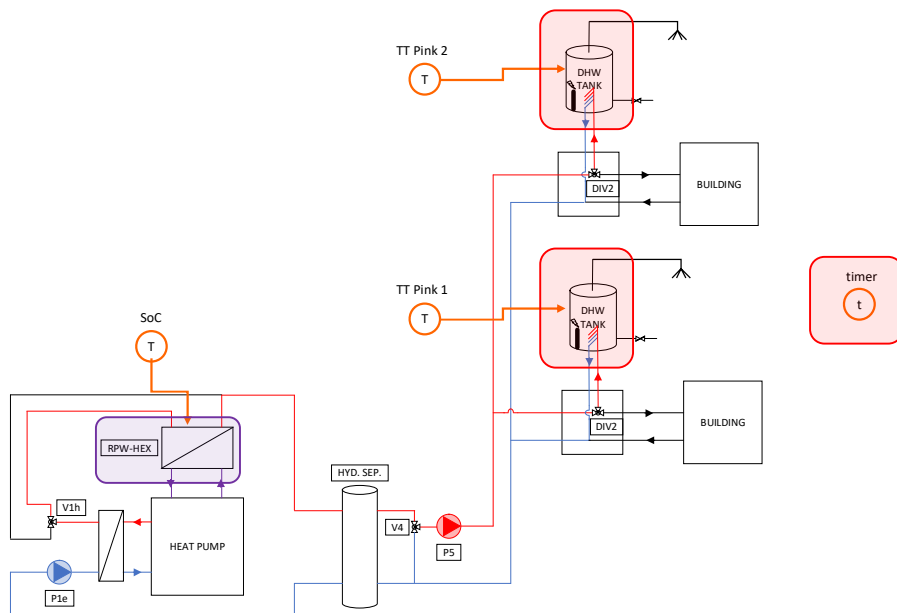
Figure 23 HYBUILD CON system, decentralized DHW tanks charging scheme with HP and RPW-HEX working in series (scheme SC_4_1). System components and sensors used for system control

To ensure DHW at every time to the users, there is an electrical resistance inside each DHW tank that works as back-up element. The activation of the electric back-up occurs if:

- the temperature at node 1 of the tank (see TT Pink # in Figure 22) is lower than 42°C (the hysteresis deadband limits in this case are respectively +3°C and 0°C).

Figure 24 shows the scheme of this operational mode where electrical resistances of the single DHW tanks are activated to ensure the desired temperature inside the storage. Please note that, the management of the back-up element of the specific DHW tank, depends only on the temperature at node 1 (see TT Pink # in Figure 22) of the considered tank. The fact that in Figure 24 both electrical resistances are represented active at the same time is only for the sake of clarity of the figure.
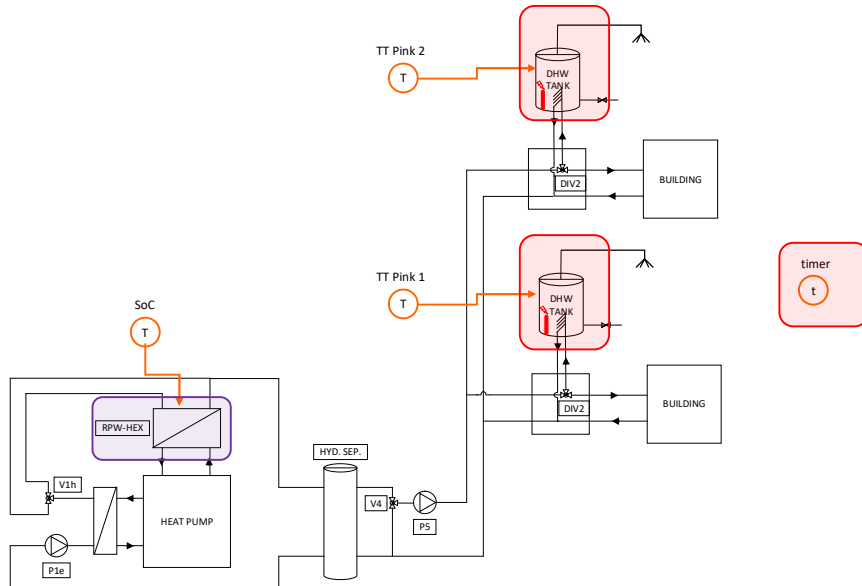
**Figure 24 HYBUILD CON system, decentralized DHW tanks charging scheme with electrical resistances. System components and sensors used for system control**

Electrical system

As for the HYBUILD MED system, also the HYBUILD CON system considers the presence of a PV + BESS system. The three main components are:

- Photovoltaic system (PV) with a total installed power of 10 kWp
- Battery Energy Storage System (BESS) with a total capacity of 15 kWh
- Controller/equipment (CONTRL) to manage the energy flow from PV, to/from Battery, to/from grid.

As can be noticed, the only differences between the HYBUILD MED and CON electrical systems are related to the different sizes of the components. On the other hand, the logics used by the controller to manage the electrical energy fluxes are the same (already reported in section 2.1.1. and shown in Figure 11). It is important to underline that also in this case, only the HP can be powered by the energy coming from the PV+BESS sub-system (see Figure 12) as the considered HP is a DC component. All other auxiliary devices (circulating pumps, electrical resistances in the decentralized DHW tanks) can be powered only using electricity coming from the grid.

2.2 Resume about PIs used to evaluate systems´ performance (from D1.3)

Performance Indicators (PIs) define useful quantities that allow evaluation of the system with respect to different objectives (performance, comfort, healthiness and cost). These quantities are explained in detail in D1.3 [5]. Here, PIs provide a first evaluation of the two HYBUILD systems. They will be used in future also as benchmark to evaluate the validity of different developed optimised control strategies. Different PIs, for different control volumes (CV) at sub-system level (L2) and overall building system level (L3) have been identified to allow a complete evaluation of the system.

Although the PIs defined in D1.3 are used to evaluate both HYBUILD MED and CON system performance, for the sake of clarity, here they are presented separately (for the two HYBUILD system, MED and CON). In this way, the specific CV and the various contributions taken into account are more clear for the reader. For this reason, in the following, section 0 presents the PIs used to evaluate performance of the HYBUILD MED system, while section 2.2.2 reports the

PIs used to evaluate performance of the HYBUILD CON system. On the other hand, being the control volume, the contributions and the concept of the electrical part of both systems basically the same, section 2.2.3 reports the PIs used to evaluate the performance of electrical part (valid for MED and CON system).

It is here important to add a specification about the calculation of the index Self-sufficiency. In the HYBUILD systems (both for the MED and CON climates), the PV+BESS sub-system is only connected to the compression chiller/heat pump compressor, as this device is fed by DC current. In this view, it is considered more appropriate to evaluate the aforementioned PI considering only the load that can be effectively powered by the PV+BESS sub-system, excluding the electrical consumption of auxiliary elements (as circulating pumps) as they are only connected to the AC grid.

2.2.1 Mediterranean system' PIs

Sub-system level (L2)

Thermal Seasonal Energy Efficiency Ratio ($SEER_{th}$)

$SEER_{th}$ characterizes energy performance of a sub-system and it is defined as the ratio of energy produced over energy required. In the case of the adsorption chiller sub-system energy required is thermal energy. Formula and conceptual scheme of this PI are reported below and in Figure 25.

$$SEER_{th,ADS,CV1} = \frac{Q_{chilled\ water}}{Q_{hot\ source}}$$
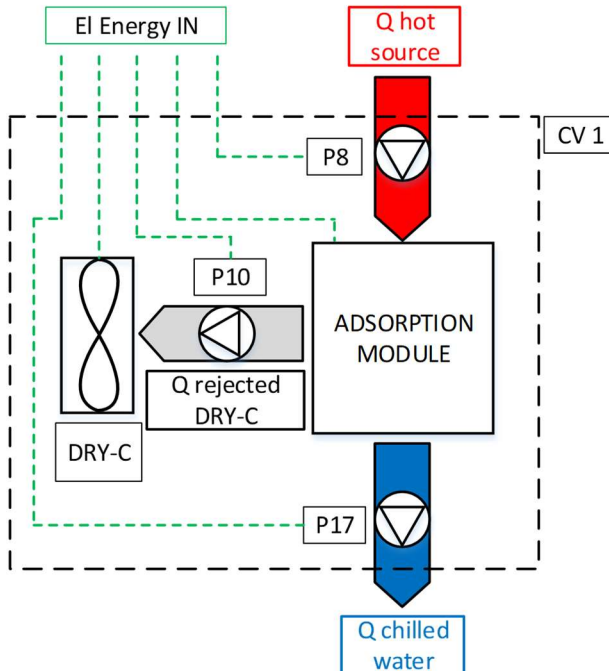
Figure 25 HYBUILD MED system, scheme for the evaluation of adsorption chiller performance

Where $Q_{chill\ water}$ is the thermal energy of the chilled water circuit that goes to the condenser of the compression chiller, while $Q_{hot\ source}$ is the thermal energy used by the machine.

Electric Seasonal Energy Efficiency Ratio ($SEER_{el}$)

The $SEER$ is used also to evaluate a device performance with respect to the consumption of electricity. In the specific, this PI is applied to the compression chiller. It is however important to consider the chiller performance in the two working modes: when it is connected to the adsorption chiller and when it is directly connected to the dry cooler. These two operational modes must be evaluated separately because different components have to be taken into account. In addition to these two $SEER_{el}$ ($SEER_{HP,CV2}$ and $SEER_{HP,CV}$), a third one represents the overall (global) performance of the chiller in the two modalities along the year ($SEER_{HP,CV3}$). In the following, the various equations used to evaluate the various $SEER$ are presented, while Figure 26, Figure 27 and Figure 28 show the schematic of the respective operative modes.

Compression chiller $SEER_{el}$ with adsorption chiller is

$$SEER_{HP,CV2} = \frac{Q_{ref} + Q_{direct\ cooling}}{El\ Energy\ IN}$$
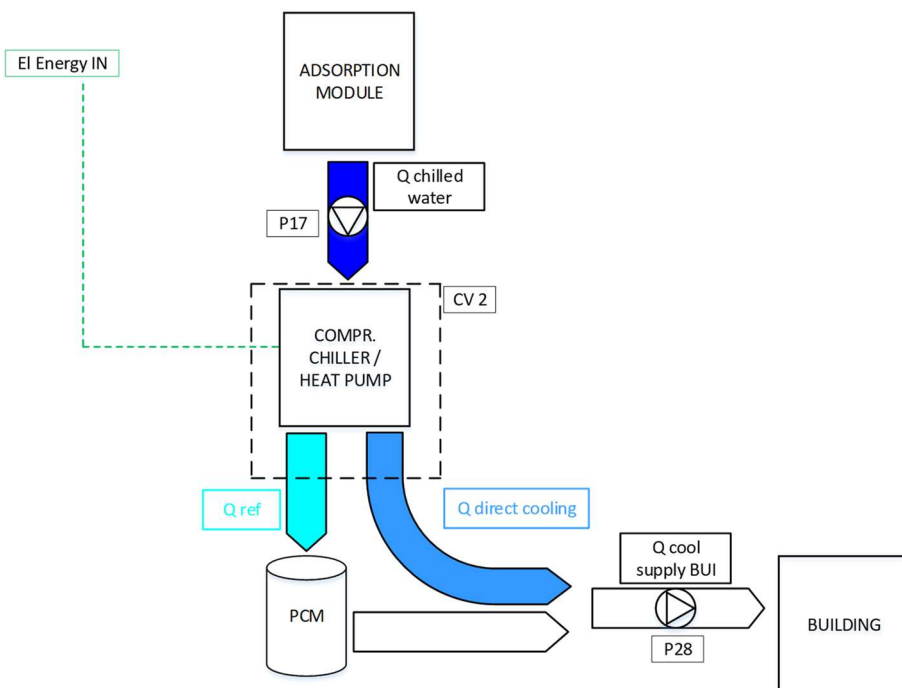
Figure 26 HYBUILD MED system, scheme for the evaluation of compression chiller performance (when it operates coupled with adsorption module)

Where Q_{ref} is the thermal energy that goes to the PCM storage and $Q_{direct\ cooling}$ is the thermal energy that goes directly to the building (using the standard evaporator). These two contributions are here evaluated with compression chiller that works coupled with adsorption module. In addition to that, $El\ Energy\ IN$ represents, in this case, only the energy consumed by the compressor.

Compression chiller $SEER_{el}$ without adsorption chiller is

$$SEER_{HP,CV} = \frac{Q_{ref} + Q_{direct\ cooling}}{El\ Energy\ IN}$$
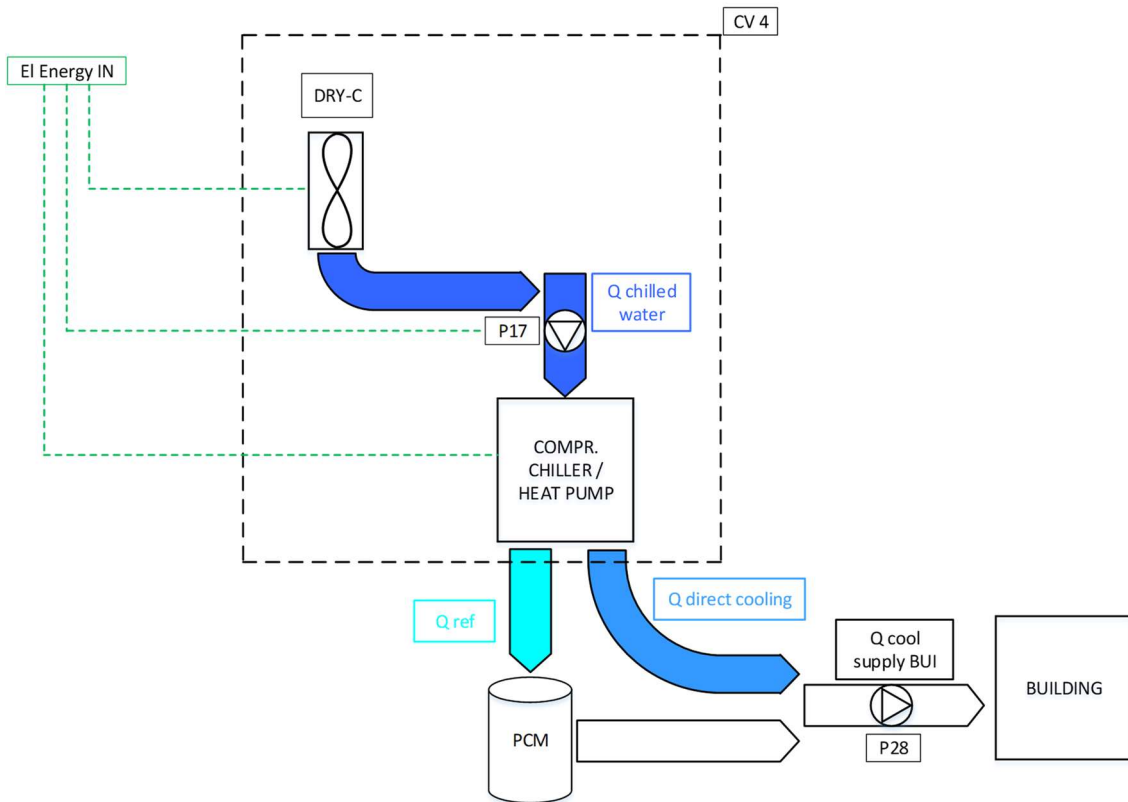
Figure 27 HYBUILD MED system, scheme for the evaluation of compression chiller performance (when it operates without adsorption module)

Where Q_{ref} is the thermal energy that goes to the PCM storage and $Q_{direct\ cooling}$ is the thermal energy that goes directly to the building (using the standard evaporator). These two contributions are here evaluated with compression chiller that works directly connected to the dry cooler. In addition to that, $El\ Energy\ IN$, in this working mode, besides the compressor electrical consumption, includes also the energy to run the dry cooler and the pump P17 when the compression chiller is directly connected to the dry cooler.

Compression chiller $SEER_{el}$ global is

$$SEER_{HP,CV3} = \frac{Q_{ref} + Q_{direct\ cooling}}{El\ Energy\ IN}$$
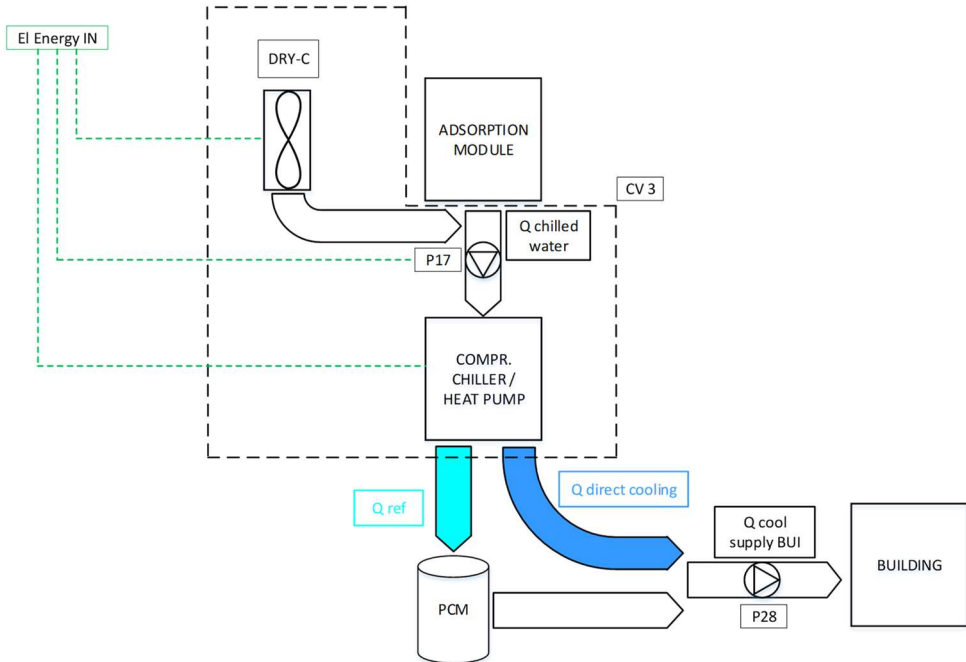
**Figure 28 HYBUILD MED system, scheme for the evaluation of compression chiller performance (global evaluation)**

Where Q_{ref} is the thermal energy that goes to the PCM storage and $Q_{direct\ cooling}$ is the thermal energy that goes directly to the building (using the standard evaporator). These two contributions are here evaluated with compression chiller that works both coupled with adsorption module and also directly connected to the dry cooler. In addition to that, $El\ Energy\ IN$, besides the compressor electrical consumption when the compressor chiller works coupled with adsorption module and also when it works directly connected to the dry cooler, includes the energy to run the dry cooler and the pump P17 when the compression chiller is directly connected to the dry cooler.

Overall building system (L3)

Annual building space heating and space cooling energy demands

Two of the most important values generally used to assess thermal properties of a building are the building space heating and space cooling energy demands. Space heating and space cooling energy demands represent the amount of energy needed to ensure that indoor temperature is maintained in a certain range (between 20°C and 25°C) along the whole year. With these two values, and knowing the boundary conditions considered (as, for example, climatic data of the considered location and internal gains contribution to the energy balance of the building), it is possible also to extrapolate indications about building envelope performance. In this section these values are evaluated over a period of one year.

Electric and thermal Seasonal Performance Factor (SPF)

Electric and thermal Seasonal Performance Factor (SPF_{el} and SPF_{th}) are PIs used to evaluate global system energy performance. Their definitions are reported below, while Figure 29 and Figure 30 show graphically the various electrical and thermal contributions considered in the respective equations.

System SPF_{el} is

$$SPF_{el,CV7} = \frac{Q_{cool\ supply\ BUI}}{El\ Energy\ IN}$$
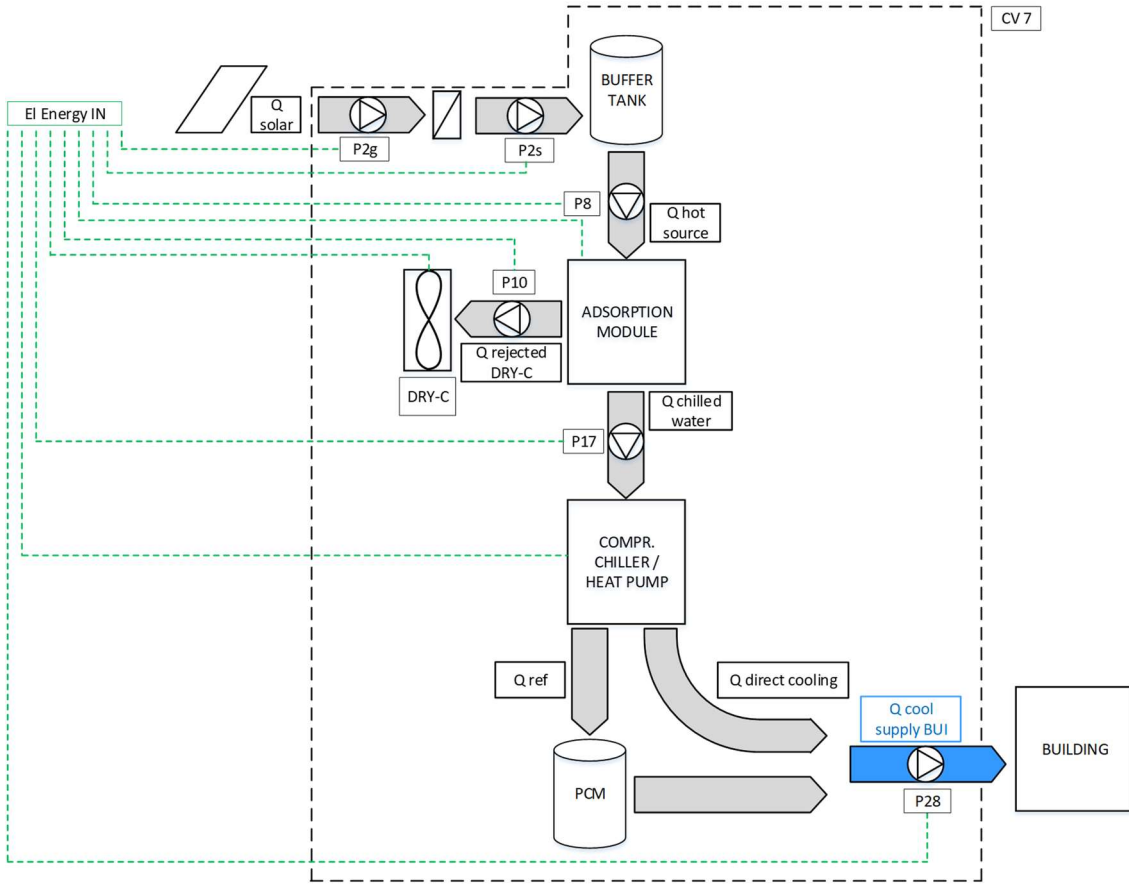
Figure 29 HYBUILD MED system, scheme for the evaluation of system SPF$_{el}$

Where $Q_{cool\ supply\ BUI}$ represents the overall cooling thermal energy supplied to the building whereas $El\ Energy\ IN$ takes into account all electrical energy contributions: electricity consumed by the adsorption machine, by the dry cooler, by the heat pump compressor, by the pump P2g, P2s and P8 of the adsorption hot circuit, by the pump P17 of the adsorption chilled circuit, by the pump P10 of the adsorption cooled circuit, by the pump P28 of the distribution circuit.

$$El\ Energy\ IN = Q_{el,ADS} + Q_{el,DRY-C} + Q_{el,HP} + Q_{el,P2g\ for\ ADS} + Q_{el,P2s\ for\ ADS} + Q_{el,P8} + Q_{el,P10} + Q_{el,P17} + Q_{el,P28}$$

Although it is not represented in Figure 29, thermal energy entering the buffer tank is not only used as heat source for the adsorption machine but also for space heating through free heating mode and DHW production. To correctly account the electrical energy spent by P2g and P2s for running the adsorption machine, their contributions are multiplied for the share of thermal energy used for cooling purpose.

System SPF_{th} is

$$SPF_{th,CV8} = \frac{Q_{cool\ supply\ BUI}}{Q_{hot\ source}}$$
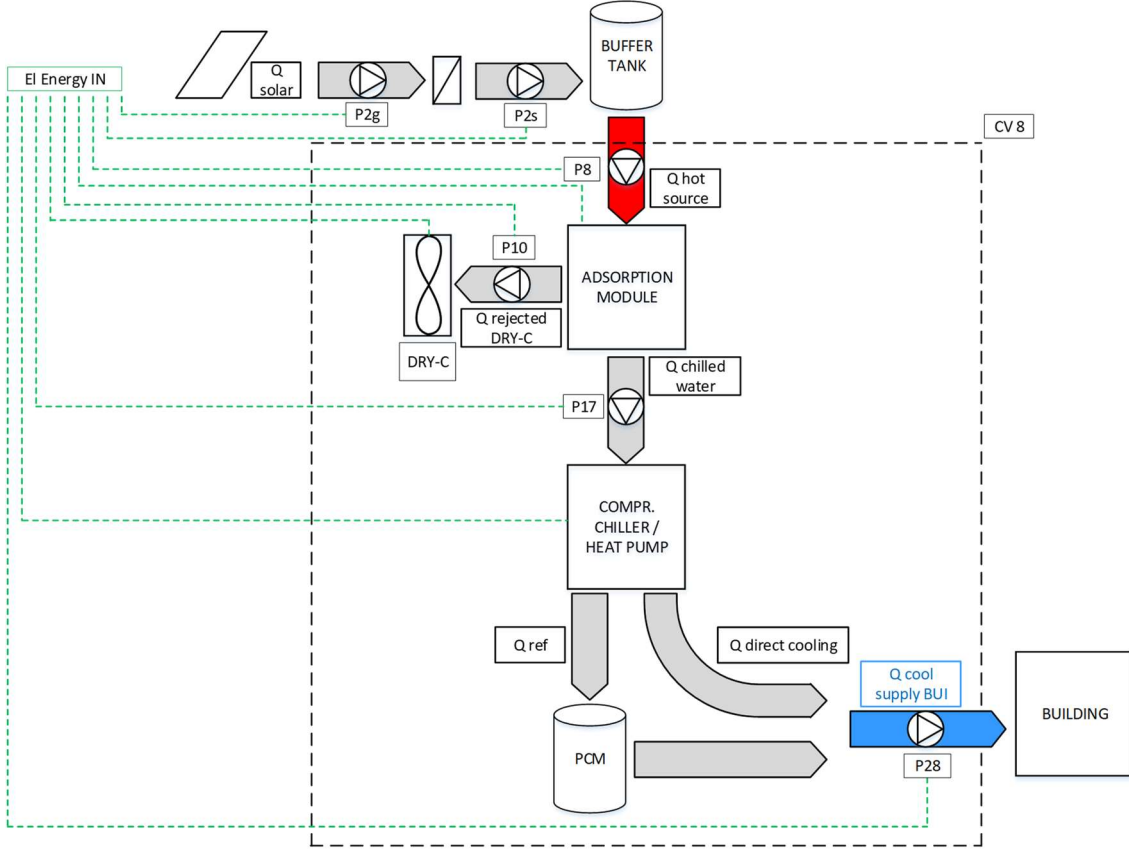
Figure 30 HYBUILD MED system, scheme for the evaluation of system SPF$_{th}$

Where $Q_{cool\ supply\ BUI}$ represents cooling thermal energy supplied to the building whereas $Q_{ho\ source}$ takes into account thermal energy spent to run the adsorption module.

Solar and auxiliary element energy contributions for DHW production

One of the peculiarities of HYBUILD MED system is the possibility to cover part of DHW demand using the thermal energy captured by solar thermal system. For this reason, it is considered useful to present some results in terms of energy contributions, from solar system and from auxiliary element (the auxiliary element foreseen is an electrical resistance inside the DHW tank), to the DHW production. Figure 31 shows the CV considered for this analysis and the energy fluxes entering and exiting the DHW tank. Solar and auxiliary contributions to DHW production are evaluated with a monthly and yearly time frame. In addition to the yearly solar contribution to DHW production, the monthly analysis allows to evaluate in more detail the two contributions along the year, highlighting months in which the auxiliary element is never activated and months in which it represents the main contribution to DHW production.
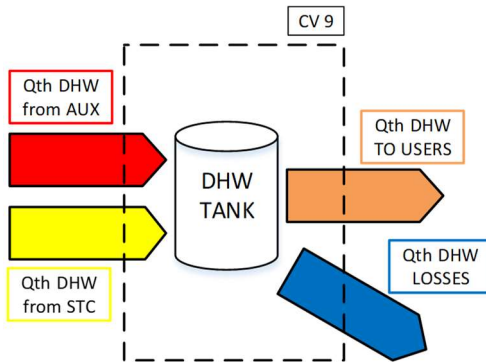
Figure 31 HYBUILD MED system, scheme for the evaluation of solar and auxiliary contributions to DHW production

***Solar and heat pump energy contributions for space heating demand covering***

Another important characteristic of HYBUILD MED system, as already mentioned, is the possibility to exploit thermal energy captured by solar thermal system to cover part of the space heating demand of the building. As for the evaluation of solar energy contribution to DHW production, also in this case, results are reported in terms of energy contributions, from solar system and from heat pump, for space heating demand covering. Also in this case, the evaluation is performed with monthly and yearly time frame. This allows to have an overall yearly estimation about solar contribution to space heating but also a more detailed analysis about the two contributions along the months, highlighting how the solar contribution varies from coldest months of winter period (December, January, February) to more temperate ones (March, April). Figure 32 shows the considered CV for this analysis, as well as the two contributions for space heating demand covering.
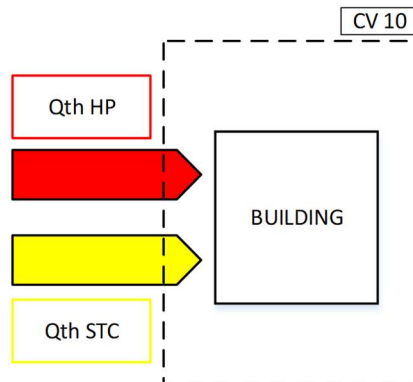
Figure 32 HYBUILD MED system, scheme for the evaluation of solar and auxiliary contributions to space heating

Final Energy use (FE)

As reported in D1.3 [5], Final Energy use is a PI that gives indications about overall energy consumption of the specific energy vector considered in a system. For electricity driven systems (as HYBUILD MED system), Final Energy use equals the electricity used to drive the HVAC system. For a more useful evaluation, in addition to overall value, Final Energy use is also divided in Final Energy use for space heating, space cooling and DHW use.

2.2.2   Continental system´ PIs

Sub-sytem level (L2)

Seasonal Coefficient Of Performance $(SCOP)$ ***and Seasonal Energy Efficiency Ratio*** $(SEER)$

$SCOP$ (Seasonal Coefficient Of Performance) and $SEER$ (Seasonal Energy Efficiency Ratio) are the PIs used to characterize energy performance of the HP in heating and cooling operation. Moreover, two different $SCOP$ are evaluated for space heating and DHW tank charging operational modes to evaluate HP performance in the specific heating scheme. Formula and conceptual scheme of these PIs are reported below and in Figure 33,Figure 34 and Figure 35.

Seasonal Coefficient Of Performance in space heating mode ($SCOP_{SH}$):

$$SCOP_{SH,CV\ HP} = \frac{Q_{th,space\ heating}}{El\ Energy\ IN}$$
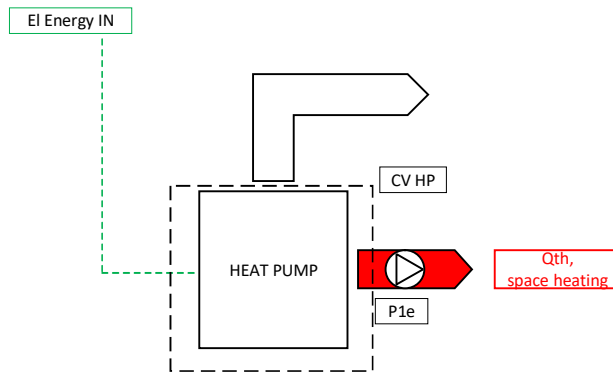
Figure 33 HYBUILD CON system, scheme for the evaluation of HP SCOP in SH mode

Where $Q_{th,space\ heating}$ is, in this case, the thermal energy for space heating exiting the HP, while $El\ Energy\ IN$ represents, in this case, the electrical energy consumed by the compressor of the HP for space heating.

Seasonal Energy Efficiency Ratio in space cooling mode ($SEER_{SC}$):

$$SEER_{SC,CV\ HP} = \frac{Q_{th,space\ cooling}}{El\ Energy\ IN}$$
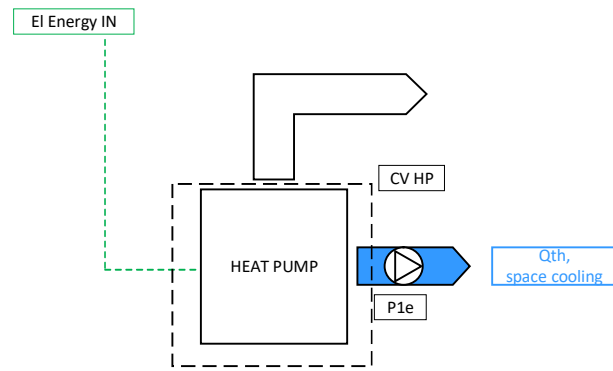
Figure 34 HYBUILD CON system, scheme for the evaluation of HP SEER in SC mode

Where $Q_{th,space\ cooling}$ is, in this case, the thermal energy for space cooling exiting the HP, while $El\ Energy\ IN$ represents, in this case, the electrical energy consumed by the compressor of the HP for space cooling.

Seasonal Coefficient Of Performance in DHW tanks charging mode ($SCOP_{DHW}$):

$$SCOP_{DHW,CV\ HP} = \frac{Q_{th,DHW}}{El\ Energy\ IN}$$
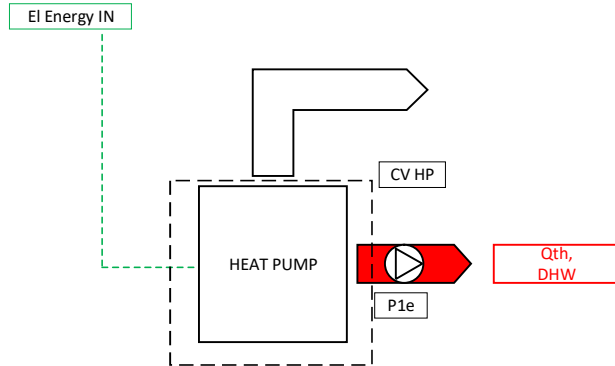
Figure 35 HYBUILD CON system, scheme for the evaluation of HP SCOP in DHW mode

Where $Q_{th,DHW}$ is, in this case, the thermal energy for decentralized DHW tanks charging exiting the HP, while $El\ Energy\ IN$ represents, in this case, the electrical energy consumed by the compressor of the HP for decentralized DHW tanks charging.

Overall building system (L3)

Annual building space heating and space cooling energy demands

As already presented for the MED case, also for the CON one, space heating and space cooling demands are used to characterize the building. Also in this case, space heating and space cooling energy demands represent the amount of energy needed to ensure that indoor temperature is maintained in a certain range (between 20°C and 25°C) along the whole year. With these two values, and knowing the boundary conditions considered (as, for example, climatic data of the considered location and internal gains contribution to the energy balance of the building), it is possible also to extrapolate indications about building envelope performance. In this section, these values are evaluated over a period of one year.

Electric Seasonal Performance Factor (SPF)

For evaluation of HYBUILD CON system performance at overall building system level (L3) one of the used PIs is the electric Seasonal Performance Factor (SPF). As done for the HYBUILD CON system performance at sub-system level, also in this case, different SPF are calculated for space heating, space cooling and DHW tanks charging operational modes. The definitions of the considered SPF are reported below, while Figure 36, Figure 37 and Figure 38 show the considered control volumes, thermal and electrical contributions in the various cases.

Seasonal Performance Factor for space heating (SPF$_{SH}$):

$$SPF_{SH,CV\ SYS\ SH} = \frac{Q_{th,space\ heati}}{El\ Energy\ IN}$$
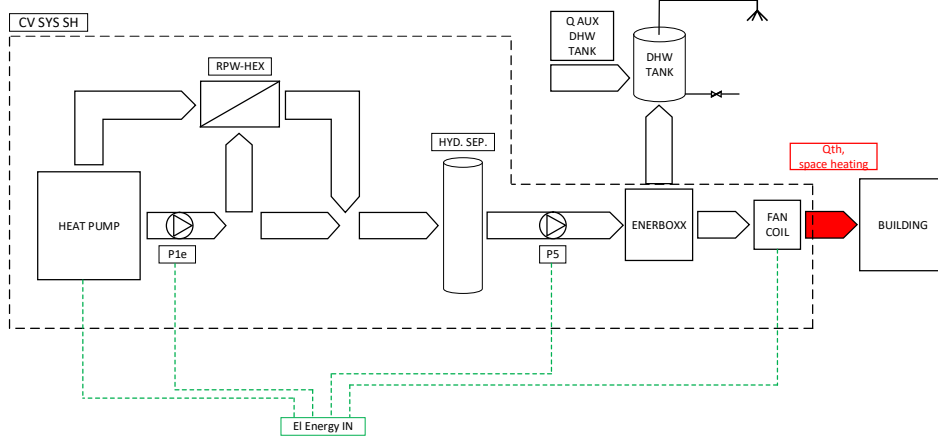
Figure 36 HYBUILD CON system, scheme for the evaluation of system SPF in SH mode

Where $Q_{th,space\ heating}$ is, in this case, the thermal energy for space heating distributed by emission units to the building, while $El\ Energy\ IN$ represents, in this case, the electrical consumption in space heating mode of HP compressor, circulating pumps P1e and P5 and electricity consumption of the various fan coils in the dwellings.

Seasonal Performance Factor for space cooling (SPF$_{SC}$):

$$SPF_{SC,CV\ SYS\ SC} = \frac{Q_{th,space\ cooling}}{El\ Energy\ IN}$$
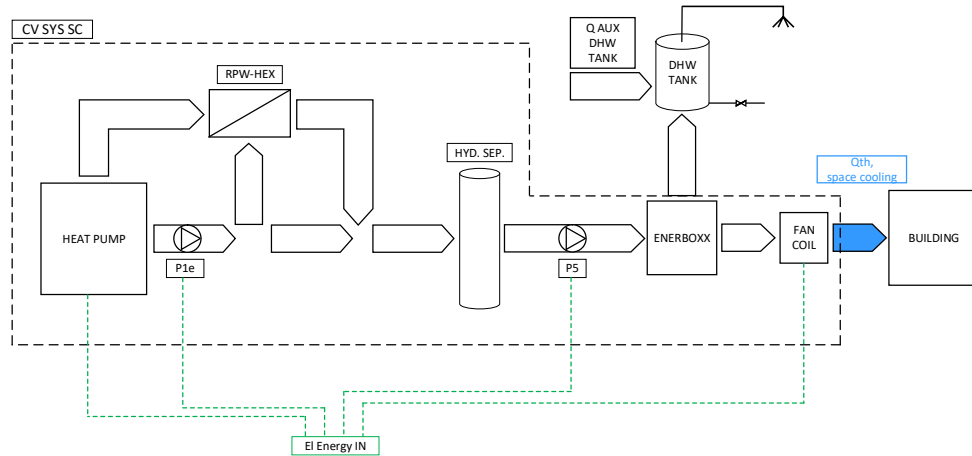
Figure 37 HYBUILD CON system, scheme for the evaluation of system SPF in SC mode

Where $Q_{th,space\ cooling}$ is, in this case, the thermal energy for space cooling distributed by emission units to the building, while $El\ Energy\ IN$ represents, in this case, the electricity consumption in space cooling mode of HP compressor, circulating pumps P1e and P5 and electricity consumption of the various fan coils in the dwellings.

Seasonal Performance Factor for DHW tanks charging mode (SPF$_{DHW}$):

$$SPF_{DHW,CV\ SYS\ DHW} = \frac{Q_{th,DHW}}{El\ Energy\ IN}$$
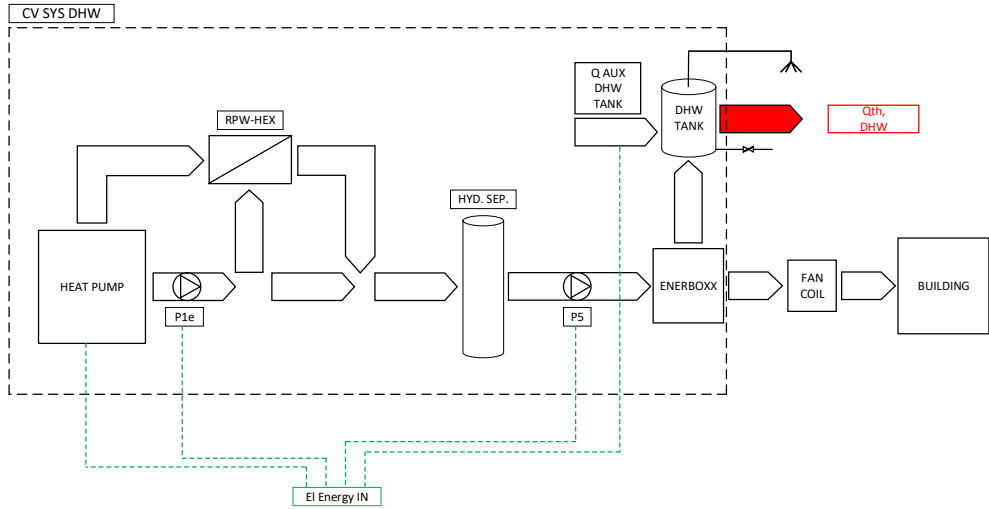
Figure 38 HYBUILD CON system, scheme for the evaluation of system SPF in DHW tanks charging mode

Where $Q_{th,DHW}$ is, in this case, the DHW thermal energy provided to the users, while $El\ Energy\ IN$ represents, in this case, the electricity consumption in decentralized DHW tanks charging mode of HP compressor, circulating pumps P1e and P5 and also the electricity consumption of the electrical resistances inside the decentralized DHW tanks.

Final Energy use (FE)

As reported in D1.3 [5] (and also in section 0) Final Energy use (*FE*) is a PI that gives indications about overall energy consumption of the specific energy vector considered in a system. For electricity driven systems (as HYBUILD CON system), Final Energy use equals the electricity used to drive the HVAC system. For a more useful evaluation, in addition to overall value, Final Energy use is also divided in Final Energy use for space heating, space cooling and DHW use.

2.2.3 Electrical sub-system PIs (for both MED and CON system)

Overall building system level (L3)

Self-consumption ($Sc_{(el)}$)

Self-consumption ($Sc_{(el)}$) is a PI that represents the fraction of energy produced by the photovoltaic system and directly consumed by the load or stored into the battery, with respect to the total PV production. Although this index is generally expressed with a yearly time frame, in this work, also a monthly evaluation is reported. This allows to investigate possible fluctuations and differences along the year. The formula adopted and a conceptual scheme for this PI are reported below and in Figure 39.

$$Sc_{(el)} = \frac{E_{RES\ (el)}}{E_{RE\quad (el)}}$$
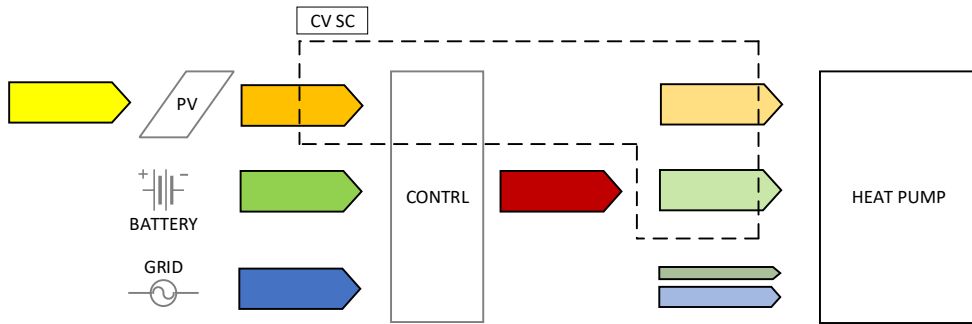
Figure 39 Scheme for Sc(el) evaluation. The coloured arrows have the following significance: yellow: solar radiation on PV modules, orange: energy produced by PV modules, green: energy from battery, blue: energy from grid, dark red: energy to the load (equal to load demand). The light arrows on the right are used to highlight PV, battery and grid contribution to the energy sent to the load. In the bottom right the energy coming from the grid is split into two contributions: renewable (dark green) and non-renewable (blue)

Where $E_{RES\,(el)}$ is the energy produced by PV and directly consumed by the load or stored into the battery, while $E_{RES-TOT\,(el)}$ represents the total PV production.

Self-sufficiency ($SS_{(el)}$)

Self-sufficiency ($SS_{(el)}$) is a PI that represents the fraction of energy produced by PV and directly consumed by the load or stored into the battery, with respect to the total load demand. As for Self-consumption, this index is generally expressed with a yearly time frame. In this work, also a monthly evaluation is reported to allow a more detailed investigation about possible fluctuations and differences along the year. Formula and conceptual scheme of this PI are reported below and in Figure 40.

$$SS_{(el)} = \frac{E_{RES\,(el)}}{E_{D\,(el)}}$$
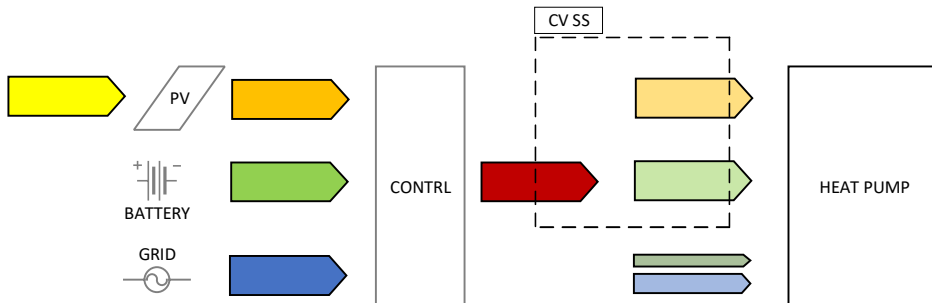
Figure 40 Scheme for SS(el) evaluation. The coloured arrows have the following significance: yellow: solar radiation on PV modules, orange: energy produced by PV modules, green: energy from battery, blue: energy from grid, dark red: energy to the load (equal to load demand). The light arrows on the right are used to highlight PV, battery and grid contribution to the energy sent to the load. In the bottom right the energy coming from the grid is split into two contributions: renewable (dark green) and non-renewable (blue)

Where $E_{RES\,(el)}$ is the energy produced by PV and directly consumed by the load or stored into the battery, while $E_{D\,(el)}$ represents the total load demand (heat pump electrical consumption).

Share of renewables ($SR_{(el)}$)

Share of renewables ($SR_{(el)}$) is PI similar to Self-sufficiency, but in this case also the renewable energy fraction of the energy taken from the grid is considered in the calculations. The index represents the fraction between the overall renewable energy consumed (coming from PV+BESS sub-system, plus the renewable part of the electricity coming from the grid) and the total demand. The Share of renewables PI has been calculated also considering the consumption of the auxiliaries. It is important to note that the renewable fraction of energy coming from the

grid is evaluated referring to the energy mix of the considered country (Greece for MED climate and Germany for CON climate) for the year 2019 available in [8]. In this case, only the yearly value of the index is elaborated as the renewable fraction in the energy mix of the considered country is an annual value. Formula and conceptual scheme of this PI are reported below and in Figure 41.

$$SR_{(el)} = \frac{E_{RES*\,(el)}}{E_{D\,(el)}}$$
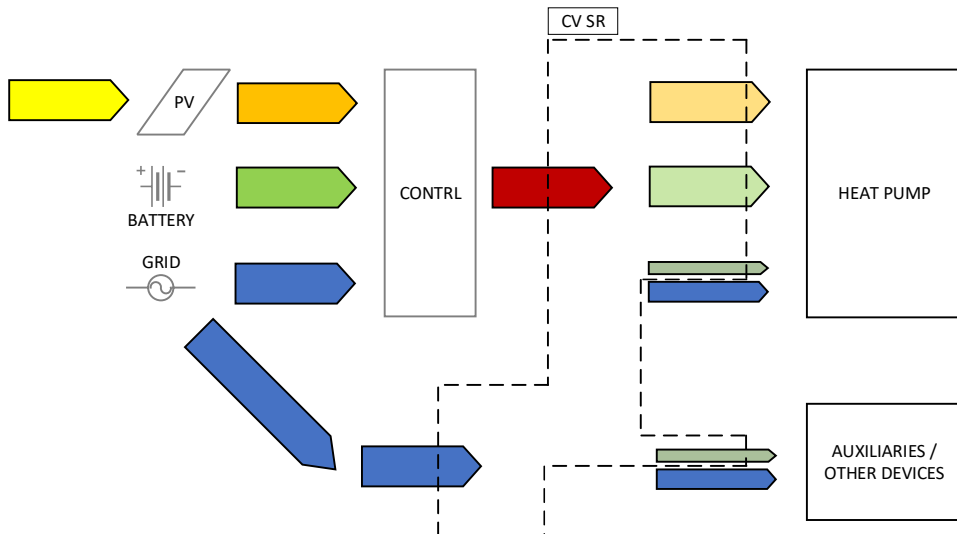
Figure 41 Scheme for SR(el) evaluation. The coloured arrows have the following significance: yellow: solar radiation on PV modules, orange: energy produced by PV modules, green: energy from battery, blue: energy from grid, dark red: energy to the load (equal to load demand). The light arrows on the right are used to highlight PV, battery and grid contribution to the energy sent to the load. In the bottom right the energy coming from the grid is split into two contributions: renewable (dark green) and non-renewable (blue)

Where $E_{RE\,*\,(el)}$ is the energy produced by PV and directly consumed by the load or stored into the battery plus the renewable energy fraction coming from the grid, while $E_{D\,(el)}$ represents, in this case, the total energy demand (heat pump electrical consumption plus the consumption of all auxiliaries).

3 Dynamic simulations results

3.1 Mediterranean system

This section reports results from TRNSYS simulations of HYBUILD MED system in the specific correspondent building (a SFH in the MED climate with the reference city of Athens) considering the control logics extensively explained in D4.2 [2]. The results are reported in terms of the above mentioned and explained PIs.

Sub-system level (L2) analysis

Adsorption chiller

According to what already presented in section 0, the thermal Seasonal Energy Efficiency Ratio $SEER_{th}$ is used to characterize adsorption chiller performance. According to the formula already presented in section 0, the value of this PI is reported below.

$$SEER_{th,ADS,CV1} = 0.57$$

This value is slightly lower than what reported in the datasheet of the device (up to 0.65), nevertheless is in good agreement with results from laboratory test of the considered machine (0.55).

Compression chiller

As expected, compression chiller performance described in terms of $SEER$ is better when condenser is fed by water coming from adsorption module at around 20°C rather than when connected directly to the dry cooler that works at ambient air temperature, generally higher when space cooling is needed. As explained above, three different $SEERs$ are defined to correctly evaluate performance of the machine in different conditions. Results are reported below.

$SEER_{el}$*with adsorption chiller*

$$SEER_{HP,CV2} = 4.6$$

In addition to the Seasonal Energy Efficiency Ratio that gives a global evaluation about compression chiller performance along the whole cooling season in the considered mode, in Figure 42, a more specific analysis is reported for Athens ref. building. In this case, EER is plotted against $T_{wc,in}$ that represents the temperature of the cold source on the condenser side when compression chiller works coupled with adsorption module. Theoretically there are three possible operational modes that foresee the work of the two devices in series: SC3b, SC4b, SC6b. These schemes are widely explained in D4.2 [2], however, below, a short recap is considered useful for the reader. SC3b is the scheme that considers the by-pass of the PCM storage and the direct connection between the compression chiller and the distribution circuit (blue and red dotted lines in Figure 6), while SC4b is the scheme in which the compression chiller, working in series with the adsorption module, only charge the PCM storage. Last, SC6b foresees the use of compression chiller, working also in this case in series with adsorption module, to charge the PCM storage and, at the same time the PCM storage is also discharged by the user that is requiring space cooling. It is useful here also to remind the significance of letter "b" present in all the mentioned schemes. Letter "b" refers to the operational modes in which compression chiller and adsorption module work in series. On the contrary, letter "a" used at the end of the scheme name indicates the same operational mode, but with the compression chiller directly connected to the dry cooler and working as a classical air to water unit. For the sake of simplicity, considering that working mode SC3b is never activated, it is not considered in this analysis.

As expected, moving from lower $T_{wc,in}$ to higher ones the EER decreases. Following the defined control strategies, outlet temperature from the chilled side of the adsorption chiller is set at 20°C and, as can be seen in Figure 42, Figure 43 and Figure 44, the density of points around 20°C and, consequently, the percentage of time in which compression chiller works in this condition is above 90%. However, in less than 10% of the total running time, the temperature at the condenser side of compression chiller ranges between 20 and 38°C.

Compression chiller EER at different condenser inlet temperature
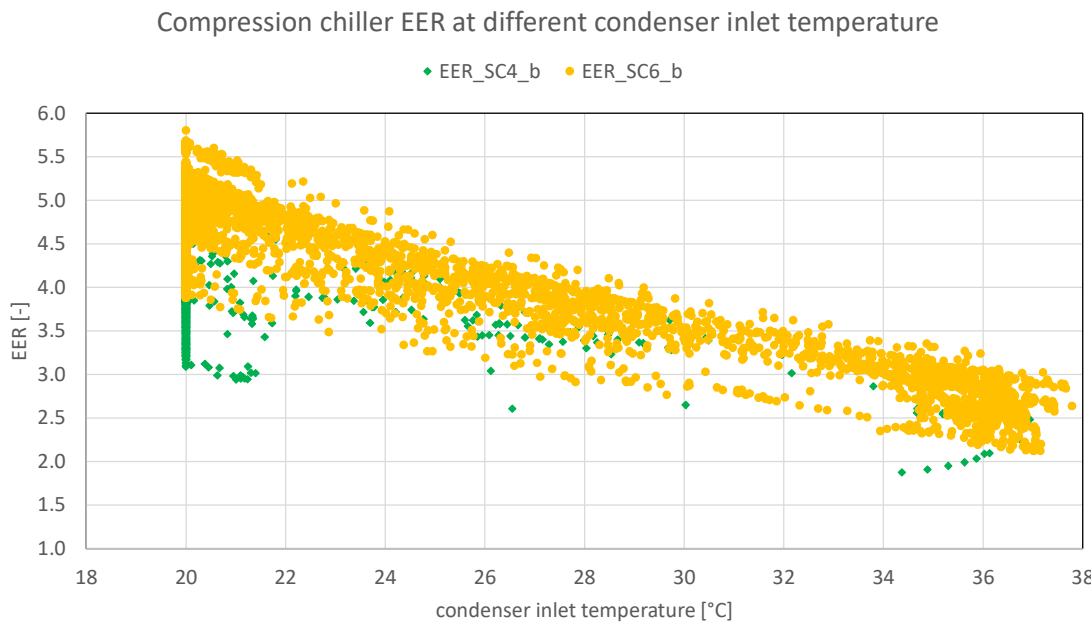
Figure 42 Compression chiller EER at different condenser inlet temperature in schemes SC4b and SC6b

Going into more detail, it can be noted as the temperature at the condenser side is not the only variable affecting the EER. In fact, influences on the EER are observed also by plotting EER with respect to the evaporator side temperature (in this case, considering that evaporator side is always connected to PCM storage the temperature considered is T_{PCM}). As it can be seen in Figure 43 and Figure 44, three different almost parallel EER trends are visible for three different T_{PCM} ranges. As expected EER decreases lowering T_{PCM} because more electrical power is needed to reach lower temperatures. However, the lowest $EERs$ obtained with the coldest T_{PCM} (between 0-2°C) and characterized by dark green (Figure 43) or gold (Figure 44) squares, have low incidence on the global performance because, for most of the time, compression machine does not work in these conditions but instead with a T_{PCM} in the range of 4-6°C. This fact is highlighted by the percentages of time worked with different T_{PCM} and $T_{wc,in}$ ranges shown using columns in Figure 43 and Figure 44.

Compression chiller EER at different condenser inlet temperature
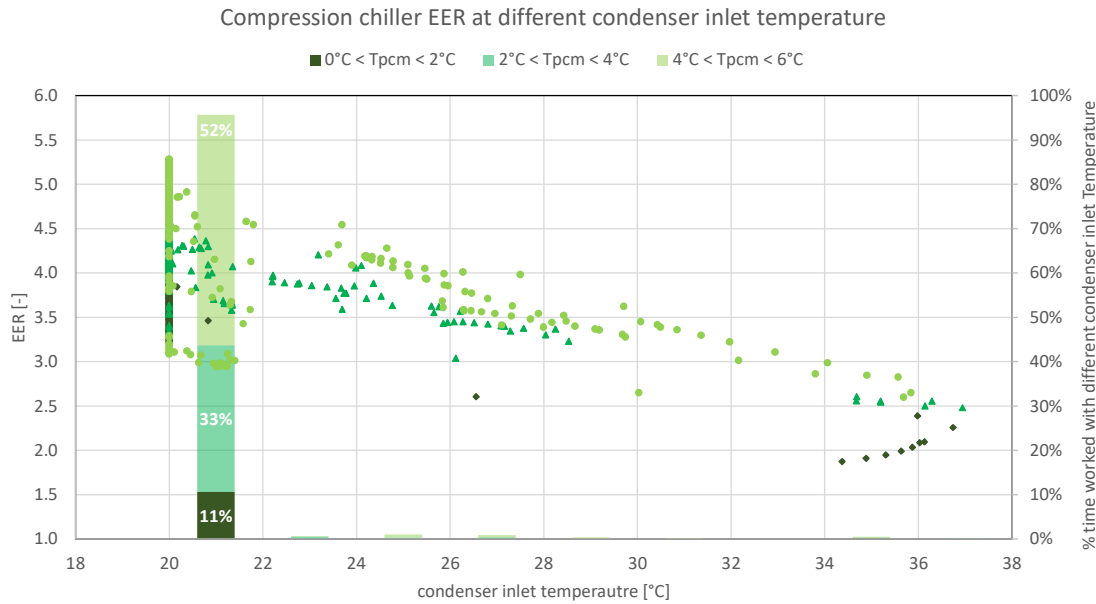
Figure 43 Compression chiller EER against condenser inlet temperature in schemes SC4b for different T$_{pcm}$ and percentage of time worked with different condenser inlet temperature and different T$_{pcm}$ ranges (secondary vertical axis)

Compression chiller EER at different condenser inlet temperature
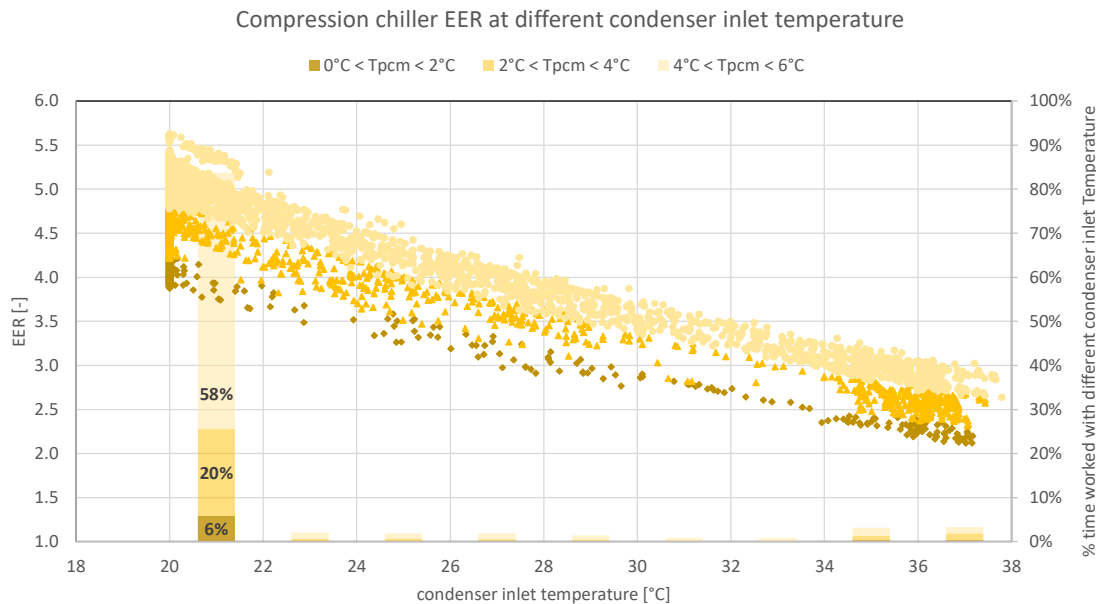
Figure 44 Compression chiller EER against condenser inlet temperature in scheme SC6b for different T$_{pcm}$ and percentage of time worked with different condenser inlet temperature and different T$_{pcm}$ ranges (secondary vertical axis)

$SEER_{el}$ *without adsorption chiller*

$$SEER_{HP,CV2} = 3.1$$

The same analysis presented in the previous section has been performed also for the case in which the condenser side of compression machine is directly connected to the dry cooler. This analysis allows, as previously, to have a more detailed comprehension about compression chiller performance using $SEER_{HP,CV2}$ that gives indications about performance of the machine when working directly connected to dry cooler over the whole cooling season.

Figure 45 shows the compression machine EER plotted against temperature on the condenser side that, in this case, is represented by ambient air temperature (WEA_TAMB). As for the operation with adsorption module, also in this case, theoretical, there are three possible operational modes where the compression chiller is directly connected to the dry cooler (SC3a, SC4a, SC6a). For the sake of simplicity, considering that also scheme SC3a (that is the direct cooling from the compression chiller to the building bypassing the PCM storage) is never activated, the operative points reported in Figure 45 represent only the relation between EER and WEA_TAMB in scheme SC4a (blue squares) and in scheme SC6a (red triangles). Both schemes SC4a and SC6a are meant to charge the PCM storage when it is empty and at the same time adsorption module cannot work. More specifically, SC4a activation occurs if, in addition to PCM storage condition, contemporaneously, space cooling demand is not present, while SC6a is activated when, at the same time, space cooling demand is identified, hence, the PCM storage is at the same time charged and discharged. The first considerations that follow are valid for both SC4a and SC6a, while the slightly difference in terms of EER will be explained at the end of this part.

As expected, moving from low WEA_TAMB to higher ones the EER decreases. In this case, however, contrarily to what occurs with adsorption chiller, $T_{wc,in}$ is not fixed and is instead strictly related to WEA_TAMB and to the dry cooler control. For simulations, the dry cooler water outlet temperature is defined as follows:

$$T_{wc,in} = WEA\_TAMB + 2.3$$

Where:
- $T_{wc,in}$ is the outlet temperature from dry cooler and inlet in the condenser side of the compression machine [°C];
- WEA_TAMB is the ambient air temperature (that constitutes the lower limit for $T_{wc,in}$) [°C];
- 2.3 is a fixed ΔT suggested by the dry cooler data sheet [°C].

As Figure 45, Figure 46 and Figure 47 show, for most of the time in which compression chiller works in "schemes_a" (SC4a, SC6a), WEA_TAMB is between 20 and 38 °C, therefore $T_{wc,in}$ is in the range of around 22- 40 °C. Being this temperature higher with respect to $T_{wc,in}$ in SC4b and SC6b (that for most of the time is 20°C as shown in Figure 43 and Figure 44), the resulting EER is, as expected, lower because more electrical energy is used by compressor to obtain the same cooling effect on the evaporator side.

Another variable that strongly affects the EER is, also in this case, T_{pcm}. Figure 46 and Figure 47 show three almost parallel trends of EER depending on T_{pcm}. In particular, the light blue (Figure 46) and pink (Figure 47) dots indicate the operative points characterized by the highest T_{pcm} range (between 4 and 6°C), while on the other side, dark blue (Figure 46) and red (Figure 47) squares represent operative points with the lowest T_{pcm} range (between 0 and 2°C). Also in these cases, the obtained results are in line with expectations because lower temperatures at evaporator side are related to a higher electrical work needed at the compressor side and consequently to a lower EER. Although EER reveals important decrements if T_{pcm} is in the lowest range of 0 - 2°C, this affects only partially the global performance of the machine and this is due to the fact that for most of the time the T_{pcm} during compression chiller operation is between 4 and 6°C in both schemes SC4a and SC6a (blue and red columns respectively in Figure 46 and Figure 47).

Lastly, the slightly higher performance shown in scheme SC6a in comparison to scheme SC4a visible in Figure 45 are due to the fact that, temperature at the evaporator side in scheme SC6a is generally slightly higher than in scheme SC4a and this, is reflected also in slightly higher EER.

Compression chiller EER at different ambient temperature
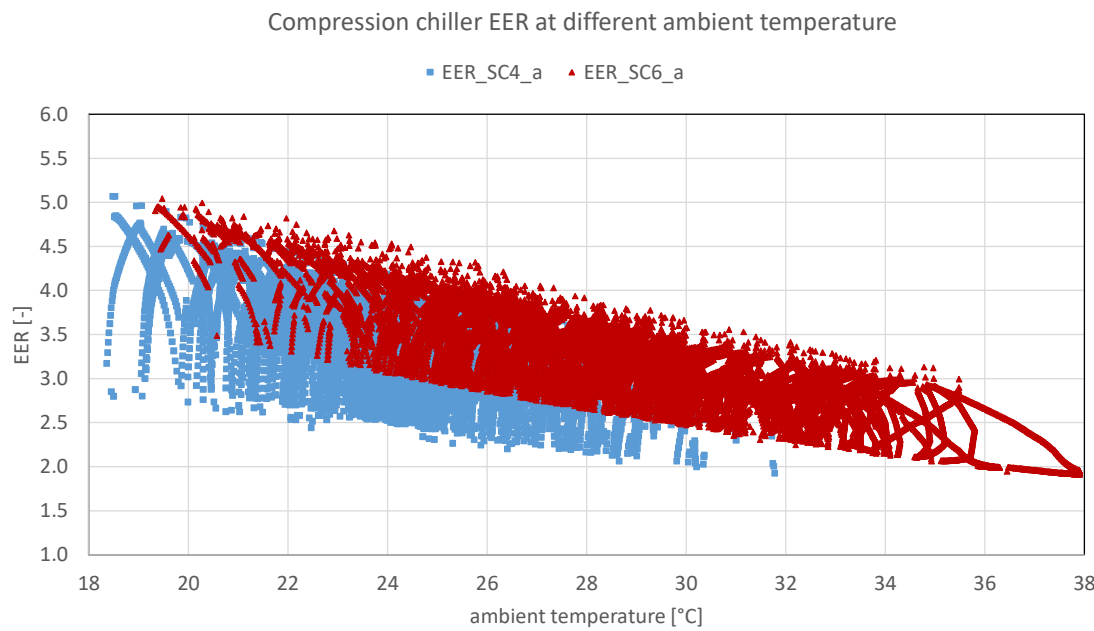
Figure 45 Compression chiller EER at different ambient temperature in schemes SC4a and SC6a

Compression chiller EER at different ambient temperature
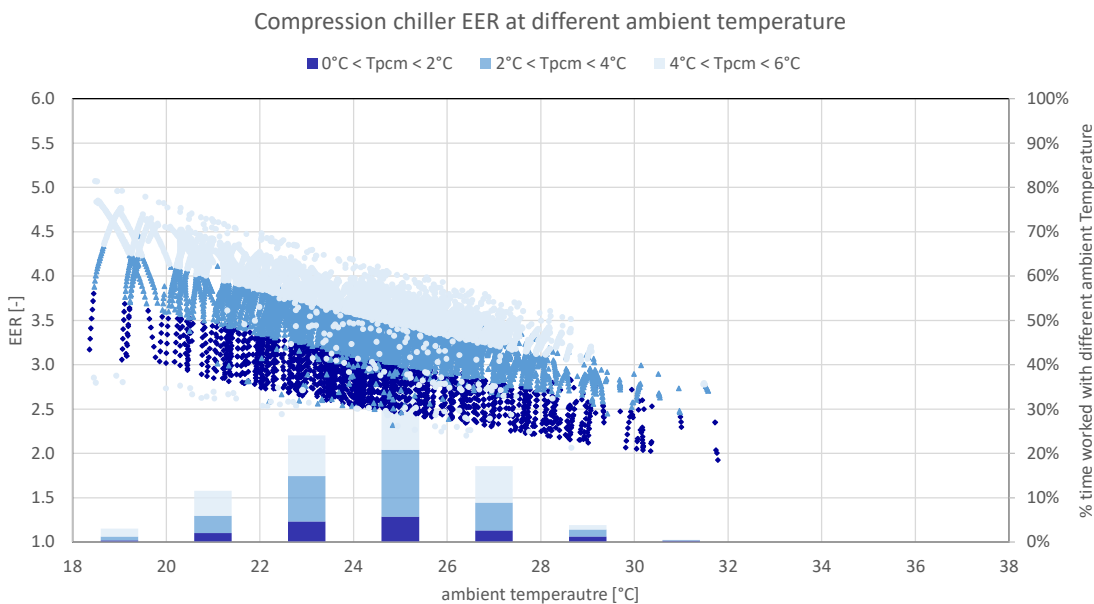
Figure 46 Compression chiller EER at different ambient temperature in schemes SC4a for different T$_{pcm}$ and percentage of time worked with different ambient temperature and different T$_{pcm}$ ranges (secondary vertical axis)

Compression chiller EER at different ambient temperature
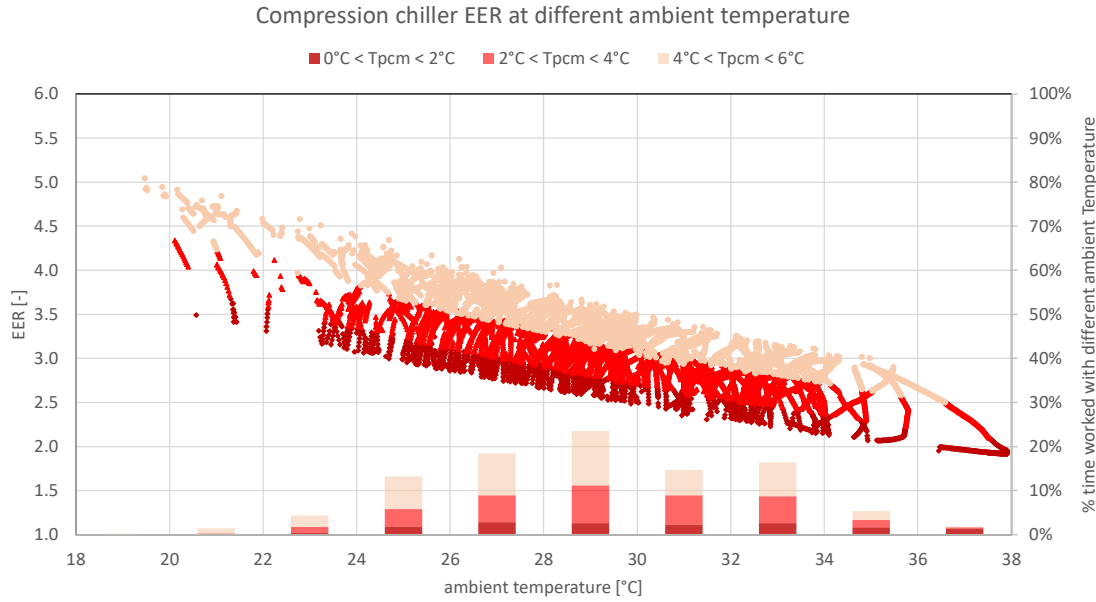
Figure 47 Compression chiller EER at different ambient temperature in scheme SC6a for different T$_{pcm}$ and percentage of time worked with different ambient temperature and different T$_{pcm}$ ranges (secondary vertical axis)

$SEER_{el}$ global

$$SEER_{HP,CV4} = 3.5$$

Compression chiller performance in different schemes (SC4a, SC4b, SC6a, SC6b) are presented in detail in the previous sections. Here instead, indications about the global performance of the compression chiller are given by using $SEER_{HP,CV4}$, calculated as the ratio of total cooling energy delivered over the total electrical energy absorbed by compressor, dry cooler and P17 (see Figure 28). Also in this case, more details can be extrapolate observing Figure 48 showing the EER against temperature at the evaporator side of the machine (T$_{evap}$). Each point indicates one operative point of the compression chiller, while the different colors identify the different operative modes (blue squares for scheme SC4a, green squares for scheme SC4b, red triangles for scheme SC6a, yellow dots for scheme SC6b). As expected, and also reported in the previous analysis, EER presents a decreasing trend moving from higher to lower T$_{evap}$. Moreover, also this figure shows the general higher EER when compression chiller works coupled with adsorption module (schemes b) with respect to the respective schemes in which it works with condenser side directly connected to the dry cooler (schemes a).

Compression chiller EER at different evaporator temperature

■ EER_SC4_a   ◆ EER_SC4_b   ▲ EER_SC6_a   ● EER_SC6_b
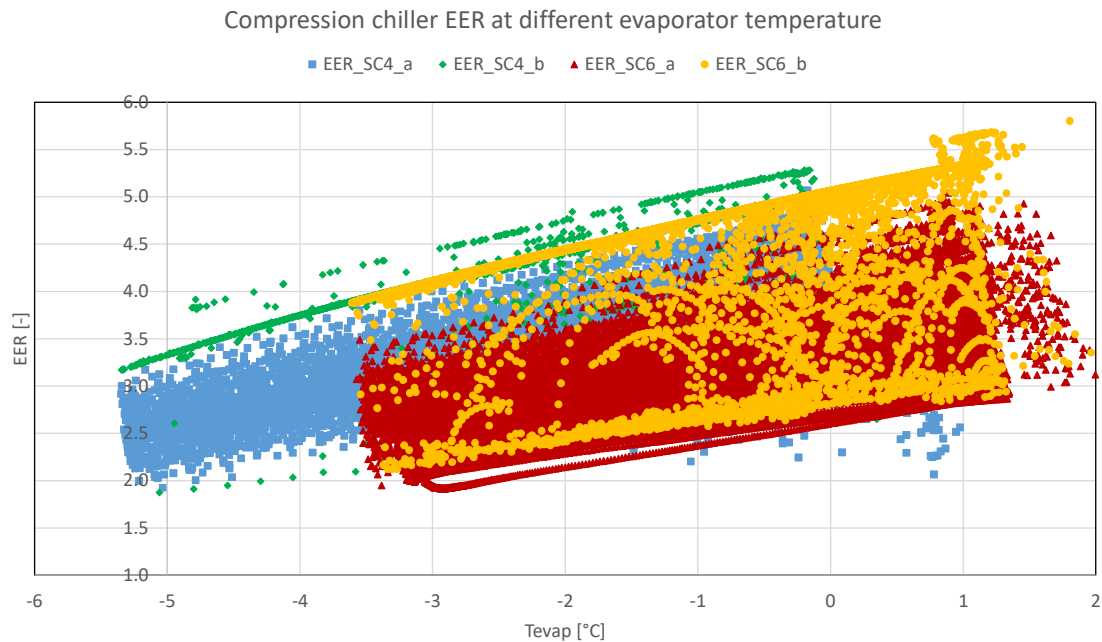
Figure 48 Compression chiller EER at different evaporator temperature T$_{evap}$ in schemes SC4a, SC4b, SC6a and SC6b

In conclusion, it is important to underline that the operational modes that foresee the work of compression chiller and adsorption module in series (schemes_b) are characterized by higher performance of the compression chiller. However, one important point that must be mentioned regards the percentage of time in which compression chiller effectively works coupled with adsorption module (schemes_b) or without this second device (schemes_a). These two percentages are reported in Figure 49. As it can be seen, for more than half of the total working time (70%) there are not the conditions for the adsorption module activation.

% of time worked in each scheme

■ SC4a   ■ SC6a   ■ SC4b   ■ SC6b
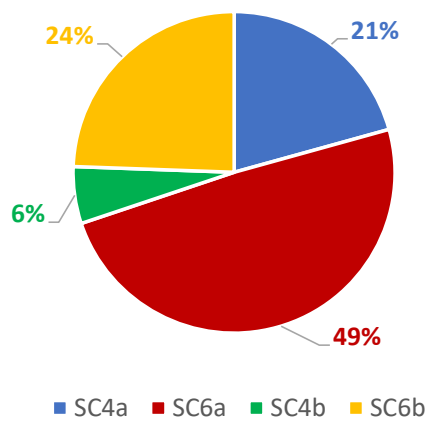
Figure 49 Compression chiller percentage of time worked in each scheme (schemes a -> without adsorption module, schemes b -> with adsorption module)

Analysing in more detail the cause behind this particularly low value, and trying to increase the fraction of time in which the compression chiller works coupled with adsorption module, it has been found that, the main cause behind the adsorption module unavailability is related to the limited availability of thermal energy for adsorption hot circuit. Considering the relatively high

solar thermal collector area already considered (60 m^2 of Fresnel solar thermal collector for a building with a total net area of 100 m^2) it has been decided to not investigate possible benefits related to an increase of this parameter, focusing instead only on increase buffer tank volume from the actual 800 l.

For this reason, some simulations with different increased buffer tank volumes (from 800 l up to 3000 l) have been run to evaluate if, a bigger thermal storage could improve the percentage of time in which compression chiller and adsorption module work in series. As can be noted in Figure 50 a buffer tank with higher volume (3000 l) could significantly increase the time in which compression chiller and adsorption module works in series (up to 58% of the operation time).

Percentage of time in which compression chiller works coupled with adsorption module considering different buffer tank capacities
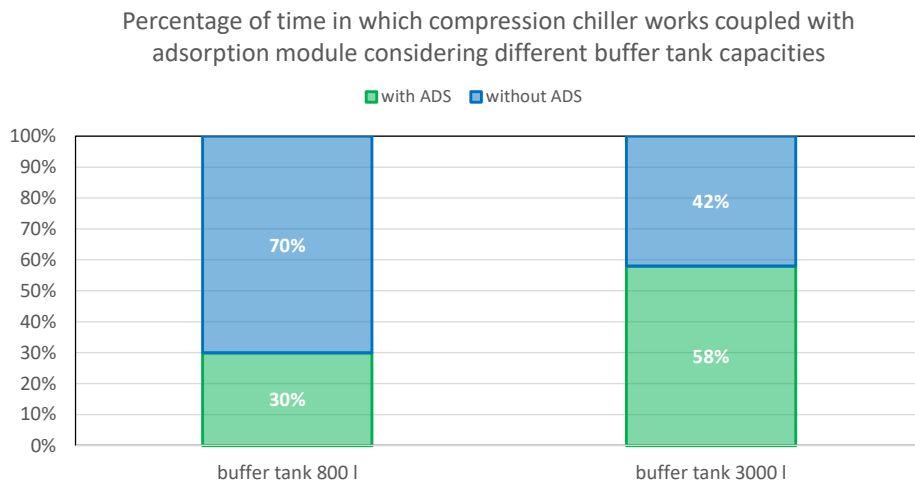
Figure 50 Percentage of time in which compression chiller works coupled with and without adsorption module considering different buffer tank capacities

The higher percentage of time in which compression chiller and adsorption module work in series leads, as expected to higher performance of the compression chiller (evaluated in this case considering $SEER_{HP,CV3}$). However, contrarily to expectations, this higher performance of compression chiller is not reflected in an increment also of performance at overall building system level (evaluated, in this case, considering $SPF_{el,CV}$). The value of $SEER_{HP,CV}$ and $SPF_{el,CV}$ are reported for the two analyzed cases (800 l and 3000 l buffer tank) in Table 2.

Table 2 Evaluation of compression chiller performance at sub-system level (L2) using the PI SEER$_{HP,CV3}$ and at overall system level (L3) using PI SPF$_{el,CV7}$ with different buffer tank volumes

	800 l buffer tank	3000 l buffer tank
$SEER_{HP,CV3}$	3.5	3.8
$SPF_{el,CV7}$	2.9	2.9

This relatively strange behavior has been investigated in more detail analyzing electrical consumptions of all components at overall building system level. For this purpose, Figure 51 shows the electricity consumption of the various components present in the HYBUILD MED system in space cooling modes, obtained from TRNSYS simulations, considering two different buffer tank sizes: 800 l in the figure on the left, 3000 l in the figure on the right. As can be noted comparing the figure on the left and the one on the right in Figure 51, the use of a bigger buffer tank leads effectively to a decrement of the electricity consumption of compression chiller (Wcomp in Figure 51), however, at the same time, there is an increment of electricity

consumption of adsorption module and dry cooler. In conclusion, these two opposite effects lead to obtain almost the same $SPF_{el,CV7}$ in both cases.
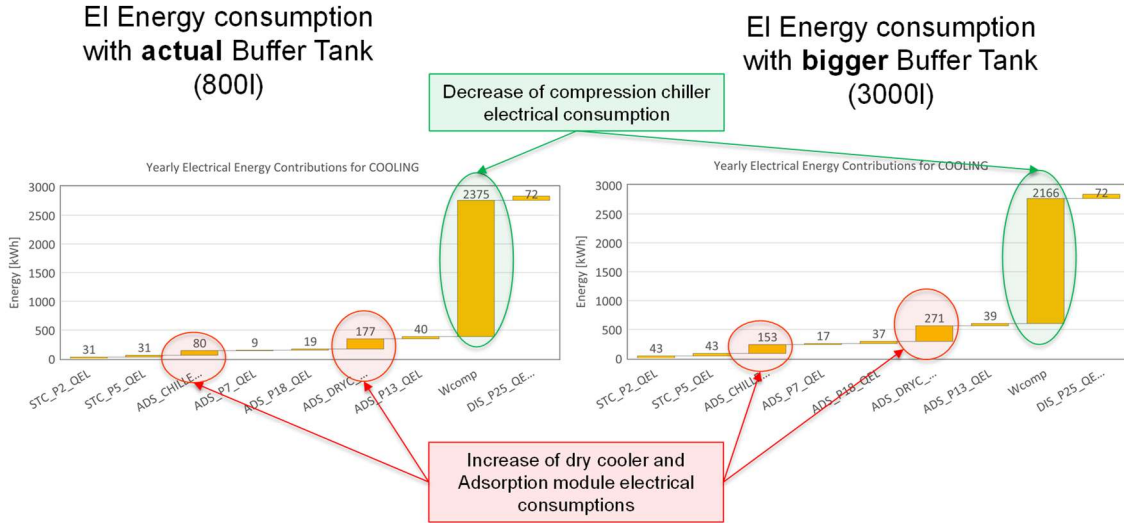

Figure 51 Yearly electrical energy consumption contributions in HYBUILD MED system in cooling season considering two different buffer tank volumes, (800 l on the left and 3000 l on the right). Green circles highlight the reduction of electricity consumption of compression chiller compressor in the 3000 l buffer tank configuration. Red circles highlight the devices that present instead a sensible increase in their electricity consumption in the 3000 l buffer tank configuration

At the end of this explanation, it is useful to highlight that, as discovered with the previous analysis, the increase of performance of one component could be not strictly connected to an increase of performance at overall building system level. This consideration must be carefully taken into account, especially for control logics optimization process, having in mind that, an optimized control logic that results in higher performance at component level could, in principle, lead to opposite results at overall system level.

Overall system level (L3) analysis

Annual building space heating and space cooling energy demands

This section reports space heating and space cooling demands coming from dynamic simulations considering the HYBUILD MED system in the MED reference building. Table 3 reports these results. As can be seen, space cooling demand constitutes the main request of the building. This is aligned with expectations. In fact, the HYBUILD MED system is mainly developed to cover space cooling demand in residential building located in the MED climate.

Table 3 HYBUILD MED ref. building yearly space heating demand with ideal and real system

Athens	Yearly demand with modelled HVAC system [kWh/m^2/y]
Space heating	66
Space cooling	85

Thermal and electric Seasonal Performance Factor (SPF)

As reported in section 0, two PI used to assess overall building system performance are SPF_{el} and SPF_{th}. As expressed in the formulas in section 0, these two quantities, referring to the overall system, include all the thermal losses in the distribution circuit and the electrical consumption of all devices ($SPF_{el,CV7}$) The results are reported below:

$$SPF_{el,CV7} = 2.9$$

$$SPF_{th,CV8} = 1.5$$

It is important to add that, this calculation does not consider the beneficial effect due to the possibility to exploit solar energy not only for covering space cooling demand but also for DHW production and space heating. These additional advantages are reported in the following sections.

Solar and auxiliary element energy contributions for DHW production

As already said in section 0, one of the peculiarities of HYBUILD MED system is its possibility to cover part of DHW demand using the solar energy captured by solar thermal collectors. However, to always ensure DHW at the right temperature (at least 45°C) to the users, an electrical resistance (considered as auxiliary element) is placed inside the DHW and can be activated if solar system is not able to guarantee the desired temperature inside the DHW tank. To have an evaluation of the share of DHW produced exploiting the energy catched from solar thermal collectors and of the contribution of auxiliary element, in the following, Figure 52 shows monthly solar and auxiliary contributions to DHW production for Athens building. It is useful to remind here that, the DHW users demand profiles have been imposed considering an estimated DHW demand, at users' side, around 20-22 kWh/m^2/year. As can be seen in Figure 52, the implementation of HYBUILD MED system, strongly reduces the usage of electrical back-up inside the DHW tank with respect to a standard case in which, electrical heater, is the only element responsible for DHW production. In particular, looking at Figure 52, it can be observed that, from April to October, DHW demand is totally covered by solar source, while important solar contributions are also visible for February, March and November. Considering instead the yearly time frame, as Figure 53 shows, HYBUILD MED system ensures to decrease electrical consumption for DHW (related to electrical resistance activation) to around 25% with respect to the standard scenario. Lastly, Figure 54 indicates thermal losses in the DHW Tank around 12%. This value is in line with expectations and comparable to the same value obtained for similar systems.

Figure 52 Monthly solar (yellow) and auxiliary (red) contributions to DHW production along the year

ATHENS SHARE OF INLET THERMAL ENERGY (SOLAR & AUX)

Qth DHW from STC   Qth DHW from AUX
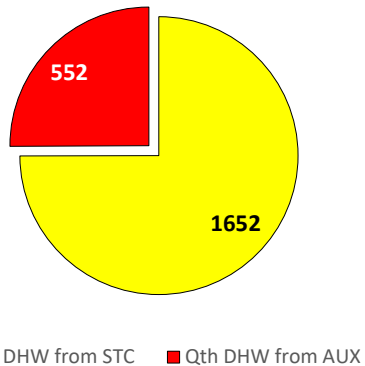
Figure 53 Yearly solar (yellow) and auxiliary (red) contributions to DHW production [kWh]

ATHENS SHARE OF OUTLET THERMAL ENERGY (QTH OUT & LOSSES)

DHW_PINK_QTH_OUT   Qth DHW LOSSES
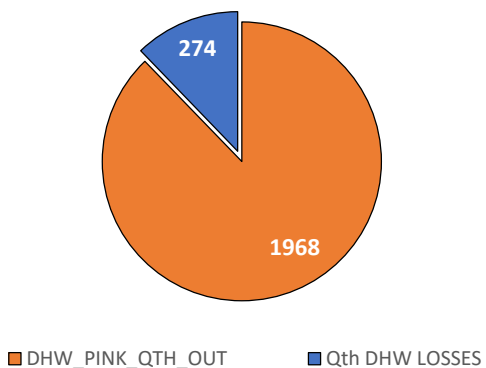
Figure 54 Yearly DHW thermal energy delivered to users (orange) and DHW Tank losses (blue) [kWh]

Solar and heat pump energy contributions for space heating demand covering

In addition to DHW production, the possibility to directly connect the buffer tank to the distribution system for covering space heating demand allows the exploitation of solar energy also for space heating through the free heating mode. From Figure 55 it can be noted that space heating load in April, May and October is almost completely covered by solar source, while in January, February, November, December it constitutes in any case an important contribution. On a yearly basis, the solar source contribution to space heating is around 30-40% of the total as it can be observed in Figure 56.

Athens solar and heat pump monthly energy contributions to space heating
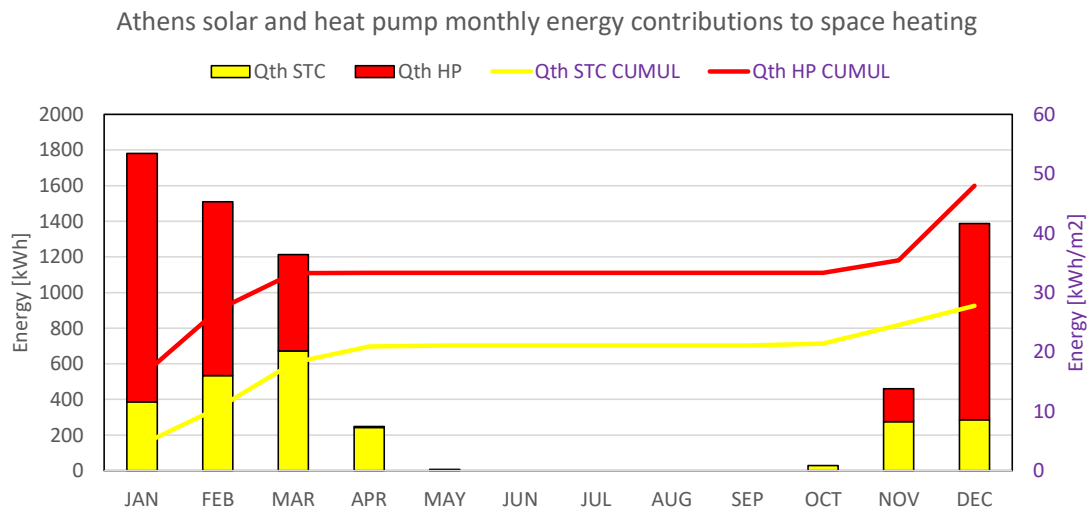
Figure 55 Monthly solar (yellow) and heat pump (red) contributions to space heating along the year

Athens contributions to space heating (solar
& heat pump)
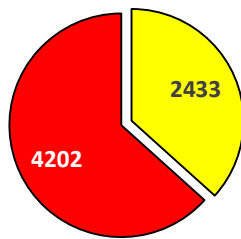
Figure 56 Yearly solar (yellow) and heat pump (red) contributions to space heating [kWh]

The main objective of HYBUILD MED system is the coverage of space cooling demand of a Single Family House in the Mediterranean climate (in this context the climatic conditions of the city of Athens are considered).

The big solar field considered (60 m2) has the primary objective to ensure the hot water needed to run the adsorption chiller.

In addition to this purpose, the solar field is also used to cover part of the DHW demand and part of building space heating demand.

Over the considered period (one year), the thermal energy gathered from solar thermal collectors is used to:
1. Run the adsorption chiller (5818 kWh, equal to around 55% of the thermal energy entering the buffer tank)
2. Cover users' DHW demand (1652 kWh, equal to around 16% of the thermal energy entering the buffer tank)
3. Cover space heating demand (2433 kWh, equal to around 23% of the thermal energy entering the buffer tank)

Moreover, 668 kWh, equal to around 6% of the thermal energy entering the buffer tank are lost as thermal losses.

These results can be seen in Figure 57.
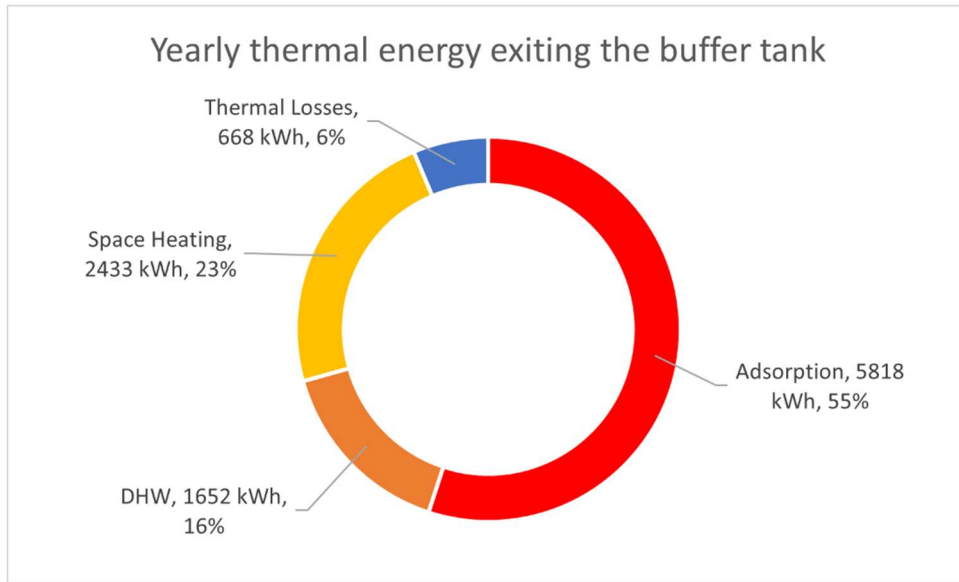
The total amount of thermal energy gathered from solar thermal collectors and used to cover building demands (SH, SC, DHW) is 10571 kWh.

Considering the area of solar thermal collectors, this value could seem relatively low. This is due to different factors, between them:

- The setup of the buffer tank: in fact, the water for space heating is extracted at around half of the tank height, maybe a different configuration of the position of the double ports in the buffer tank could improve the amount of thermal energy available for space heating. Moreover, as reported at pag. 47 of D4.4, also a specific sizing of the buffer tank volume could influence the system operation and performances.
- Regardless the solar thermal collector area, winter months, especially December and January, are characterized by low external temperature and low solar irradiation, leading to low production of the solar system and high building space heating demand. Moreover, the system prioritizes the production of DHW and therefore the solar system contributes to cover space heating demand only if the DHW tank results charged.

The high temperature level of the water needed to run the adsorption chiller (65-95 °C as specified at pag.12 of D4.4): in fact, the use of a high temperature level inside the buffer tank leads in general to a reduction of the performances of the solar system.

This explains the low value for the contribution from solar in Figure 56.

Self-consumption

As already explained in section 2.2.3, Self-consumption has been evaluated with monthly and yearly time frame to have indications about the amount of electricity used to drive the compression chiller and coming from the PV+BESS sub-system, with respect to the total PV production. Table 4 reports the yearly Self-consumption value. Due to the seasonality of the load, also a monthly calculation has been added to the analysis: results have been reported in Figure 58. As can be observed in Figure 58, the yearly value (40%) does not represent well the behaviour of the system. Monthly Self-consumption values in summer are around 70%, confirming the expected well coupling of cooling demand and PV production. During the heating periods, Self-consumption is around 50%, a lower value compared to the summer period caused

by the mismatch between heating needs and photovoltaic production during winter. On the contrary, in mild periods (March, April, May, October, November) Self-consumption drops to values lower than 30%. The cause of this effect is the low electricity consumption of the compression chiller in these months: for example, in October any space heating or space cooling demand is identified and the Self-consumed energy is equal to zero.

Table 4 HYBUILD MED system yearly Self-consumption

| Yearly Self-consumption |
|:---:|
| 40% |

PV system, monthly Self-consumption

Figure 58 HYBUILD MED system monthly Self-consumption

Self-sufficiency

As for Self-consumption, also Self-sufficiency has been evaluated with monthly and yearly time frame. Self-sufficiency is the amount of electricity used to drive the compression chiller and coming from PV+BESS, with respect to total energy demand. Table 5 reports the yearly value while Figure 59 shows the monthly Self-sufficiency values. As Figure 59 highlights, the fraction of energy demand covered by the PV+BESS sub-system is almost always higher than 40% as expected from the evaluations done during the sizing phase. Moreover, during mild seasons (April, May, September, November) the monthly Self-sufficiency index is particularly high (almost always higher than 80%). These high values are caused by the low thermal demand of the building for space heating or space cooling that is reflected also in low demand from the compression chiller. Therefore, the PV+BESS sub-system covers most of the demand with Self-consumed energy. During the summer period where the cooling demand is high, the PV+BESS can cover around 50% of the cooling load. Finally, as already discussed for the Self-consumption index, the low values for October can be explained by the absence of space heating or space cooling demand.

In addition to that, Figure 60 shows the two contributions to Self-sufficiency: the energy produced by PV and directly consumed by the load (yellow columns in Figure 60) and the energy sent to the load from the battery (green columns in Figure 60). As can be noted, during cold winter months (January, February, November and December) the energy from PV is rarely directly sent to the load. On the other hand, most of the Self-sufficiency is guaranteed by the battery. This behaviour can be explained by the time mismatch between the PV production and the demand from the compression chiller and the absence of advanced control logics that could increase direct self-consumption shifting part of the load during daytime hours. This condition

is even more visible in mild seasons (see Figure 60, for example in April and May). On the contrary, during the summer period, the most important contribution to Self-sufficiency is given by the energy produced by PV and directly consumed by the compression chiller. Contrarily to what happens in the winter period, during summer the PV production and the thermal load (in this case space cooling load) shows similar daily trends and consequently a higher matching between production and consumption.

Table 5 HYBUILD MED system yearly Self-sufficiency

Yearly Self-sufficiency
56%

PV system, monthly Self-sufficiency
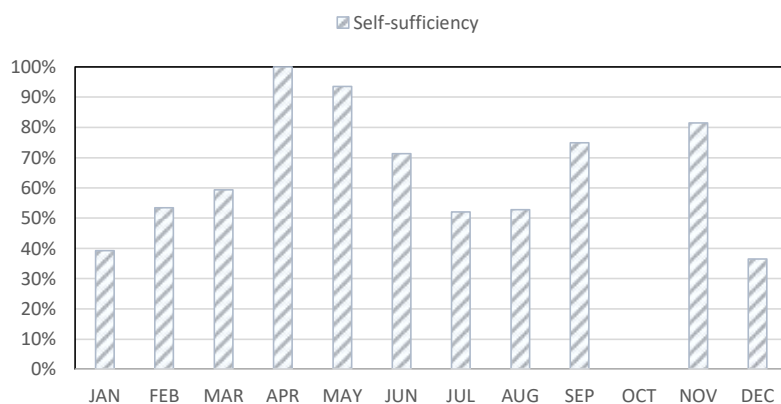
Figure 59 HYBUILD MED system monthly Self-sufficiency

PV system, monthly Self-sufficiency contributions
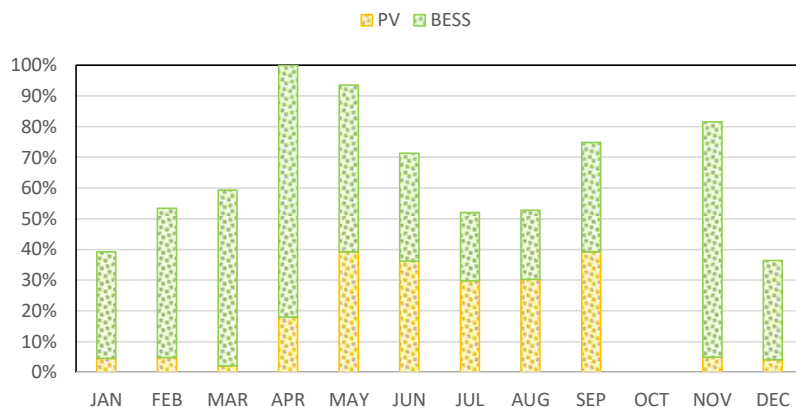
Figure 60 HYBUILD MED system monthly Self-sufficiency contributions: yellow: PV contribution, green: BESS contribution

Share of renewables

As already presented in section 2.2.3, the Share of renewables is an index similar to Self-sufficiency where also the renewable part of the electricity coming from the grid (value dependent on the energy mix of the considered country) is considered in the calculation of the renewable energy self-consumed. For the MED climate, Athens is considered as a reference location; therefore, the renewable fraction of the energy mix of Greece for the year 2019 has

been considered (31.30% according to [8]). Contrarily to Self-consumption and Self-sufficiency, the Share of renewables is presented only for a yearly time frame in Table 6. The index has been calculated both considering only the compression chiller as load, but also considering the energy demand of the entire system. The obtained values are relatively high and indicate that a relevant part of the energy consumption of the HYBUILD MED system is covered using renewable energy. Comparing the Share of renewables indicator (70%) calculated considering only the compression chiller consumption with the Self-sufficiency index (56%), it is possible to highlight the impact of the share of renewable of the energy mix that in this case correspond to an increase of 14% of the consumptions.

Table 6 HYBUILD MED system yearly Share of renewables

Share of renewables (HP only)	Share of renewables (HP + auxiliary)
70%	60%

Final Energy use (FE)

As already reported in section 0, FE is a useful PI representing the electricity used to drive the HVAC system. Table 7 reports the Final Energy used for space heating, space cooling and DHW production, as well as the total value.

Table 7 Athens FE for space heating, space cooling, DHW production and total value

Studied city	FE space heating [kWh/y]	FE space cooling [kWh/y]	FE DHW [kWh/y]	FE total [kWh/y]
Athens	1345	2843	577	4766

3.2   Continental system

This section reports results from TRNSYS simulations of HYBUILD CON system in the specific correspondent building (a small Multi-Family House in the CON climate with the reference city of Stuttgart) considering the control logics extensively explained in D4.2 [2]. The results are reported in terms of the above mentioned and explained PIs.

Sub-system level (L2) analysis

Seasonal Coefficient Of Performance $(SCOP)$ *and Seasonal Energy Efficiency Ratio* $(SEER)$

Seasonal Coefficient Of Performance in space heating mode ($SCOP_{SH}$)

The heat pump performance in space heating mode, as already presented in section 2.2.2 is described using the $SCOP_{SH}$. Below the calculated value is reported.

$$SCOP_{SH,CV\ HP} = 4.3$$

The previous value gives an indication about the overall yearly performance of the heat pump when it works to cover space heating demand. Nevertheless, one peculiarity of HYBUILD CON system is the possibility to store in the RPW-HEX part of the sensible energy of refrigerant, after being elaborated by the HP compressor and before entering the condenser, when the machine works to cover space heating (and also space cooling) building demand. This stored energy is

then used for DHW tanks charging with HP and RPW-HEX working in series in the predefined periods devoted to DHW tanks charging. It is therefore important to assess that, when the machine is working in space heating mode and, at the same time is charging the RPW-HEX (scheme SC_2_1), the device performance, in terms of $SCOP_{SH,CV\ HP}$, are not sensibly lower with respect to the operational mode in which the HP only works to cover space heating demand (scheme SC_2_2). The black dots in Figure 61 show the $SCOP_{SH,CV\ HP}$ calculated with the machine that works in SH mode and, at the same time is charging the RPW-HEX (black dot in scheme SC_2_1 in Figure 61) and when the machine is working to cover only SH building demand (black dot in scheme SC_2_2 in Figure 61). As can be noted in the same figure, there is a slight decrement of $SCOP_{SH,CV\ HP}$ when the machine works in scheme SC_2_1. Being so small the difference between the $SCOP_{SH,CV\ HP}$ in the two schemes SC_2_1 (4.27) and SC_2_2 (4.37) it can be concluded that the operational mode that foresees, in addition to the covering of space heating demand, also the RPW-HEX charging, does not present a sensible decrement of the HP performance in terms of $SCOP_{SH,CV\ HP}$. It is also interesting to note that most of the building space heating demand is covered with the HP that, at the same time, is also charging the RPW-HEX (scheme SC_2_1). This fact can be observed looking at the orange columns in Figure 61 that represent the annual thermal energy delivered by the HP for space heating respectively in scheme SC_2_1 and SC_2_2.
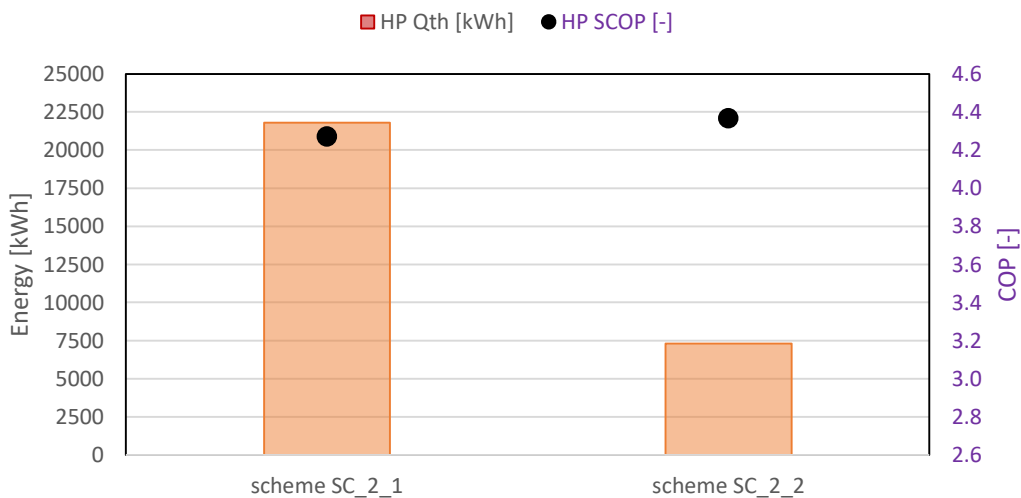
Figure 61 Heat pump thermal energy delivered for space heating (orange columns) and SCOP (black dots, right axis) in the two space heating operational modes SC_2_1 (HP works to cover space heating demand and, at the same time, charges the RPW-HEX) and SC_2_2 (HP works only to cover space heating demand)

Seasonal Energy Efficiency Ratio in space cooling mode ($SEER_{SC}$)

As presented in section 2.2.2 the energy performance of HP in space cooling mode is assessed through the Seasonal Energy Efficiency Ratio. The value of this index is reported below.

$$SEER_{SC,CV\ HP} = 6.6$$

The obtained value is particularly high with respect to other commercial heat pumps. However, this high value is related to high EER values included in the performance map characteristic of the considered machine. The data reported in the performance map are reliable as they come from laboratory tests performed on the studied machine. It has also to be noted, that the

considered HP works for a very limited amount of time in space cooling mode as the space cooling demand of the considered building is very low (see Table 8).

Seasonal Coefficient Of Performance in DHW tanks charging mode ($SCOP_{DHW}$)

The heat pump performance in DHW tanks charging mode, as already presented in section 2.2.2 is described using the $SCOP_{DHW}$. In the following the calculated value is reported.

$$SCOP_{DHW,CV\ HP} = 3.8$$

As already presented for space heating, also in this case the previous value gives an indication about the overall yearly performance of the HP in DHW tank charging mode. However, as previously mentioned in section 2.1.2, one of the peculiarities of HYBUILD CON system is the possibility to charge the decentralized DHW tanks exploiting not only the energy from the HP but also the energy previously stored in the RPW-HEX. It is therefore important to evaluate the benefits (in terms of increased $SCOP_{DHW,CV\ HP}$) during DHW tanks charging phase when this is performed with HP and RPW-HEX that work in series. The black dots in Figure 62 represent the $SCOP_{DHW,CV\ HP}$ when the HP works in series with RPW-HEX to charge the decentralized DHW tanks (scheme SC_4_1) and when the RPW-HEX is empty, hence the HP works alone to ensure DHW tanks charging (scheme_SC_4_2). As can be noted, there is a slight increase in the $SCOP_{DHW,CV\ HP}$ when HP works in series with RPW-HEX to charge DHW tanks (4.01) with respect to the scheme in which only HP is used to charge the DHW tanks (3.78). However, the effect of the slightly higher COP in scheme SC_4_1 on $SCOP_{DHW,CV\ HP}$ is very limited because, for the majority of the time, the charging of the decentralized DHW tanks is ensured by the HP only (through scheme SC_4_2) as the RPW-HEX is not available. Red columns in Figure 62 show graphically this last concept, representing the energy delivered to DHW tanks for their charging in scheme SC_4_1 (DHW tanks charging with HP and RPW-HEX working in series) and in scheme SC_4_2 (DHW tanks charging using only the HP).
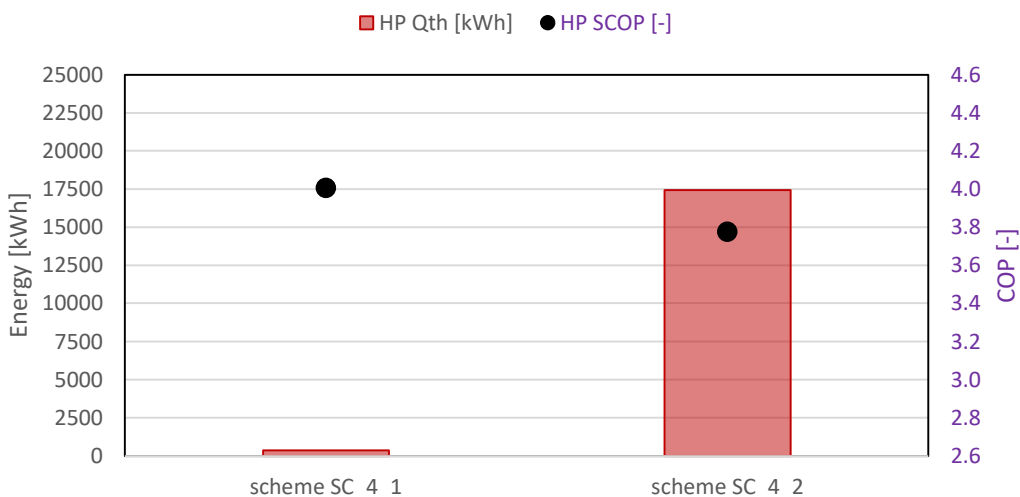
Figure 62 Heat pump thermal energy delivered for DHW tanks charging (red columns) and SCOP (black dots, right axis) in the two DHW tanks charging operational modes SC_4_1 (HP works in series with RPW-HEX to charge DHW tanks) and SC_4_2 (HP only works to charge DHW tanks)

At the end of this section it is useful to add some partial conclusions obtained from a more detailed analysis of dynamic simulation results. As already discussed, the operational mode that foresees the charging of DHW tanks with HP and RPW-HEX connected in series (schemes

SC_4_1) presents benefits in terms of $SCOP_{DHW,CV\ HP}$. The same concept could be seen also in Figure 63 that shows all the COP values calculated with a time frame of one hour for an entire year in space heating (orange triangles) and DHW tank charging mode (red circles). In addition to that, in the same figure also EER values of the heat pump in space cooling mode are reported with blue crosses. As can be noted the COP in space heating and DHW tank charging mode decreases, as expected, moving towards low external air temperatures. On the contrary, the EER in space cooling mode shows an opposite trend with, as expected, lower values at higher external air temperatures.

Moreover, Figure 63 shows that, for DHW tanks charging operation, there are two almost parallel trends of COP. The two almost parallel COP trends are related to DHW tanks charging performed with HP working in series with RPW-HEX (higher COP, higher red circles trend in Figure 63) and without RPW-HEX (lower COP, lower red circles trend in Figure 63). As can be noted, the higher COP points in DHW tanks charging mode are practically overlapped with orange triangles that represent the COP of heat pump when it works in space heating mode. This confirms that, when the DHW tanks are charged with HP and RPW-HEX connected in series, the HP COP is aligned with the COP obtained in space heating mode.

In addition to that, the columns in Figure 63 show the number of hours along the year in which the HP works for different purposes (space heating, orange, space cooling, blue, DHW tanks charging, red) with different external air temperature ranges. As Figure 63 highlights, for the majority of the time, the HP works with external air temperature in the range -5 - 15°C.
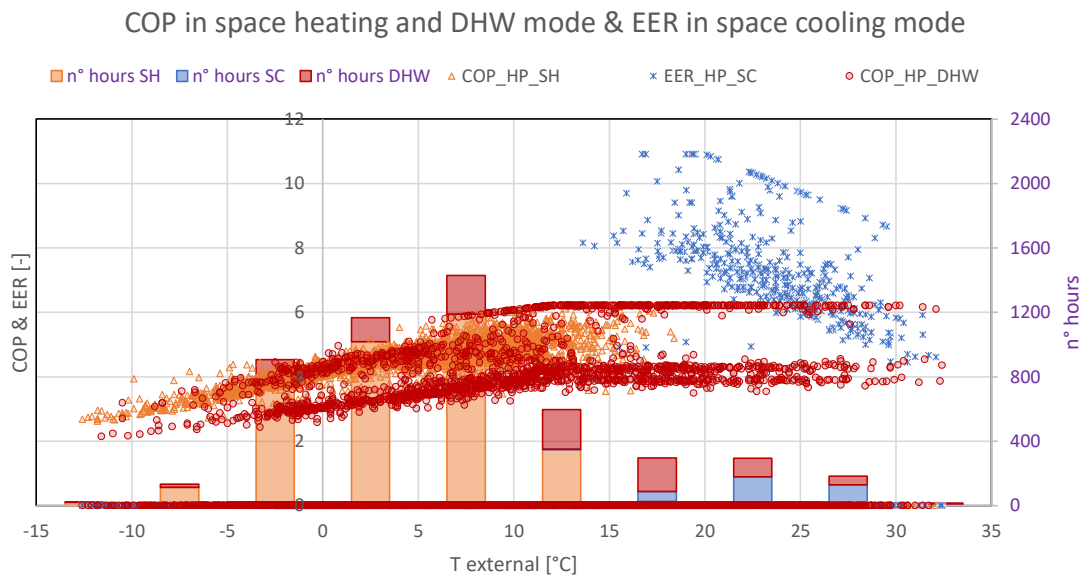
Figure 63 Heat pump COP in space heating mode (SH, orange triangles) and in DHW tanks charging mode (DHW, red circles) and EER in space cooling mode (SC, blue crosses) against external air temperature (T external). In addition, number of hours along the year in with the HP works for the various purpose (SH, orange columns, SC, blue columns, DHW, red columns) with different external air temperature ranges

Considering the beneficial effect related to the use of HP and RPW-HEX connected in series for DHW tanks charging, some simulations with an RPW-HEX characterized by a higher thermal storage capacity (up to 10 kWh) have been run to try to increase the time in which DHW tanks are charged with the HP and RPW-HEX working in series. However, no improvements have been obtained. Analysing the simulation results in more details, it has been found that this is mainly due to the fact that, the real limit, is not related to the thermal storage capacity of RPW-HEX but, instead, to the limited power available from HP to charge the RPW-HEX. In fact, RPW-HEX can be charged only when HP is working in space heating or space cooling mode and the power

that can be delivered to RPW-HEX for its charging is limited. This fact is particularly important in mild seasons in which the space heating or space cooling demands are very small resulting in a still lower amount of thermal energy available for RPW-HEX charging. This concept can be observed in Figure 64 that shows the monthly energy entering the RPW-HEX (from the HP) and the energy exiting the RPW-HEX (and used for DHW tanks charging). Figure 64 is obtained considering 7 kWh as RPW-HEX thermal storage capacity. As can be seen, the months in which the RPW-HEX energy contribution to DHW tanks charging is higher are the months characterized by cold external air temperature and, therefore high usage of HP in space heating mode. Due to the high HP usage in space heating mode, consequently, a high amount of thermal energy is also available for RPW-HEX charging. The optimization of the management of RPW-HEX and DHW tanks charging operation is a process that is still ongoing and will continue with different tests in simulation environment, as well as in the CON demo site to improve the contribution of RPW-HEX in DHW tanks charging phase.
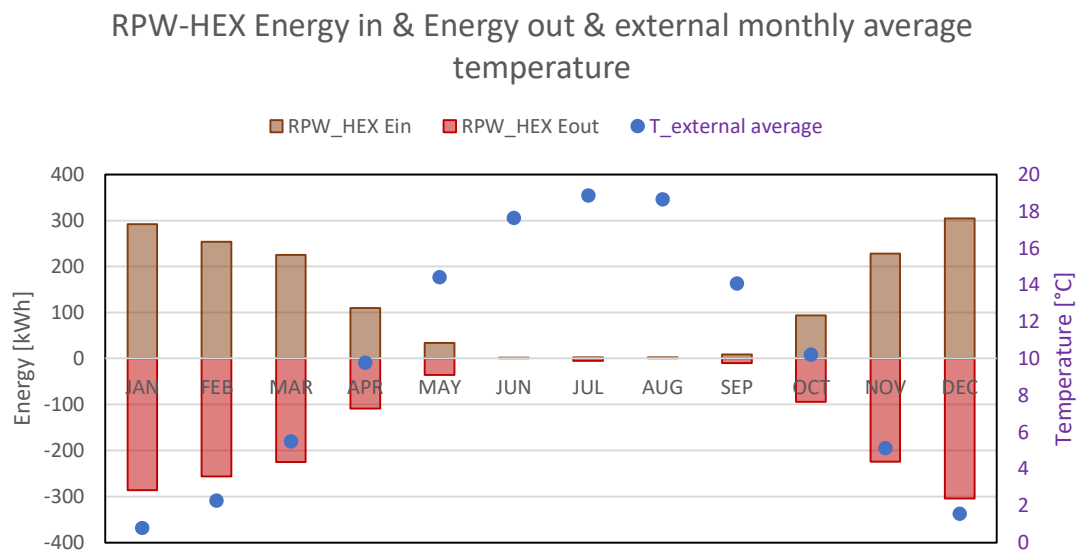
Figure 64 Monthly energy balance of RPW-HEX. Energy entering the RPW-HEX (from HP, brown columns) and energy exiting the RPW-HEX (to DHW tanks for their charging, red columns). In addition, monthly average external air temperature (blue dots)

Overall building system (L3)

Building space heating and space cooling energy demands

This section reports space heating and space cooling demands coming from dynamic simulations considering the HYBUILD CON system in the CON reference building. Table 8 reports these results. As can be seen, the main building request is represented by space heating demand. This is in accordance with expectations. In fact, the HYBUILD CON system is mainly developed to cover space heating and DHW demands in residential buildings located in the CON climate.

Table 8 HYBUILD CON ref. building yearly space heating demand with ideal and real system

Stuttgart	Yearly demand with modelled HVAC system [kWh/m²/y]
Space heating	46
Space cooling	3

Electric Seasonal Performance Factor (SPF)

Seasonal Performance Factor for space heating (SPF_{SH})

As already presented in section 2.2.2, SPF_{SH} is used to evaluate performance at overall building system level (L3) of HYBUILD CON system in space heating mode. The resulting SPF_{SH} is reported below.

$$SPF_{SH,CV\ SYS\ SH} = 3.3$$

As already discussed, this value is calculated considering the energy delivered to the various dwellings of the building to cover space heating demand with respect to the overall electricity consumed in this mode. It includes the energy delivered to fan coils to cover dwellings' space heating demand in both two possible space heating schemes (SC_2_1, in which HP works to cover space heating demand and, at the same time, charges the RPW-HEX, and SC_2_2, in which HP works only to cover space heating demand as the RPW-HEX is fully charged).

Seasonal Performance Factor for space cooling (SPF_{SC})

Regarding instead the assessment of HYBUILD CON system performance at overall building system level (L3) in space cooling mode this is done considering the SPF_{SC}. The obtained value for this PI is reported below.

$$SPF_{SC,CV\ SYS\ SC} = 3.0$$

As presented above for SPF_{SH} also in this case the index is calculated considering the energy delivered to the various dwelling to cover, in this case, space cooling demand, with respect to the overall electricity consumed in this mode. Also to cover space cooling demand the HP could work in two different operational modes; the energy delivered using both space cooling demand in accounted in SPF_{SC}. In the first scheme (SC_3_1) the HP works to cover space cooling demand and, at the same time, charges the RPW-HEX, while, in the second (SC_3_2) the HP works only to cover space cooling demand as the RPW-HEX is fully charged. It is also important to remind here that, the focus of HYBUILD CON system is mainly on space heating and DHW demands covering. This fact is enforced by the low space cooling demand of the building considered that, it is important to remind, represents the target building for future exploitation of HYBUILD CON system.

Seasonal Performance Factor for DHW tanks charging mode (SPF_{DHW})

As already discussed in section 2.2.2, the index used to evaluate system performance at overall building system level (L3) in DHW tanks charging mode is the SPF_{DHW}. The value of this PI is reported below.

$$SPF_{DHW,CV\ SYS\ DHW} = 2.1$$

As already presented in section 2.2.2, this value is calculated considering the energy delivered to the various DHW tanks present in the various dwellings of the building with respect to the overall electricity consumed in DHW mode. As for SPF_{SH} and SPF_{SC} it includes the energy delivered to DHW tanks in both two possible DHW tanks charging schemes (SC_4_1, in which HP works in series with RPW-HEX to charge the DHW tanks, and SC_4_2, in which HP alone works to charge DHW tanks as the RPW-HEX is not available).

Although this value is not particularly low there is room for improvements. In fact, the SPF_{DHW} value strongly depends on the management of the DHW tanks charging periods. A different

management of the DHW tanks charging periods could result in a higher or lower need of electrical resistances contribution, and, consequently in a higher or lower value of SPF_{DHW}.

With the aim of trying to decrease the back-up elements contribution to DHW production, it has been performed a more detailed evaluation to assess in which hours of the day the activation of back-up element for the specific DHW tank occurs more frequently.

Figure 65 reports the results of this analysis for six different DHW tanks, in particular, the two placed in the dwellings at ground floor, the two placed in the dwellings at third floor and the two placed in the dwellings at top floor. For each DHW tank, the cumulated energy delivered by its electrical resistance, in the specific hour of the day (vertical axis), and for all the months (horizontal axis), is reported in different colours based on the specific value (colour scale on the right of the various figures). It is here important to remind that, DHW tanks charging periods considered in this work are from 3:00 a.m. to 5:00 a.m. and from 3:00 p.m. to 5:00 p.m. For this reason, it is not expected to find notably back-up contributions during these periods.
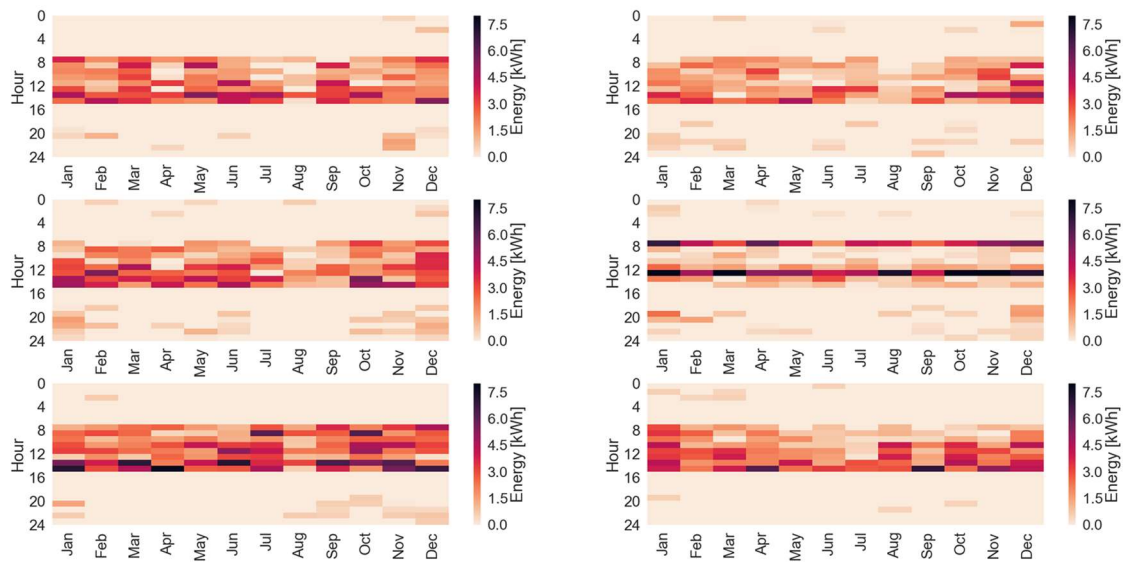

Figure 65 Energy exploited by electrical back-ups in different DHW tanks for the specific hour of the day and for the various months. The two graphs in the lower part of the figure report the energy exploited by electrical back-ups in DHW tanks placed at ground floor. The two graphs in the middle part of the figure report the energy exploited by electrical back-ups in DHW tanks placed at third floor. The two graphs in the higher part of the figure report the energy exploited by electrical back-ups in DHW tanks placed at top floor

From Figure 65 different important aspects can be observed.

The first regards the hours of the day in which the activation of electrical back-up occurs. As can be noted the activation of back up resistance occurs in general in the period from 8:00 a.m. to 3:00 p.m. This indicates that the time between the early morning charge (finishing at 5:00 a.m.) and the afternoon charge (starting at 3:00 p.m.) is too high with respect to the storage capacity of the decentralized DHW tanks (140 l). Another aspect that enforce this thesis can be noted observing the general increment of back-up element activation (dark colour in Figure 65) moving towards the hours immediately before the second daily charging period (just before 3:00 p.m.). For this reason, one possible improvement could be a different management of the DHW tanks charging periods or, the introduction of an additional DHW tanks charging period in the late morning.

The second conclusion that can be drawn from analysing Figure 65 is that there are not big differences regarding the activation of back-up resistances in winter and summer months. This also means that the external air temperature, although it influences the performance of the HP,

has not a notably impact on the ability of the HYBUILD CON system to charge the DHW tanks in different periods of the year.

The third aspect still regards the ability of HYBUILD CON system to charge DHW tanks. In this case, the focus is on the ability to complete the charge of all DHW tanks present in the building in the predefined charging periods (characterized by a duration of two hours). This aspect is verified considering that any important increment can be observed between the use of back-up element in the DHW tanks placed at top floor with respect to those placed at ground floor. Considering the sequence of DHW tanks charging, that is performed with two DHW storages at the same time, starting from the two placed at ground floor and proceeding with those at the upper floors only when the firsts are fully charged, an undersized system would not be able to complete the charge of DHW storages placed at the top floor within the predefined charging period (two hours). This fact would lead to a higher exploitation of the back-up elements in DHW storages at top floor with respect to those placed at ground floor with a notably higher electrical consumption that would be detected in Figure 65.

As presented in the last paragraphs some additional analysis have been performed to better understand the peculiarities of the HYBUILD CON system, in particular, regarding the DHW tanks charging phase. As already mentioned, there is room to improve this operational mode. More specifically, points that will be investigated in more details are related to the management of DHW charging periods along the day and to the coupling with PV+BESS electrical energy availability. The scope of these analysis is to be a support for possible upgrades in the management of control logics to improve the DHW charging mode and in general the performances of HYBUILD CON system.

Self-consumption

As already explained in section 2.2.3, Self-consumption has been evaluated with monthly and yearly time frame to obtain indications about the amount of electricity used to drive the heat pump coming from PV+BESS, with respect to total PV production. Table 9 reports the yearly Self-consumption value, while Figure 66 shows the monthly Self-consumption values. As can be observed in Figure 66, during the winter period the monthly Self-consumption are relatively high (up to around 60%). This is the result of two different contributions: on one hand, the reduced PV production in winter months and on the other hand, the increased demand due to the higher exploitation of the HP to cover space heating demand. On the contrary, during summer Self-consumption values decreases (around 30-40%). The motivations behind this decrement are related to the higher PV production during summer and to the limited HP demand during the summer period related to the CON climate.

Table 9 HYBUILD CON system yearly Self-consumption

| Yearly Self-consumption |
|---|
| 44% |

PV system, monthly Self-consumption
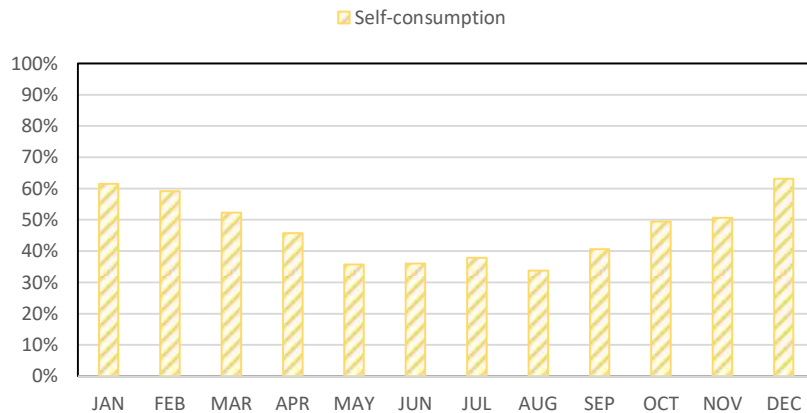
Figure 66 HYBUILD CON system monthly Self-consumption

Self-sufficiency

As presented above for Self-consumption, also Self-sufficiency has been evaluated with monthly and yearly time frame. Self-sufficiency indicates the amount of electricity used to drive the heat pump, and coming from PV+BESS, with respect to total energy demand. Table 10 reports the yearly value of Self-sufficiency, equal to 45%. As Figure 67 highlights, the fraction of energy demand covered by the PV+BESS sub-system is limited during the winter period (in January and December values around 20% have been obtained). This is motivated by the fact that in these periods the PV production and, therefore, the fraction of load that can be covered by the PV+BESS sub-system is low. In addition to this fact, in the same period, the load is particularly high due to the high exploitation of the HP for space heating. On the contrary, during summer periods, PV production is at its peak, while the HP load decreases. This is reflected in high values of Self-sufficiency in the period between May and September in which almost all the demand (around 90%) is covered by the PV+BESS sub-system. In addition to that, Figure 68 shows the two contributions to Self-sufficiency: the energy produced by PV and directly consumed by the load (yellow columns in Figure 68) and the energy sent to the load from the battery (green columns in Figure 68). During cold winter months (January and December) the battery contribution to self-consumption is well below the yearly average, mainly because most of the PV production is directly self-consumed by the system (low PV production, high consumption for space heating). On the contrary, the high PV production of summer months causes an excess of energy compared to the one directly self-consumed that is used to charge the battery increasing the BESS contribution to self-sufficiency.

Table 10 HYBUILD CON system yearly Self-sufficiency

| Yearly Self-sufficiency |
|---|
| 45% |

PV system, monthly Self-sufficiency
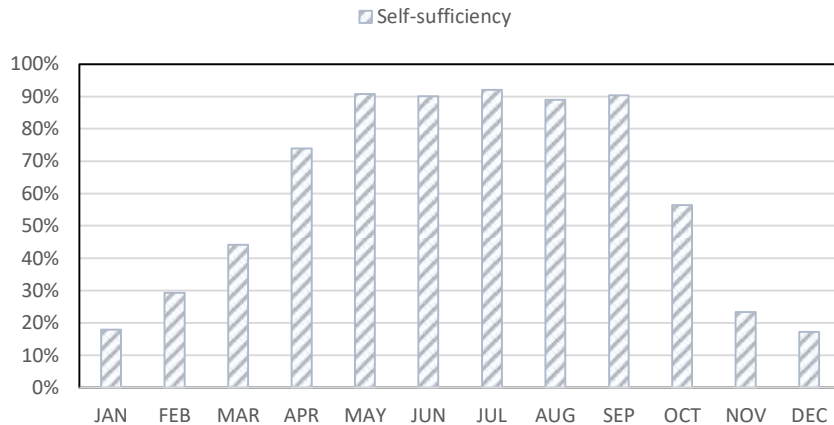
Figure 67 HYBUILD CON system monthly Self-sufficiency

PV system, monthly Self-sufficiency contributions
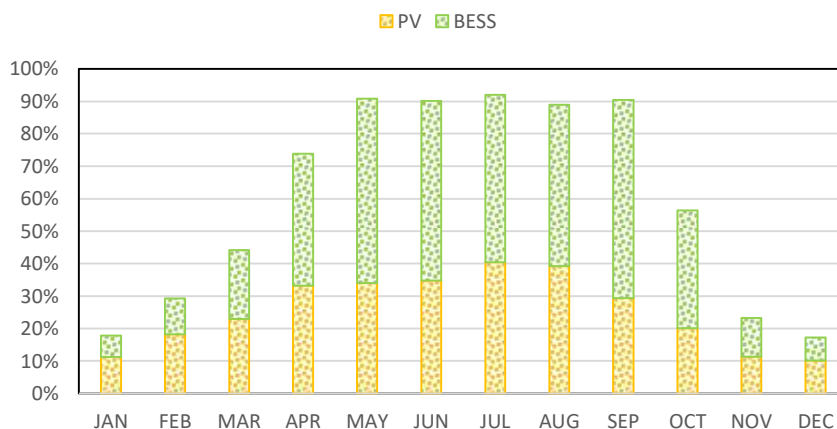
Figure 68 HYBUILD CON system monthly Self-sufficiency contributions: yellow: PV contribution, green: BESS contribution

Share of renewables

As already presented in section 2.2.3, the Share of renewables is a PI similar to Self-sufficiency with the difference that also the renewable part of electricity coming from the grid (value dependent on the energy mix of the considered country) is considered. The reference building for the CON climate has been located in Stuttgart. For this reason, the renewable fraction of Germany energy mix for the year 2019 has been considered (40.82% according to [8]). Contrarily to Self-consumption and Self-sufficiency, the Share of renewables has been calculated only with a yearly time frame in Table 11 for both the cases considering only the energy consumption of the heat pump and the overall electricity consumption of the system. The obtained value is in line with the ones obtained for the MED system and indicates that a relevant part of the energy demand is covered with renewable energy. Comparing the Share of renewables calculated considering only the HP demand (68%) with the Self-sufficiency (45%) it is possible to highlight the impact of the renewable fraction in the energy mix. In this case, the increase corresponds to 23% due to the higher renewable fraction of the German energy mix compared to the one of Greece used for the MED system.

Table 11 HYBUILD CON system yearly Share of renewables

Share of renewables (HP only)	Share of renewables (HP + auxiliaries)
68%	62%

Final Energy use (FE)

As already reported in section 2.2.2, FE is a useful PI representing the electricity used to drive the HVAC system also in HYBUILD CON system. Table 12 reports the Final Energy used for space heating, space cooling and DHW production, as well as the total value.

Table 12 Stuttgart sMFH Final Energy use for space heating, space cooling, DHW production and total value

Studied city	FE space heating [kWh/y]	FE space cooling [kWh/y]	FE DHW [kWh/y]	FE total [kWh/y]
Stuttgart	7714	525	8009	16248

3.3   Next steps

The results presented above constitute a useful evaluation about system performance at different levels (sub-system level and overall building system level). Moreover, the additional analysis performed for Mediterranean and Continental HYBUILD systems gives a more complete assessment of the behaviour of the two systems. All these results represent a realistic benchmark to compare the results in terms of the studied PIs obtained considering the first optimized logics developed. Another activity foreseen for the future is the use of these results to upgrade the performance of the system with particular focus on some specific aspect as, for example, the improvement of DHW tanks charging phase management in the HYBUILD Continental system. The optimized control logics that, tested in simulation environment, indicate an effective improvement in terms of system performance will be also tested in the real demo sites to have a final real assessment of their benefits.

4 Optimisation results

Beside the basic control analysed in the previous section, two different approaches based on Artificial Intelligence (AI) have been studied to extend the functionalities for the BEMS proposed within the HYBUILD project. The two approaches, proposed by UDL and ENG, are not directly comparable, since they implement two different methodologies to pursue different objectives: in particular, the first approach is an optimised alternative to the execution of the basic control rules versus which it is compared, while the second approach is the only method specifically tailored and able to optimise the KPIs defined for the exploitation of the flexibility of the system components as part of the collaboration with external actors, such as grid operators, for the provisioning of auxiliary services to the grid. The two proposals have been fully described in D4.3 [3]. In this section, the main results coming from the two optimisation methodologies are reported, and their performances are analysed as specified.

4.1 Cost and system efficiency optimisation results

The details regarding the approach used by UDL for the smart control based on deep reinforcement learning (DRL) technique were presented in deliverable D4.3. In that report, some preliminary results obtained for the theoretical Mediterranean HYBUILD system based on a cost optimisation strategy were provided and compared with three different rule-based control (RBC) approaches. The results confirmed that using a DRL approach the operation costs of the HYBUILD system were considerably reduced with respect to any RBC approach (a 35% cost reduction was obtained using a DRL approach with respect to the best RBC approach).

However, the simplified models for some of the components of the theoretical HYBUILD system, developed within WP2 and WP3 activities and used in the smart algorithm, were not yet validated against experimental test data, either because the components characteristics were different with respect to the ones tested in the lab, or because they were not yet tested at the demo sites. Therefore, to check the influence that uncertainties in the components models may have in the final results, a sensitivity analysis was performed. To do this, the values of some of the main model parameters were randomly deviated within an interval ±20% with respect to the reference values, as shown in Table 13.

Table 13 Values used to check the robustness of the model

Variable	Symbol	Lower limit	Ref. value	Upper limit	Units
Optical efficiency Fresnex	η_{opt}	0.8×Ref	Data from Fresnex [9]	1.2×Ref	-
PV efficiency	η_{PV}	0.12	0.16	0.20	-
Maximum battery charging or discharging power	$MaxB$	2.4	3.0	3.6	kW
Battery charging efficiency	η_B	0.8	0.9	1.0	-
Sorption thermal efficiency	COP_{th}	0.5	0.55	0.6	-
Dry cooler electricity consumption	W_{dc}	0.8×Ref	Eq. 5.6 of [10]	1.2×Ref	kW
Heat pump cooling power	Q_r	0.8×Ref	Eq. 6.4 of [10]]	1.2×Ref	kW
Heat produced by the compressor	Q_{comp}	0.8×Ref	Eq. 6.5 of [10]	1.2×Ref	kW
Buffer tank thermal resistance	R_{buffer}	350.0	403.3	456.6	K/kW

RPW-HEX thermal resistance	$R_{RPW\text{-}HEX}$	350.0	425.5	499.0	K/kW
DHW tank thermal resistance	R_{DHW}	650.0	830.8	1061.6	K/kW

No significant deviations (less than 2%) were observed in the results obtained with the deviated values of the model parameters, confirming that the accuracy of the simplified models is not a key point of the smart control strategy.

In addition to the optimisation based on the minimisation of operation cost of the system, other approaches could also be adopted to develop a smart control able to ensure an optimal operation of the system from the performance point of view. Such approaches could rely on the use of some of the key performance indicators (KPIs) identified in Task 1.5 and reported in deliverable D1.3 [5]. Among all KPIs identified within Task 1.5 activities, the share of renewables was selected as a key KPI to be considered in the objective function of the smart optimisation algorithm from an energy efficiency perspective.

According to deliverable D1.3 [5], the most common definition of the share of renewables is given by the ratio between the energy demand ($E_{RES(el,th)}$) covered by renewable energy sources (RES) over the total energy demand ($E_{D(el,th)}$), as shown in the equation below:

$$SR_{(el,th)} = \frac{E_{RES*(el,th)}}{E_{D(el,th)}} \cdot 100$$

where sub-indexes *el* and *th* refer to the electric or thermal generation or demand. It is important to consider that, in order not to underestimate the share of renewables, the $E_{RES*(el,th)}$ should consist of three attributes, which are:

- $E_{RES-onsite\,(el,th)}$: renewable energy produced onsite that is directly used to cover the demand (either electrical or thermal) over a time interval;
- $E_{RES-stored\,(el,th)}$: renewable energy coming from electric or thermal storage and used to cover the demand in the considered time interval; and
- $E_{RES-gridFactor\,(el,th)}$: quantity of the energy coming from the grid that is given by RES.

This last attribute considers the contribution of renewable energy sources to the energy mix of the electricity grid or district heating. This factor changes substantially from one European country to another and from one day to another; therefore, it should be considered different for different locations of the system and seasons.

In the case of the theoretical Mediterranean HYBUILD system, the thermal demand is entirely met by renewable energy sources (Fresnex solar collectors), so the share of renewables for thermal energy will be constant and equal to 1. Therefore, the KPI that was used in the optimization algorithm is the electrical share of renewable (SR_{el}) defined in the equation below:

$$SR_{el} = \frac{E_{RES,HP} + E_{RES,aux}}{E_{HP} + E_{aux}} \cdot 100$$

where $E_{RES,HP}$ (in kWh) is the renewable energy consumption of the heat pump, $E_{RES,aux}$ (in kWh) is the renewable energy consumption of all auxiliary equipment, E_{HP} (in kWh) is the total energy consumption of the heat pump, and E_{aux} (in kWh) is the total energy consumption of the auxiliary equipment.

The renewable energy consumption of the heat pump ($E_{RES,HP}$) is calculated using the following equation:

$$E_{RES,HP} = (x_G \cdot HP_G + x_B \cdot HP_B + HP_{PV}) \cdot \Delta t$$

where x_G is the share of renewable energy of the grid, x_B is the fraction of energy stored in the battery that was charged from renewable energy sources, HP_G (in kW) is the electricity consumption of the HP from the grid, HP_B (in kW) is the electricity consumtion of the HP from the battery, and HP_{PV} (in kW) is the electricity consumption of the HP from the PV panels during a given time interval (Δt).

The share of renewable energy of the grid (x_G) can be obtained from different sources available on the web. In this study, data from the Spanish electricity network webpage [11] was used because it is the one more familiar to the authors of this research. An example of the share of renewable evolution during one-week period is shown in Figure 69.
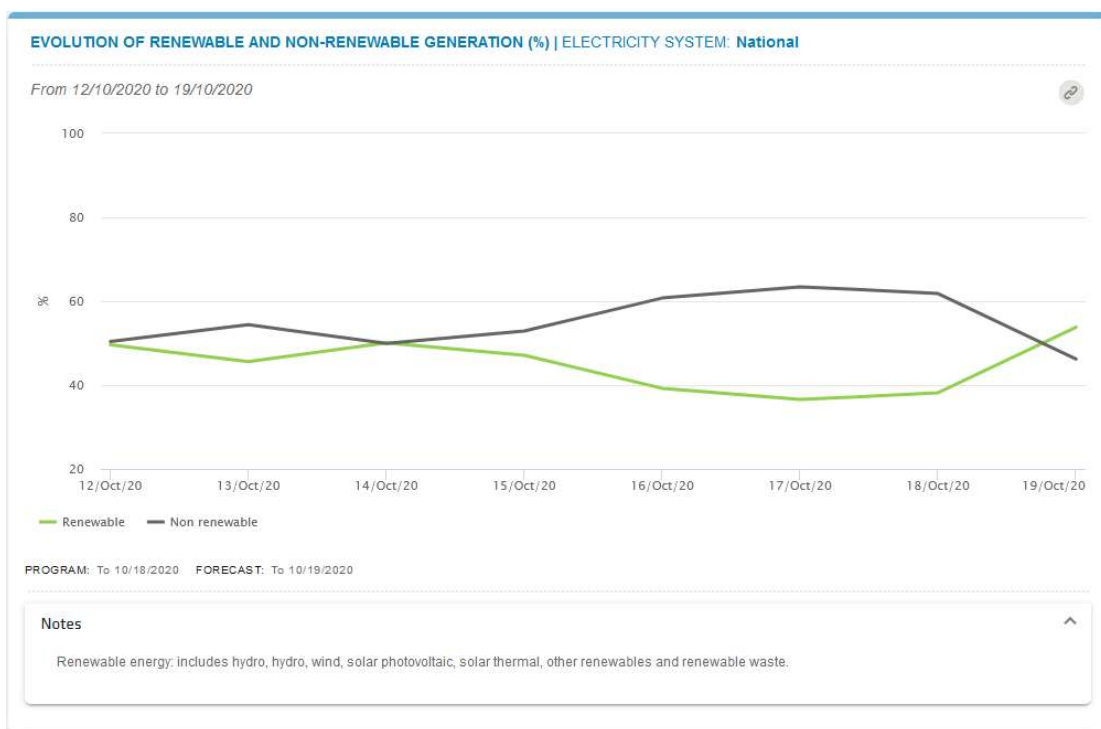
Figure 69 Evolution of the share of renewable during one week in Spain [11]

For the sake of simplicity, we will refer to x_B as the *fraction of renewable energy stored in the battery*. This variable is defined as the amount of energy stored in the battery that came from renewable energy sources divided by the total amount of energy stored in the battery. Since there is one operation mode in which the battery can also be charged with electricity from the grid, this variable is time-dependent because of variations in the share of renewable of the grid and also in the availability of renewable energy along a given time period. Therefore, at any time t, x_B can be calculated from its value at the previous time step ($t - \Delta t$), knowing the operation mode of the DC-bus, PV panels production, and the share of renewables of the grid (x_G).

Battery charging mode

In this mode, the battery is charging at the maximum charging power of the battery, $MaxB = 3$ kW, with electricity from the grid and possibly also from the PV panels. The fraction of renewable energy stored in the battery at time step t ($x_{B,t}$) can be obtained from the following equation:

$$x_{B,t} = \frac{x_{B,t-\Delta t} \cdot B_{S,t-\Delta t} \cdot C_{B,max} + \eta_B \cdot \left(B_{PV} + x_{G,t-\Delta t} \cdot B_G\right) \cdot \frac{\Delta t}{3600}}{B_{S,t-\Delta t} \cdot C_{B,max} + \eta_B \cdot MaxB \cdot \frac{\Delta t}{3600}}$$

where $x_{B,t-\Delta t}$ is the fraction of energy stored in the battery at the previous time step ($t - \Delta t$), $B_{S,t-\Delta t}$ is the state of charge of the battery at the previous time step ($t - \Delta t$), $C_{B,max} = 7.3$ kWh is the maximum storage capacity of the battery, $\eta_B = 0.9$ is the efficiency of battery charging process, B_{PV} (in kW) is the power supplied to the battery from the PV, $x_{G,t-\Delta t}$ is the share of renewable energy of the grid at the previous time step ($t - \Delta t$), B_G (in kW) is the power supplied to the battery from the grid, and Δt (in seconds) is the time step.

Battery buffer mode

In this mode, the battery is disconnected from the grid, but it can be charging or discharging, depending on the relation between the PV generation and the heat pump consumption. The fraction of renewable energy stored in the battery at time step t ($x_{B,t}$) can be obtained from the equation below:

$$x_{B,t} = \begin{cases} x_{B,t-\Delta t}; & if\ HP > PV \\ \dfrac{x_{B,t-\Delta t} \cdot B_{S,t-\Delta t} \cdot C_{B,max} + \eta_B \cdot B_{PV} \cdot \dfrac{\Delta t}{3600}}{B_{S,t-\Delta t} \cdot C_{B,max} + \eta_B \cdot B_{PV} \cdot \dfrac{\Delta t}{3600}}; & if\ HP \leq PV \end{cases}$$

Battery discharging mode

In this mode, the battery is discharging at the maximum discharging power ($B = -MaxB = -3$ kW) to the grid and possibly also to the HP, so that electricity cannot flow towards the battery. Therefore, since there is no income of renewable energy to the battery, the fraction of renewable energy stored in the battery remains unchanged, i.e. $x_{B,t} = x_{B,t-\Delta t}$.

The renewable energy consumption of all auxiliary equipment ($E_{RES,aux}$) is the addition of the renewable energy consumption of the DHW tank electric heater, circulation pumps, controllers, dry-cooler, and fan-coils. Since all these auxiliary components are directly connected to the grid, $E_{RES,aux}$ will only depend on the share of renewable of the grid (x_G), as shown in the following equation:

$$E_{RES,aux} = x_G \cdot E_{aux}$$

The results obtained for a test period of 18 days during the cooling season using an optimisation approach based on the share of renewable were then compared with the results obtained using a cost minimisation approach, as shown in Table 14.

Table 14 Optimal cost policy vs. optimal efficiency policy

Policy	Total cost (€)	Average SR_{el} value (%)
Optimal cost	11.3	52
Optimal efficiency	27.0	62

From Table 14 it is clear that the approach based on the maximisation of the share of renewable does not provide good results from the point of view of operation cost, while only achieving a 10% increase in the average value of the share of renewable. Further improvement could still be possible in the case of energy efficiency-based policy, if a multi-objective optimisation based on both cost and energy efficiency were applied.

Therefore, depending on the objective of the control strategy, the behaviour of the smart control can be distinct in each case and very different results can be obtained.

To see the different behaviour of the system as a result of the two optimisation policies, some of the main system parameters are plotted in Figure 70 for a test period of 18 days during the cooling season.


(a)

(b)
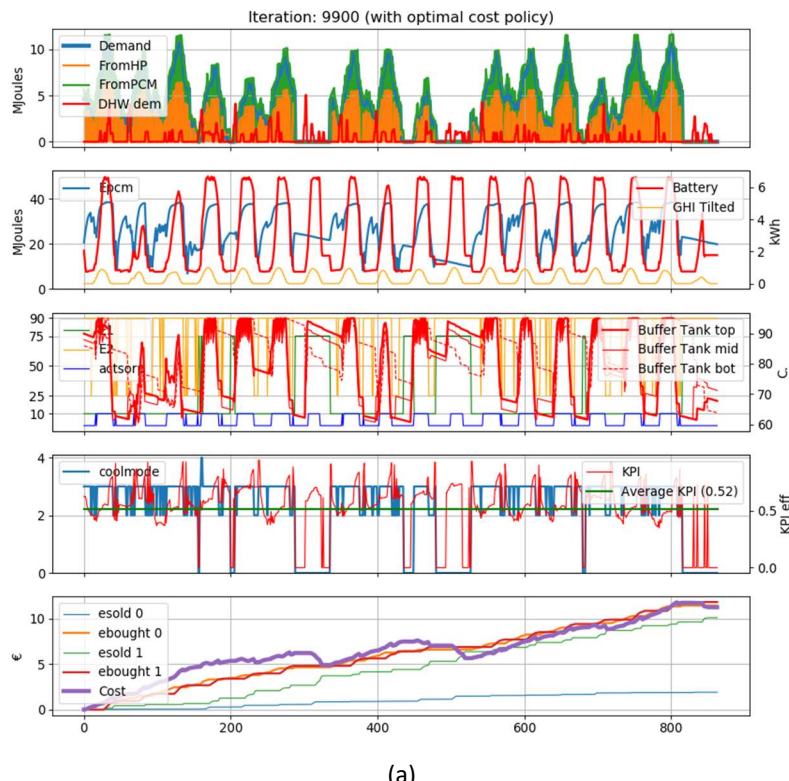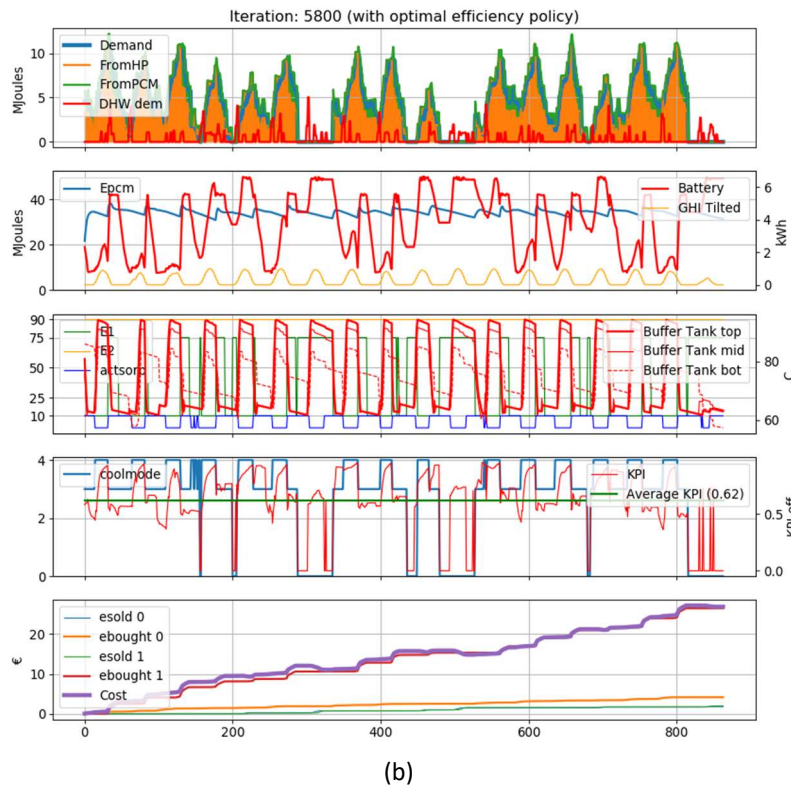
Figure 70 Comparison between the (a) optimal cost and (b) optimal efficiency policies

One of the main and key differences between the two optimisation policies is the behaviour of the electric battery. As can be seen in the second chart of Figure 70(a), the battery is fully exploited in the cost-optimisation policy, meaning that it is fully charged (up to the maximum allowed charging level of 90% of battery capacity) during periods of high solar radiation and/or low electricity price, and fully discharged (up to the minimum allowed charging level of 10% of battery capacity) during high electricity price periods. On the contrary, the full potential of the battery is not exploited in the optimal efficiency policy, since it rarely reaches a full charge or discharge level, as shown in Figure 70(b).

Another main difference in the control behaviour of the two policies consists in how the latent storage is managed. While in the cost-optimisation policy case the latent storage is exploited, in the optimal efficiency policy case the latent storage is never used, as can be seen by comparing the second charts of Figure 70(a) and Figure 70(b), respectively.

Finally, another difference that can be observed is the behaviour of the temperature evolution inside the buffer tank. By looking at the third charts of Figure 70(a) and Figure 70(b), it can be seen that, using a cost-optimisation policy, water temperature inside the buffer tank exhibits an irregular behaviour and that it is not always fully exploited. On the contrary, using an optimal efficiency policy, the buffer tank has a very regular behaviour, and it is fully charged during high solar radiation periods and fully discharged afterwards.

4.2   Flexibility optimisation results

ENG approach to BEMS optimisation is based on the exploitation of the flexibility of the building, in the perspective of the provision of auxiliary services to an hypothetical Distribution Service Operator (DSO) to support the stability of the distribution grid. It relies upon a multi-objective optimisation framework performed by the implementation of a heuristic algorithm, the Non-

dominated Sorting Genetic Algorithm II (NSGA-II). The algorithm has been described in D4.3, and its main aspects are briefly recalled in the appendix to this deliverable for sake of completeness.

4.2.1   Summer season tests

In this paragraph, a typical summer day optimisation for the MED reference building is presented. The objective is to demonstrate that the building is able to follow a particular energy consumption profile (total electric supply taken from the grid) as requested by the DSO as ancillary/auxiliary service to the grid, and at the same time to guarantee the comfort of the inhabitants, maintaining the temperature at the desired setpoint.

The test have been done setting the algorithm parameters as a population of 50 individuals (i.e., a complete of set decision variables in the entire time horizon), and 20 generations (i.e., iterations of the genetic algorithm). This configuration takes less than 25 minutes, which is a good compromise in day-ahead conditions. This can be reduced by setting lower population and generation values, as an example in case of a necessary reconfiguration and replanning at run time. In the followings, a specific analysis of the execution time will be given. The next chart reports the major evidence of the optimisation approach. The simulated DSO request to fulfill is shown in blue, with its tolerance depicted with dashed lines. The algorithm aims at demonstrating that the system can exploit the building storages, as well as can manage the PV production with the charging and discharging of the battery according the request from the DSO. The DSO request is fulfilled while constantly maintaining the building and DWH tank temperatures at the desired values (25 °C and 48 °C). This is made possible considering the power demand profiles (resulting from dynamic simulation for both space cooling and DHW generation) as *constraints* for the optimisation. The electricity absorption profile of the building, estimated after the application of this optimization strategy, is represented by the green bars. As it can be appreciated, the total consumption is within the tolerance range, allowing to gain the incentive or reward agreed with the DSO for the provision of such a service.

Figure 71 Optimal building power demand to maintain the building and DHW temperatures at desired setpoints (25 °C and 48 °C) and fulfilling at the same time the provisioning of flexibility services to the grid (summer)

This kind of approach is useful to fulfil the requirements for the optimization of the flexibility KPI reported in D1.3 [5], which defines the ability of the building to follow a predetermined consumption profile, externally provided, without specific focus on the cost and/or system efficiency. Nevertheless, the economical sustainability of this second approach can be guaranteed as well in case of rewarding mechanism by the DSO for the provision of such a kind of service [12].

The software developed by ENG includes a simulation module used inside the algorithm execution, which share the same simplified component models developed by UDL and used inside the cost/efficiency optimiser. This guarantees coherence between the results of the two different approaches. As already introduced, the optimiser produces several charts and commands as results of its elaborations: in the following figures, some of the charts coming from the simulations for the modelled building components are reported.
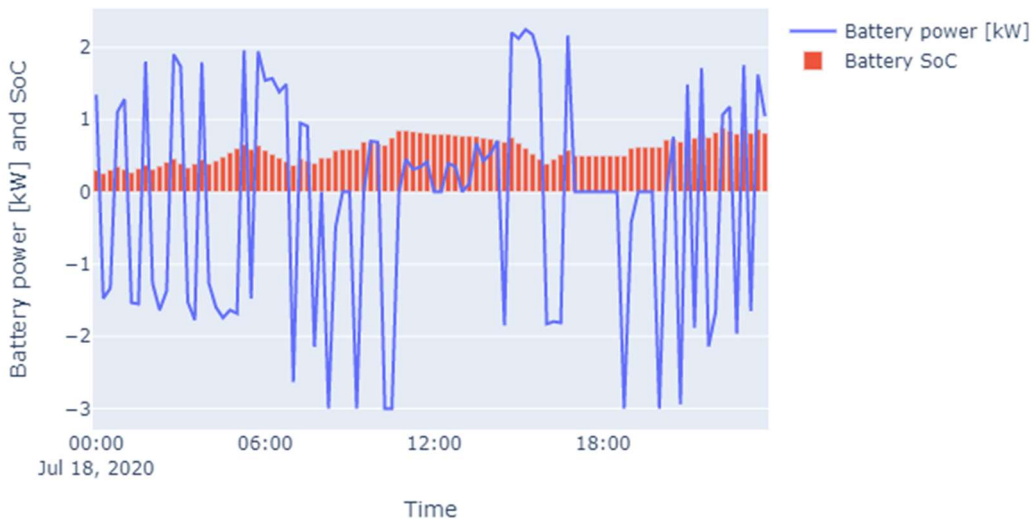

Figure 72 Electrical battery utilisation in case of flexibility service provisioning (summer)

Figure 73 Latent storage utilisation in case of flexibility service provisioning (summer)

In particular, the charts highlight the contribution over the day given by the two storage systems: the electrical battery and the RPW-HEX system. Leveraging on the flexibility provided by these devices, thus exploiting their capability in absorbing and injecting electricity and thermal power, the fulfillment of DSO request and the related economic rewards are possible, while assuring the comfort of the building inhabitants maintaining the inner temperature at 25 °C.

4.2.2 Winter season tests

The flexibility optimization has been tested also for the winter period. In the following picture, an example of results coming from the simulated implementation of the flexibility optimization in the winter season is reported. In this case, the execution was done on February 26th, the setpoint for the inner temperature was set at 20 °C and thermal/electrical demand for the winter season have been used, as well as the weather forecast and radiance data for the day after in Athens. DHW temperature setpoint has been maintained at 48 °C as in the summer season.

Figure 74 Optimal building power demand to maintain the building and DHW temperatures at desired setpoints (20 °C and 48 °C) and fulfilling at the same time the provisioning of flexibility services to the grid (winter)

In this case, a typical Demand-Response (DR) service was simulated, e.g., a *peak shaving* request from an hypothetical DSO, which has cognition of the topology of the grid and the forecasted consumption/production capacity of the *prosumers* connected to the grid (i.e., "consumers" which can act also as "producers"). In this simulation, the HYBUILD system is intended to be run into one of these prosumers and to collaborate with the DSO to support the stability of the grid. At the same time, the HYBUILD system must be able to provide the necessary heating to the building, which is always seen as the main priority in any case. The results of the optimization demonstrates that the HYBUILD system, also in the winter season, is able to maintain the temperature of the building at the desired setpoint (20 °C) guaranteeing at the same time an almost constant power consumption/supply profile to the grid, i.e., avoiding "peaks" in power demand/supply, always inside the tolerance thresholds. The possibility of avoiding intermittent and fluctuant power consumption/production is a valuable support to the grid, which can be rewarded by the DSO as a form of incentivisation/compensation to mitigate the energy purchase costs and make convenient to the prosumer the participation to this kind of DR program [13].

Also in this case, the fulfilment of such a kind of service is possible by means of the exploitation of the HYBUILD storage systems. In particular, in this case, the provisioning of this DR service to the DSO is performed by means of the orchestration of heating and DHW modes, and electrical battery management, as reported in the following figures.

Optimised battery data
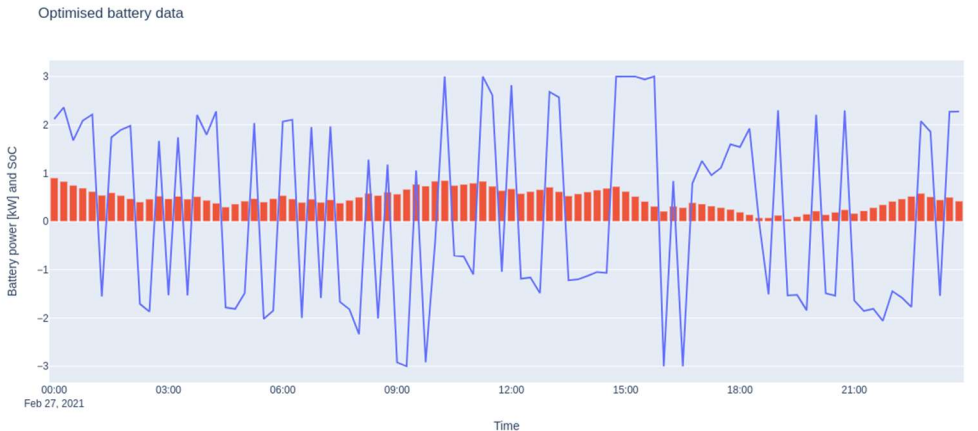
Figure 75 Electrical battery utilisation in case of flexibility service provisioning (winter)

Major electric power flows
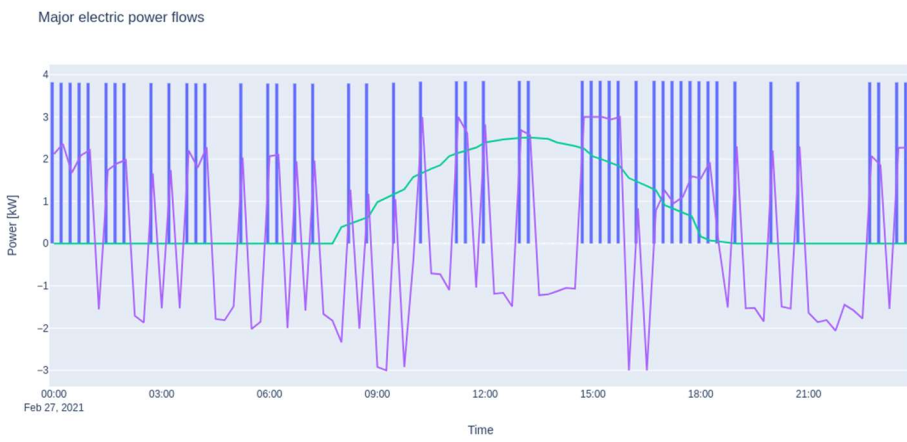
Figure 76 Main power consumption indicators in case of flexibility service provisioning (winter)

4.2.3   Comparatives and next steps

Another interesting aspect of the flexibility optimiser has been analysed, once a number of simulations have been run and results collected. As reported in the appendix, the main parameters for the configuration of the AI-based algorithm used for the flexibility optimiser are basically the number of individuals composing the population and the number of generations for which the genetic algorithm is run. The flexibility optimiser has been run with a different combinations of these parameters, with the same external inputs provided. Then, slightly different inputs have been provided to the algorithm with the same configuration of the parameters, in order to test the variations in terms of quality of the obtained results and time of execution.

In the following table, the summary of these tests is reported. The table is ordered by value in the first column, which calculates the value of the objective function minimised by the genetic algorithm. It is directly referrable to the flexibility KPI reported in D1.3 [5] (the less, the better), so indicating the adherence of the total power consumption profile to the given one. The fifth column, instead, reports the average execution time (in minutes) for the tests executed with the same number of individuals (second column) and generations (third column). As it can be seen in the fourth column, tests have been done for both the MED system and a reduced adapted one representing the system that will be deployed in the AGL demo site.

Table 15 Flexibility optimiser results and execution time indicators

electric_opt	population	generations	buildingName	executionTime
8.127359245	25	50	MED	108.4634
8.207933048	25	100	MED	150.0034
8.256781632	30	50	MED	119.8760
8.271906541	25	10	MED	19.6141
9.214493975	30	10	MED	20.4835
11.02241302	20	10	MED	18.6154
15.36130704	30	100	AGL	168.2073
15.85292870	20	100	AGL	116.5275
17.07532146	30	200	AGL	371.8926
17.54606961	30	50	AGL	77.0142
17.56539562	20	50	AGL	48.5938
24.32812856	25	10	AGL	21.8759

In all cases, the execution time is fully compatible with the requirements of a day-ahead optimisation, spanning from less than 20 minutes to not more than 3 hours (excluding stress tests not intended to be done in production). The parameter which mostly influences the time execution and quality of the results is the number of generations: from the tests executed, the number of individuals inside the population has a minor impact on the algorithm performances. Not surprisingly, the results for the theoretical MED system are generally better than the ones for the reduced system deployed in AGL since there are much more optimisations variables available. Instead, it is worth noting the very good performance of the algorithm, especially in the case of the HYBUILD MED system, also with "fast" configurations consisting of lower numbers of individuals and generations. This means that the algorithm may be successfully adopted also in all those cases in which a fast reconfiguration of the system is needed, e.g., in case of unexpected deviations from the initial simulation results, during the execution of the optimisation plan. This may happens, for example, as a consequence of the human behaviour or errors in the weather forecasts. Providing the algorithm with the new context data, and running the algorithm with lower parameters, generally allows to obtain a new plan in less than 20 minutes, coherent with the new different conditions. Being far more simpler, with also less constraints among the fewer optimisation variables, the effect of the increased number of individuals and generations in the second case (AGL) has a better impact than in the first case (MED). For this reason, in the case of the reduced system resembling AGL demo site, a day ahead optimisation with a higher number of individuals and generations makes more sense.

The flexibility optimiser has been fully implemented for the theoretical HYBUILD MED system, for which the simplified components models have been fully described [10]. Nevertheless, as shown before, the underlying algorithm has been shaped also for the reduced system which will be tested in Aglantzia. Preliminary simulated results have been obtained also for this reduced system which must be validated on site, once the deployment will be done.

In the case of the Continental demo site, a custom optimisation system has been produced in agreement with the demo owners, shaped in terms of practical rules which have been identified

and will be fully refined during the operational phase. The custom high level controller integrated in the BEMS for the CON system has been deployed in Langenwang and running 24/7 since December without any issue so far, and is designed to be integrated into the existing thermal control system described in appendix.

This work is part of the general topic of the adaptation of the BEMS for the different demo sites, which will continue beyond the end of WP4. The objective is to provide the demo sites with a customised control system, based on the RBC defined in D4.2 [2] and then refined by demo owners and technology providers to be implemented by ENG. A first adaptation have been done for all the demo sites. The control system is ready to be tested in the real demo sites, for further investigations and fine tuning.

As an example, in the following figure, the revised cooling mode flowchart for ALM demo site is shown, as a result of the field tests performed in CNR labs by ENG and ITAE, implemented and successfully tested with the same subsystem (electrical rack + HP + RPW-HEX + sorption module) that will be deployed in Almatret.
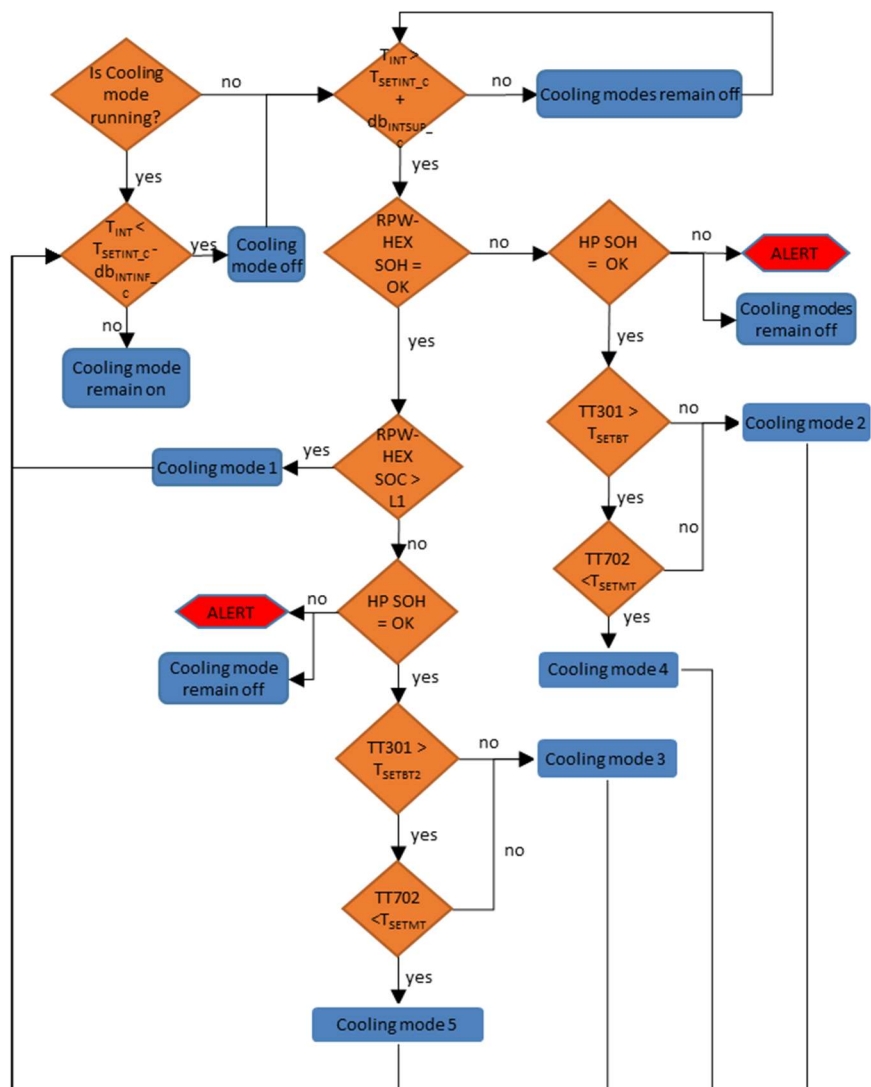

Figure 77 Basic control rules adapted for ALM demo site after the first experimental results

5 Conclusions

In this document the performances of the HYBUILD system applied to the HYBUILD MED and CON buildings have been reported, for both the RBC and the optimised control.

HYBUILD MED and CON system have been modelled and simulated, coupled with the specific reference building. Simulation results in terms of already defined PIs for the two studied HYBUILD systems have been reported. These results allow a useful evaluation of systems performance at both sub-system level (L2) and overall building system level (L3). Moreover, through the additional analysis reported, it has been presented which difficulties emerge when dealing with optimization of the control strategy in complex systems, as the ones proposed in HYBUILD, where the interactions between the different components become crucial and, therefore, an overview of the whole system is fundamental.

Smart control based on artificial intelligence techniques were proved to provide better results than simple rule-based control strategies. Depending on the variable that is intended to be optimised, the smart control is able to reduce system operation costs or to enhance the performance of the system in terms of energy efficiency. However, further investigation might still be needed to find potential ways to improve the smart control strategy by using suitable optimization functions able to provide optimal results in terms of stakeholders requirements.

The potentialities of the HYBUILD system in terms of provisioning of flexibility service inside the participation to hypothetical DR programs have been explored, as well. The HYBUILD system has been proven to be able to follow specific consumption profiles given by an hypothetical DSO to support the stability of the grid. Specific technical requirements may emerge during the operational phase: we expect that this may led to the definition of the set of the conditions in which the execution of such a kind of optimisation is valid and convenient or not. In this sense, the rapidity of the algorithm in finding new solutions also with lower values for the configuration parameters is an added value, which may allow to quickly rearrange the system accordingly.

The knowledge acquired through the detailed analysis of HYBUILD systems performance in different operational modes, constitutes an important outcome of this work and will be used also in future to improve the HYBUILD systems exploitation.

6 References

[1] HYBUILD D4.1 - Smart system algorithms.

[2] HYBUILD D4.2 - Functional requirements specification.

[3] HYBUILD D4.3 - HYBUILD optimised building management system.

[4] HYBUILD D3.1 - Modular flow sheet simulation of the hybrid (sub-)system.

[5] HYBUILD D1.3 - Requirements: Key Performance Indicators, system components and performance targets.

[6] HYBUILD D1.1 - Requirements: context of application, building classification, and dynamic uses consideration.

[7] Emhofer, Johann & Marx, Klemens & Barz, Tilman & Hochwallner, Felix & Cabeza, Luisa F. & Zsembinszki, Gabriel & Strehlow, Andreas & Nitsch, Birgo & Wiesflecker, Michael & Pink, Werner. (2020). Techno-Economic Analysis of a Heat Pump Cycle Including a Three-Media Refrigerant/Phase Change Material/Water Heat Exchanger in the Hot Superheated Section for Efficient Domestic Hot Water Generation. Applied Sciences. 10. 7873. 10.3390/app10217873.

[8] Eurostat, https://ec.europa.eu/eurostat/web/energy/data/shares, available on-line: 15.03.2021.

[9] Hartmut Schneider, Fresnex. Output simulation results_Fresnex collector_no cover_2020-04-27.xlsx; 2020.

[10] Gabriel Zsembinszki, Cesar Fernandez, Luisa F. Cabeza, UDL. Description of the simplified models for the optimisation of the Mediterranean theoretical HYBUILD system; *Report_models_for_CONTROL_MED_v7*; 2020.

[11] Red Eléctrica de España. https://www.ree.es/en. Last checked in September 2020.

[12] D. Arnone, F.S. Nucci, G. Paternò, A. Rossi, M. G. Ippolito, E. Riva Sanseverino, G. Tondi, F. Cazzato, S.E. Jenkins. Simulation-based analysis of the potentiality of incentives for prosumer flexibility. First South East European Regional CIGRÉ Conference. Portoroz, Slovenia, 7—8 June 2016.

[13] Croce, Vincenzo & Raveduto, Giuseppe & Verber, Matteo & Ziu, Denisa. (2020). Combining Machine Learning Analysis and Incentive-Based Genetic Algorithms to Optimise Energy District Renewable Self-Consumption in Demand-Response Programs. Electronics. 9. 945. 10.3390/electronics9060945.

[14] influxDB, https://www.influxdata.com/

[15] OPC UA, https://opcfoundation.org/about/opc-technologies/opc-ua/

[16] Modbus, https://modbus.org/

[17] MQTT, https://mqtt.org/

[18] Node-RED, https://nodered.org/

[19] Grafana, https://grafana.com/

[20] Python, https://www.python.org/

[21] Docker, https://www.docker.com/

[22] Postgres, https://www.postgresql.org/

7   Appendixes

7.1   Details about the BEMS implementation

In this paragraph, we briefly present the software architecture designed and implemented, for the monitoring and control of the demo sites and the evaluation of the system performance. In the following picture, the software architecture is shown.
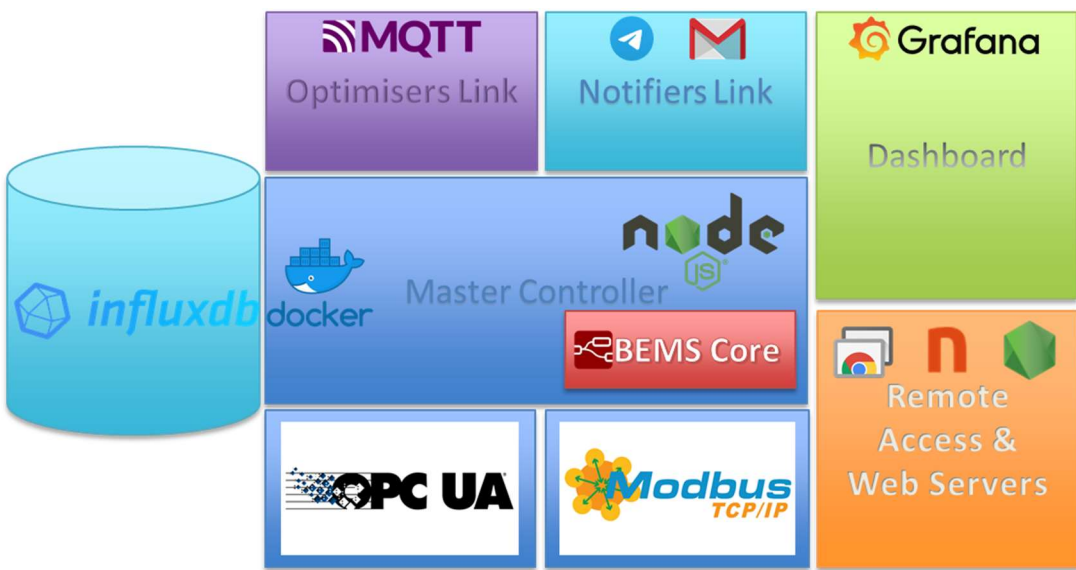
Figure 78 Sofware architecture of the BEMS

The BEMS is mainly composed by the following modules:

- Master Controller: main module of the BEMS, responsible of the high level control of the demo sites (in RBC or optimised way); the core is responsible of the application of the basic control rules and all the basic ICT (Information and Communication Technology) processes of the platform (scheduling, interfacing and orchestration of the modules, configuration of the system, etc.);
- influxDB [14]: time series database used for the storage of the monitoring data and alarms;
- OPC UA [15] and Modbus [16] TCP/IP layer: link to the low level controller by means of standard protocol and interfaces for the monitoring and high level control implementation;
- Optimisers Link: higher layer for the link the optimisers by means of standard protocols (MQTT [17], but also HTTPS) for the optimised control of the building;
- Notifiers Link: tool for event notification, by means of instant messages or standard emails, especially for security reasons and communiations of relevant status changes to demo managers and maintainers;
- Dashboard: main local GUI (Graphical User Interface) for the visualisation of real-time and historical monitoring data, used also for the provisioning of data to external actors;
- Remote Access & Web Servers: mainly used for maintenance, it allows remote access to the platform for its administration, and the visualisation of the dashboard also remotely to the allowed users.

In particular, the BEMS core has been implemented in Node-RED [18], a flow-programming framework which has been proven as effective for the condivision of control mechanisms and is one of the cutting-endge technologies used nowadays in the IoT Iinternet of Things) field.

The BEMS interface, used for the manual or automatic control of the building, is composed by different applications and pages. In the following figure, the home page of the BEMS interface is shown.
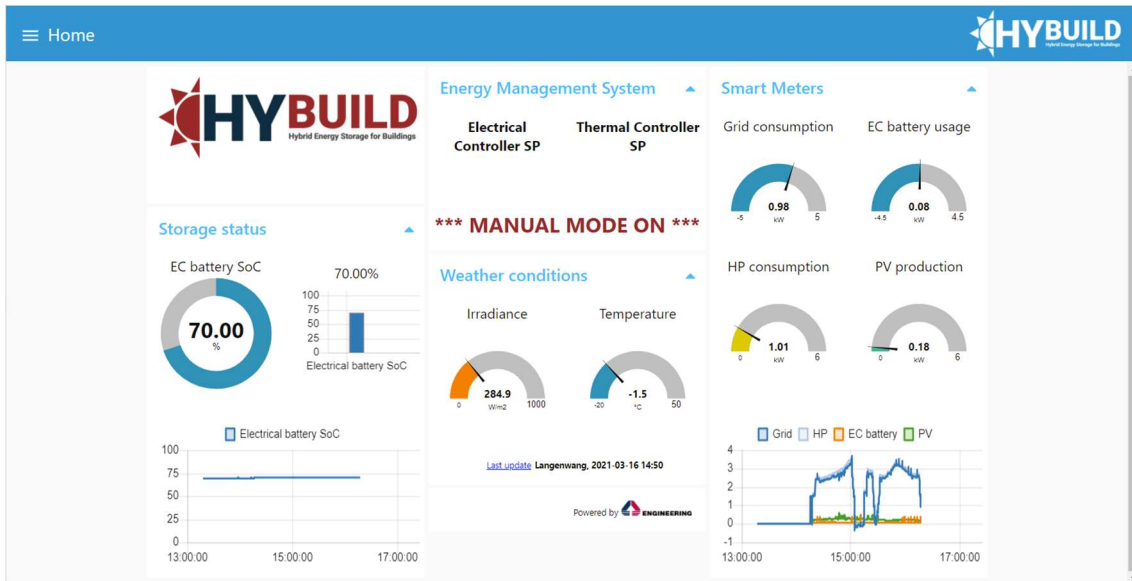

Figure 79 Home page of the BEMS interface

The interface is intended to be used locally by demo site managers and administrators for the high level control of the building. Three modalities have been implemented:

- Manual mode: used in case of direct human intervention, in case of maintenance or specific tests on the building components;
- Automatic mode: main modality of the system, implementation of the basic control rules adapted for each demo site (RBC);
- Optimisation mode: experimental modality used to run a plan provided by the different optimisers, in terms of sequence of OMs to be executed.

The BEMS Dashboard has been implemented with Grafana [19]: differently from the BEMS interface, it does not allow the control of the system, and is particularly suitable for the structured visualisation of the most important indicators of the demo sites. It is a candidate technology also for the following project activities about the data management and provisioning for public access. In the following figure an example of Grafana interface is given. The BEMS interface and Grafana dashboards share the same persistence layer, populated and maintained by the Master Controller, which guarantees coherence and interoperability of the data inside the platform.
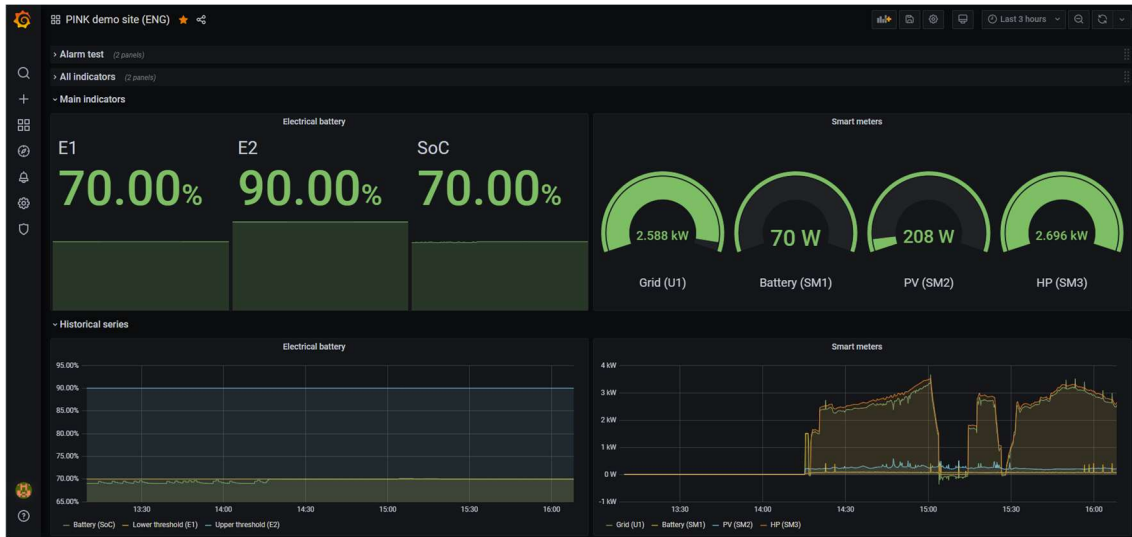
Figure 80 Grafana dashboards integrated with the BEMS

7.2 Flexibility optimisation process

The following picture shows a high level representation of the architecture and operations of the building flexibility optimizer. First, the initialisation layer is in charge of collecting all the relevant information about the building environment: the building configuration, the parameters of the optimisation itself, including the DSO request and the thermal demand. Then, the core layer addresses the optimisation process, starting from the mapping of the Operational Modes (OMs) to the presentation of the solutions. The last layer is dedicated to the visualization: at the end of the process some charts are displayed for evaluating the fulfillment of DSO request, the related economic assessment of this service provision and the data about the simulation of energy flows, temperatures and SoC.
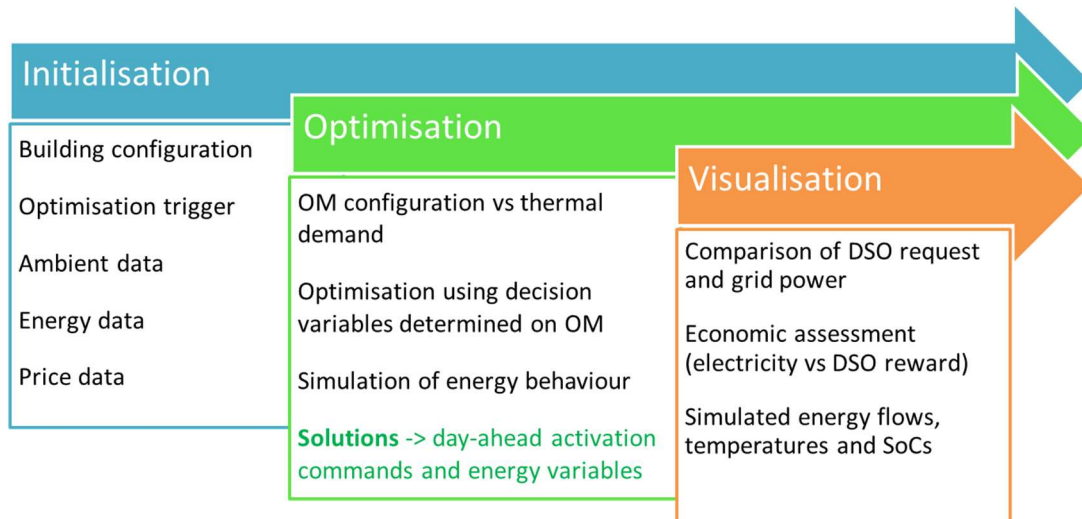

Figure 81 High level representation of the architecture and operations of the flexibility optimizer

The software algorithm proposed by ENG addresses the energy management of the building by means of a day-ahead approach implementing the multi-objective optimisation, so able to optimise simultaneously different objectives. In this case, it takes into consideration the provision of flexibility-as-a-service to network operators and the economic assessment related

82

to the balance between the operational cost (mostly supply of energy) and the DSO rewards. Technically, the *comfort* is handled as *constraints* for the optimisation problem (always satisfied), while the *power profile tracking* is handled as an *objective function*, which the genetic algorithm will try to maximise.

The algorithm starts by mapping the OMs with the thermal and DHW demands; the decision variables are shaped to reflect the OMs as well; so the genetic algorithm techniques are applied for scheduling and orchestrating these OMs to fulfill the objectives; during the optimisation, each possible solution is simulated for assessing its technical feasibility and to provide the needed information for the evaluation of the objectives; finally, the results are given in output, in terms of activation command and related energy variables that can be used as setpoints. For the complete details about the algorithm, please refer to the description presented in D4.3.

7.3 NSGA-II implementation

The Non-dominated Sorting Genetic Algorithm II is a frequently used evolutionary multi-objective optimization algorithm. The objective of the NSGA-II algorithm is to improve the adaptive fit of a population of candidate solutions to a Pareto front constrained by a set of objective functions. The algorithm uses an evolutionary process with surrogates for evolutionary operators including selection, genetic crossover and genetic mutation. The population is sorted into a hierarchy of sub-populations based on the ordering of Pareto dominance. Similarity between members of each sub-group is evaluated on the Pareto front, and the resulting groups and similarity measures are used to promote a diverse front of non-dominated solutions.

Considering V the number of critical variables, their optimal selection is the one that minimizes the M objective functions. Each set of V elements from the whole space of possible critical variables is considered an individual. The genetic algorithm proceeds to generate N individuals forming the initial population and calculating the M objective functions against each individual. A child population is then created combining the crossover and mutation genetic operators with μ and $\hat{\mu}$ probabilities. The two populations are then joined together and sorted based on the results of the objective functions. Finally, the best N individuals are selected to form a new population. This process is repeated G times, refining the population after each iteration.

We applied this process to find a subset of operational modes (OM) which, applied to the simulations of the related building, would provide the best results in terms of cost and proximity to demand.

The functionalities of the optimiser are exposed to the operators and to the others software components of the platform by the optimisation server, via a dedicated REST API. The optimisation server already includes the software models describing the behaviour of the assets characterizing each of the buildings included in the trials, such as PV production, power consumption for space cooling/heating, or DHW thermal demand. The API takes as parameters a building identifier (e.g., *Aglantzia*, *Almatret,* or *Athens*) and the building type (i.e., *Mediterranean* or *Continental*), together with the parameters specific for each optimisation request: energy price, heating price, DHW comfort temperature, thermal comfort temperature, the DSO request profile, and the request rewards. The optimiser fetches the weather data needed for the simulation (e.g., temperature, wind speed, solar radiation) from the weatherbit.io service. For this reason, it is necessary to include a valid weatherbit API key in each of the requests.

The actual optimisation takes place asynchronously, using MQTT. Each optimisation request is associated with a unique identifier, which is returned as part of the HTTP response body. Once

complete, the optimisation result is published on the MQTT queue using the following topic specifier:

```
/optimisation/[building_name]/[request_identifier]
```

In this way, it is possible for a client to subscribe to a specific request using the full topic, to subscribe to everything related to a specific building (without the need to specify a request identifier), or to subscribe to every optimisation result (not specifying the building name nor the request identifier).

7.4 Platform Deployment

The optimisation server has been developed in Python [20] and released as a software container image. Containers do not require dependencies on the hosting machine, reducing the complexity for operation and resulting extremely easy to replicate. The host system runs each software container through a daemon (with Docker [21] being the most used of them), which usually is also able to fetch for the updates container images every time an application has been updated.

The optimisation server comes already with a pre-configured set of sidekick containers needed by the main application such as a Postgres [22] database and a MQTT broker. The configuration is highly customisable, so it is possible, as an example, to replace the containerised database or MQTT broker with pre-existing ones simply replacing the appropriate environment variables. Other environment variables are used to customise the network settings or the behaviour of the optimiser: as an example, it is possible to change the number of generations or population to use (identified as G and N in the previous section).The pre-defined configuration is provided below, showing the three different software containers and the related environment variables:

```
version: "3.9"

services:
  app:
    build:
      context: .
      dockerfile: Dockerfile-app
    container_name: app
    hostname: app
    expose:
      - "3000"
    ports:
      - "3000:3000"
    environment:
      - DATABASE_HOST=postgres
      - DATABASE_PORT=5432
      - DATABASE_NAME=HYBUILD_BEMS
```

```
        – DATABASE_USER=hybuild
        – DATABASE_PASSWORD=password
        – MQTT_HOST=mosquitto
        – MQTT_PORT=1883
        – HOST=0.0.0.0
        – PORT=3000
        – POPULATION=25
        – GENERATIONS=10
  postgres:
    build:
      context: .
      dockerfile: Dockerfile-postgres
    container_name: postgres
    hostname: postgres
    expose:
      – "5432"
    volumes:
      – db-data:/var/lib/postgresql
    environment:
      – POSTGRES_DB=HYBUILD_BEMS
      – POSTGRES_USER=hybuild
      – POSTGRES_PASSWORD=password
  mosquitto:
    image: eclipse-mosquitto:1.6.12
    container_name: mosquitto
    hostname: mosquitto
    expose:
      – "1883"
      – "9001"
    ports:
      – "1883:1883"


volumes:
  db-data:
```

7.5 CON thermal control

As reported in the body part of the deliverable, in the case of the CON system, the high level control and the optimisation layer have been fused into a single set of practical rules that integrates and extends the already existent thermal controller in the CON system. The set is in its early stage of definition, since it is intended to be progressively extended during the curse of the operations according the the experimental results collected, the emerging needs and

feedback. In the following figure, the first set of rules implemented in Nod-RED inside the BEMS core provided to the CON system is shown.
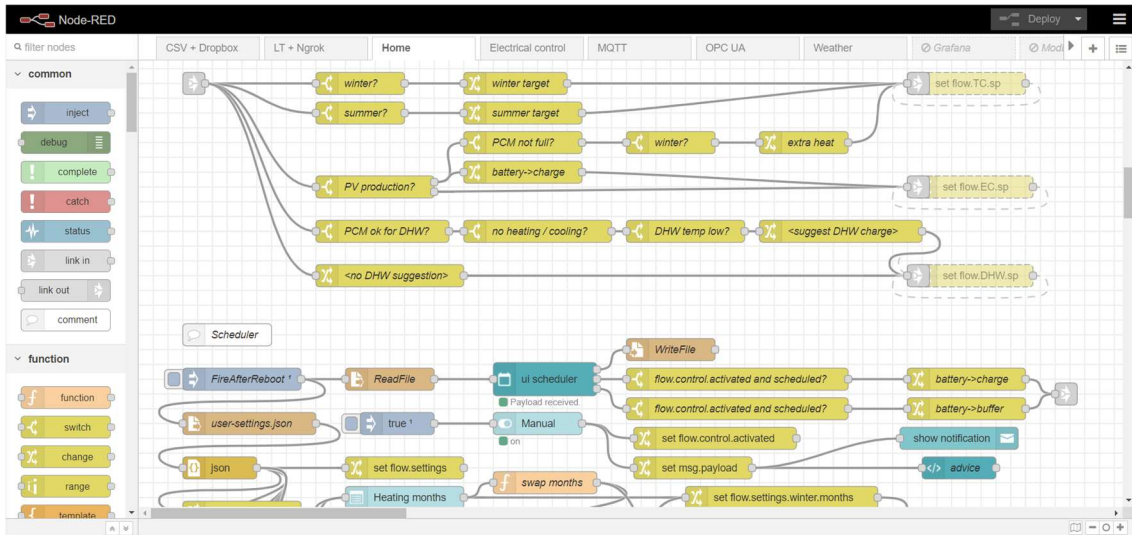

Figure 82 Pratical rules implementation in the CON system

The rules have been deployed, as well as the entire BEMS platform, in PINK demo site, and have been running 24/7 since last December without any major issue so far. The BEMS platform has been enriched with a set of tools to integrate all the functionalities not covered by the existing thermal controller, such as the control of the electrical rack, as shown in the following picture.
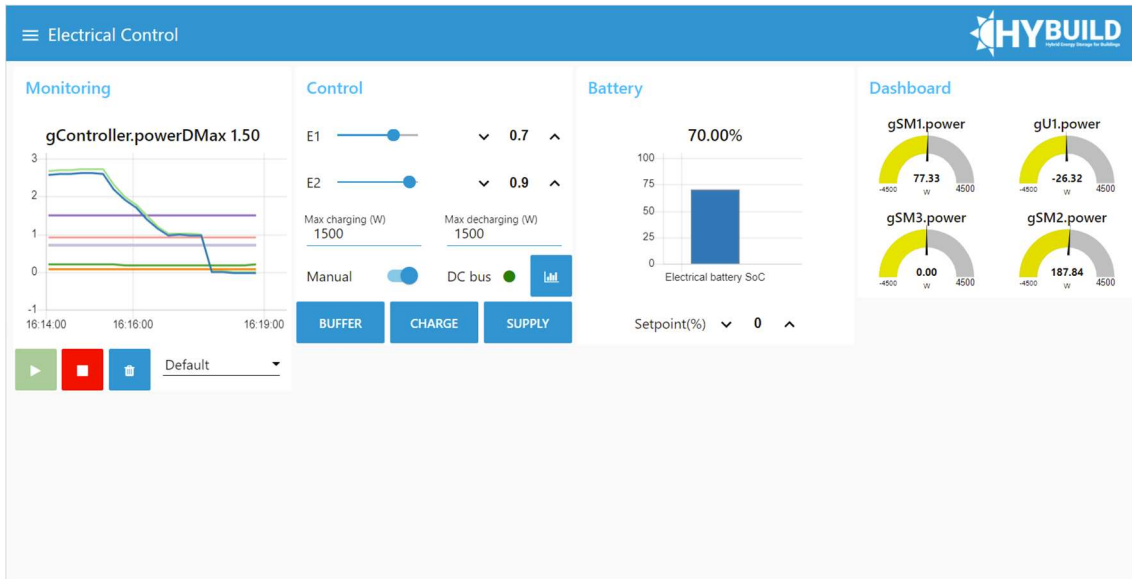
Figure 83 Electrical control interface of the BEMS

In general, the implemented practical rules aim at the maximisation of the exploitation of renewable energy sources, with the full charge the electrical battery and the latent storage when energy is produces by the PV. Since stand-alone charging modes are not available in the CON system, i.e., without the simultaneous provisionin of space heating or cooling, for the particular design of the CON system itself, the optimiser will exploit the building thermal storage with a period of extra heating or extra cooling to fill up the latent storage. The same considerations will apply also in case of low tarif periods, in order to minimise the cost of the

energy purchase. The final version of these rules will be reported an analysed in later deliverables, when the first experimental data will ba available, allowing the fine tuning of this customised rule-based control system.

The thermal controller ensures the supply of the individual apartments with hot water as well as heating energy and possibly also cooling energy, because this affects not only the reliability of the energy supply but also the energy losses and thus the total energy consumption and the efficiency of the system.

A significant advantage of the decentralized storage of hot water compared to other systems is the constant availability of hot water, whereby a simultaneous operation of the supply network is not always necessary. The figure shows the possibility of hot water withdrawal with simultaneous shutdown of the supply lines. As a result, the heat loss of the supply lines, which can be up to 70% of the total energy demand in systems with decentralized water heating due to continuous operation, can be significantly reduced.
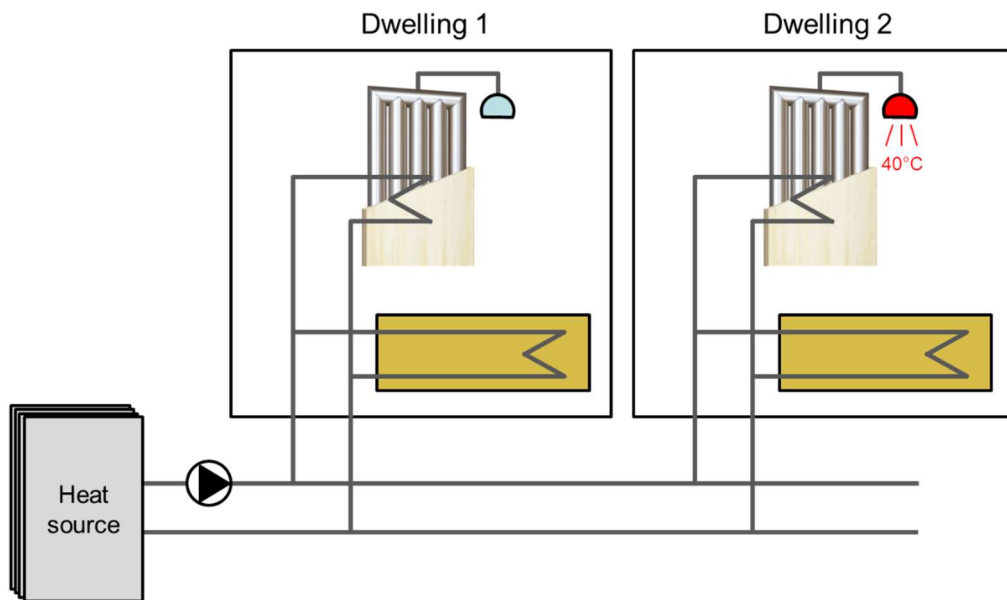

Figure 84 Scheme of water tapping during deactivated supply line

In this system the hot water is prepared by activating the supply lines while operating at high temperatures of 55 ° C, whereas this can be limited to short periods of the day and the remaining time can be completely deactivated.
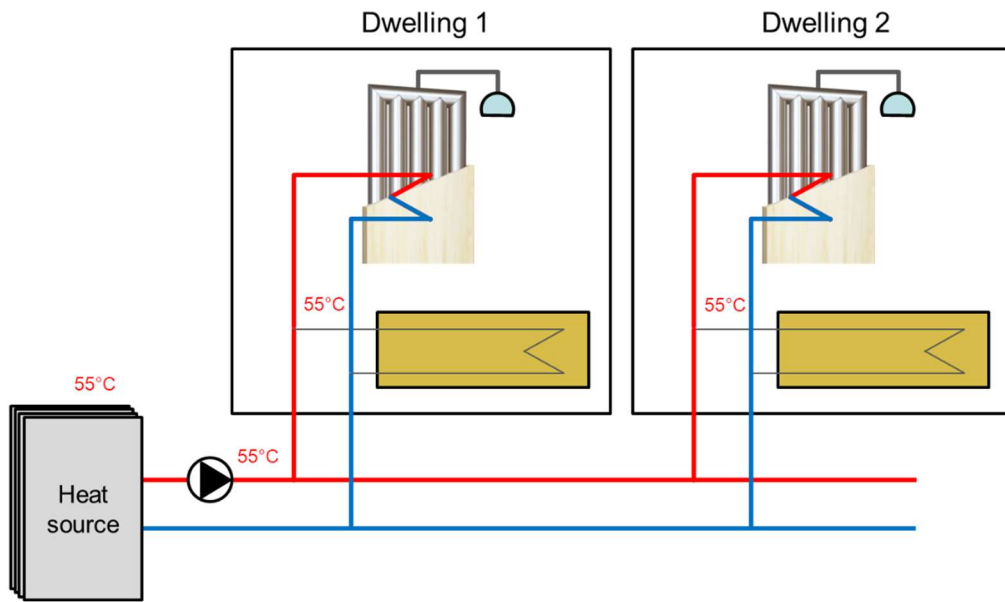
Figure 85 Scheme of DHW preparation with high temperatures in the supply line

During the heating season the system can, if a low-temperature heating system such as underfloor heating is installed in the dwellings, be operated at far lower temperatures, which can significantly reduce losses in the pipelines. As shown in the figure, the consumption of DHW is again possible at any time.
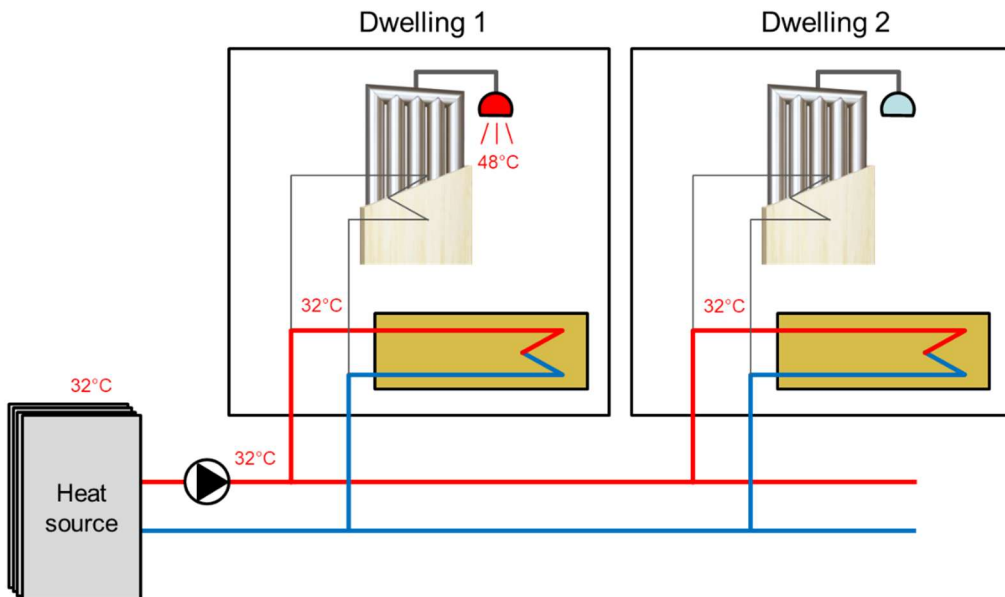

Figure 86 Scheme of heating with low temperatures in the supply line

The time sequence of two loading periods (DHW) at 5:00 am in the morning and 6:00 pm in the evening with flow temperatures of ~ 60 ° C as well as the heating periods (HEATING) of the building with flow temperatures of ~ 35 ° C is show over the period of a whole day in Figure 87. The measured data clearly shows the very short areas of around 1.5 hours, during which the supply system must be operated with high supply temperatures, the rest of the time a much lower supply temperature is sufficient.
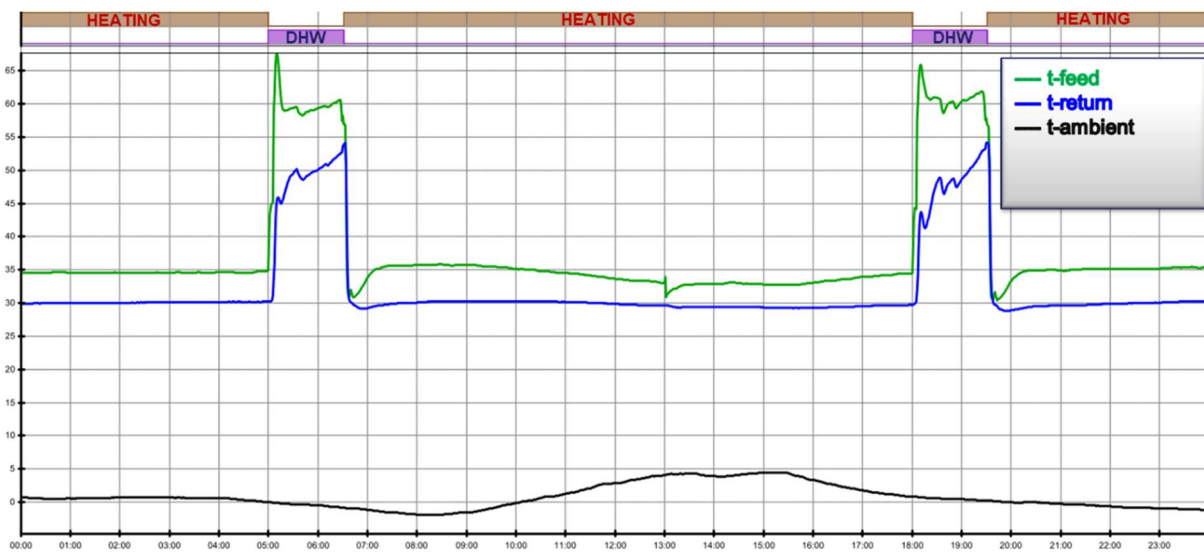
Figure 87 Time sequence of a whole day, with Heating and DHW preparation

However, a problem with a parallel DHW preparation of all storage tanks, which are integrated into a supply network, is given by the very large heat transfer, which results from the large temperature differences in combination with the large surface of internal heat exchanger.

The simulated values of the thermal load and the temperatures in the storage tank as well as in the supply system in Figure 88 clearly shows these issues, as system with three storage tanks is loaded parallel. At the beginning, the storage temperatures in the bottom range (t-0% to t-60%) are less than 20 °C (empty storage tank).

With a supply temperature of 60 °C a thermal power of the system (Q) of nearly of 24 kW (8 kW per tank) is reached at the beginning of the loading process. Only when the temperatures of the tanks rise due to the heating of the water, the load is reduced. For example, after 30 minutes the power has been decreased to 12 kW (4 kW per tank), after 100 minutes the storage tanks are fully loaded, and the thermal load is almost zero.
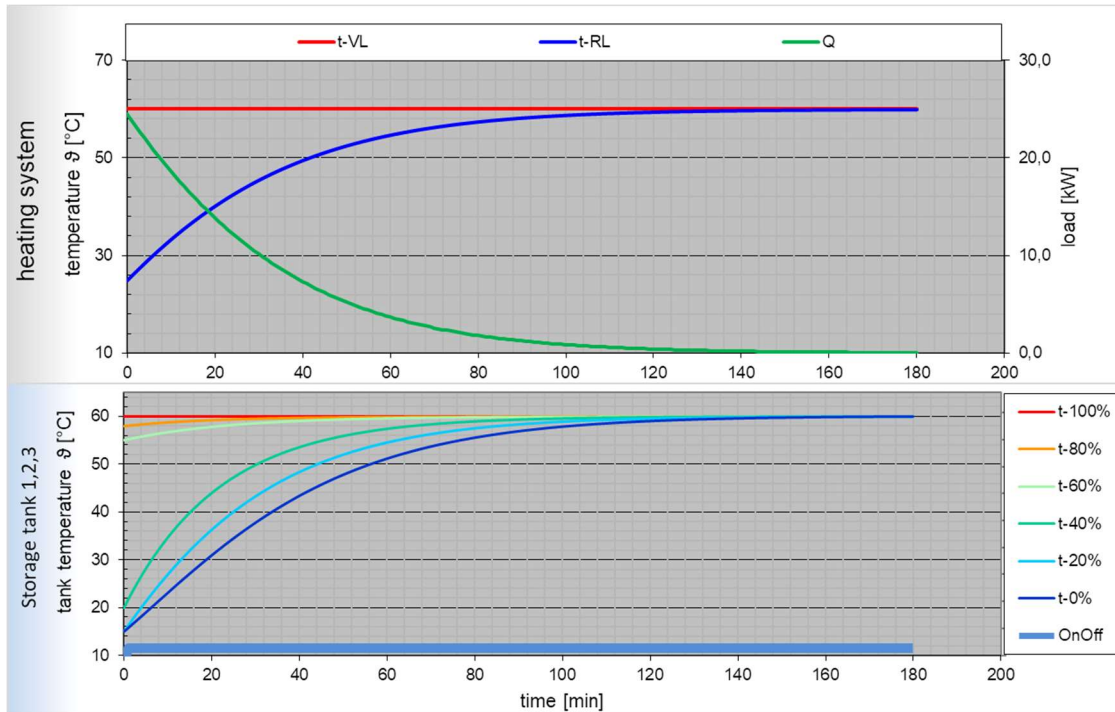
Figure 88 Thermal power and temperatures in parallel DHW preparation of 3 storage tanks

If the same system with three integrated storage tanks is not loaded in parallel, but only one of the three storage tanks is loaded at a time consecutively, as anticipated in the developed control strategy, the disadvantages in terms of high loading power can be eliminated. The view of the loading process in Figure 89 with three different loading zones shows the significant improvement in maximum load. Although the peak output of 8 kW per tank is achieved in the same way as before, but since the other two tanks are not loaded at the same time, the output for the entire system never exceeds 8 kW.

After 30 minutes the loading of the next storage tank can be activated, the other two tanks are again not loaded. After 60 minutes the last tank also can be loaded for 30 minutes. If after 90 minutes all three storage tanks have been loaded for 30 minutes each, the parallel charging of all three tanks will be activated at the same time. Due to the higher storage temperatures, however, there is a clearly reduced charging power of less than 3 kW per tank, which means that the total power of the system is again only 8 kW.
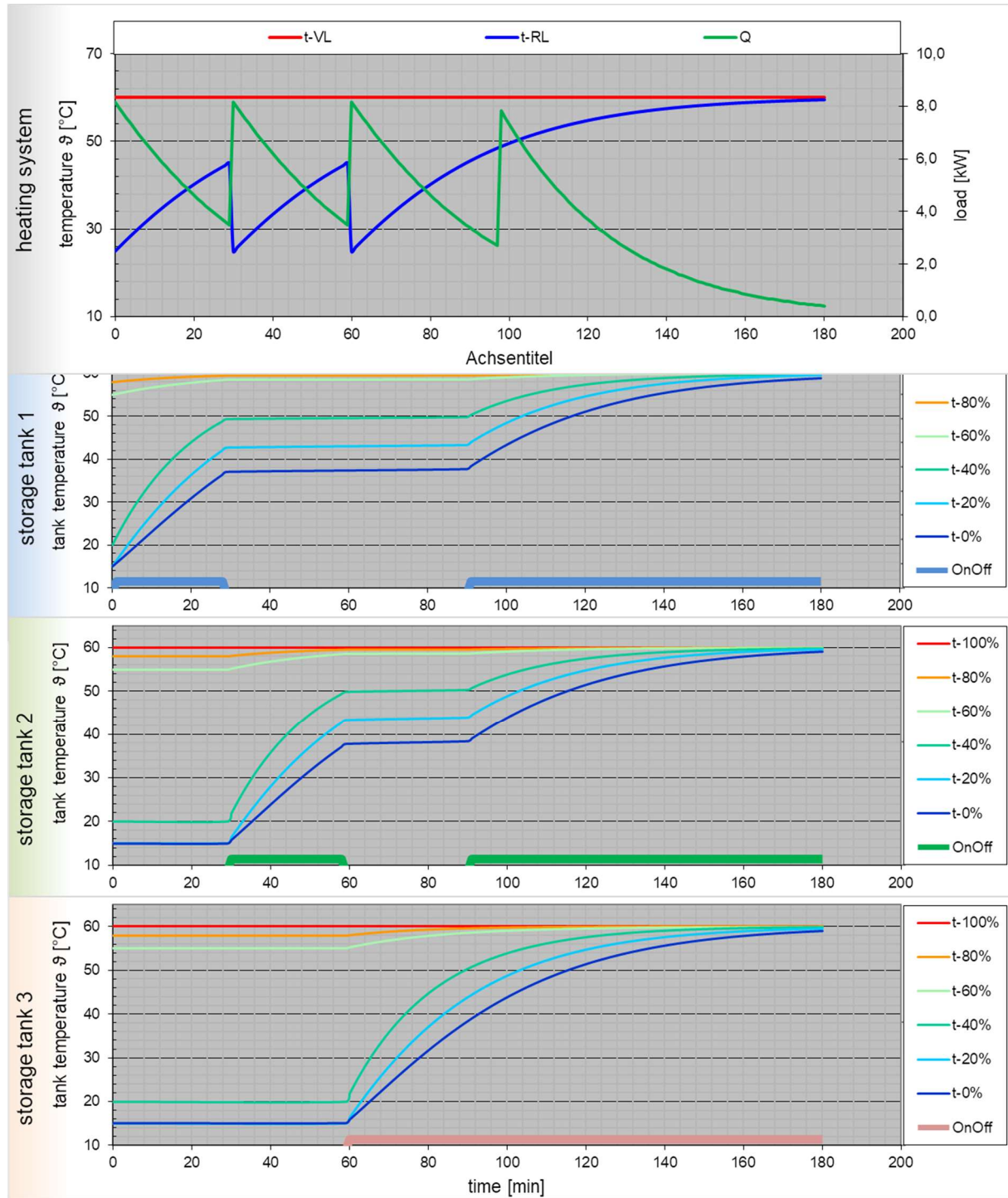
Figure 89 Thermal power and temperatures in consecutive DHW preparation of 3 storage tanks